UNIVERSITY OF OKLAHOMA

GRADUATE COLLEGE

SURFACE MODIFICATION OF TiO_2 FOR PHOTOCATALYTIC SELECTIVE OXIDATION OF ORGANIC COMPOUNDS IN BIPHASIC AND SINGLE PHASE SYSTEMS

A THESIS

SUBMITTED TO THE GRADUATE FACULTY

in partial fulfillment of the requirements for the

Degree of

MASTER OF SCIENCE

By

TANIA GIZETH VITERY ERAZO
Norman, Oklahoma
2016

SURFACE MODIFICATION OF TIO_2 FOR PHOTOCATALYTIC SELECTIVE OXIDATION OF ORGANIC COMPOUNDS IN BIPHASIC AND SINGLE PHASE SYSTEMS

A THESIS APPROVED FOR THE
SCHOOL OF CHEMICAL, BIOLOGICAL AND MATERIALS ENGINEERING

BY

_____
Dr. Steven Crossley, Chair

_____
Dr. Daniel Resasco

_____
Dr. Lance Lobban

To my mother Betty and my siblings Sarith, Liliana, Paola, Alex, and Andrés.

To my father in heaven, thanks for watching over us. You will always be in my heart.

Acknowledgements

First of all, I would like to thank my advisor, Dr. Steven Crossley, who gave me the opportunity to pursue my master studies at the University of Oklahoma. Thank you so much for sharing your knowledge with me but also for your patience, motivation, guidance, and support throughout the past two and half years. Likewise, especial thanks for your never-ending positive attitude and encouragement.

I would like to thank the rest of the committee members, Dr. Resasco and Dr. Lobban, for their valuable suggestions and for taking the time to evaluate my thesis. Moreover, many thanks to Dr. Wang for being always open to answer my questions and trying his best to give me a complete and accurate answer. I am also incredibly grateful to Dr. Daniel Santhanaraj for the guidance and advice given to me especially at the start of this adventure. Also, I would like to thank all present and former CBME group members, particularly to Terry who was always kind and caring.

I would like to extend my deepest gratitude to all the biofuels group members, above all to Maria, Sweta, Cristian, Gap, Tuong, Tyler, and Felipe. Thank you so much for the support, priceless help, and friendship.

Last but not least, I would like to acknowledge and thank my family for the kind support and unconditional love. I will always be grateful for instilling in me a sense that I could do anything if I worked for it. Mom, thanks for being my best friend and my best teacher; my love for you means more than I can ever express. I am lucky to have lived my life surrounded by such remarkable women. I appreciate and I am truly grateful for everything you have done.

Table of Contents

List of Tables

List of Figures

Abstract

Living style of human kind in this era has a large dependence on energy and petroleum based products. As the population grows; the world's fossil fuels, minerals, and natural resources are being depleted. Currently, as many nations are developing and new markets and economies are emerging, the need for the development of new products is becoming a critical factor to increase the standard of living. Furthermore, environmental and political concerns regarding pollution and global warming, motivate the search for new and innovative routes for the synthesis of chemicals in a sustainable and environmentally friendly manner.

The catalytic oxidation of cyclohexane is a worldwide chemical process used for the synthesis of KA oil (mixture of cyclohexanol and cyclohexanone). KA oil is then used as raw material for the production of caprolactam and adipic acid, which are precursors to nylon 6 and nylon 66.[1] A sustainable, non-conventional, and environmentally friendly route for this chemical process is the liquid phase photocatalytic selective oxidation of cyclohexane using TiO_2 as catalyst.

The effect of several factors on the reaction activity and selectivity have been extensively investigated. Some factors include, reaction solvent, oxygen flow bubbled throughout the reaction, light wavelength, particle size and crystal phase of the catalyst, and surface modifications of the catalyst (surface silylation and ion doping). Although the use of TiO_2 to selectively oxidize cyclohexane to cyclohexanol and cyclohexanone has been a popular research topic, fast deactivation and therefore low conversion have been found to be the two major drawbacks. Research studies have concluded that strongly adsorbed intermediates and products such as cyclohexylperoxides, cyclohexanol, and

especially cyclohexanone are further oxidized to carboxylates and carbonates, which are responsible for the fast deactivation of the TiO_2 surface. It was also found that a superior photocatalytic performance is obtained by enhancing the rate of desorption through surface silylation of TiO_2. Even though, the hydrophobic catalyst promoted the desorption of the reaction intermediates that have strong polar affinity to the surface, it did not retain its hydrophobic nature under the photocatalytic reactions conditions.[2]

In this work, two different approaches were followed in order to enhance the stability of the hydrophobic catalyst. In the first approach, a catalyst named as TiO_2@$mSiO_2$ + OTS was synthesized. This catalysts consists of a mesoporous silica shell covering TiO_2 nanoparticles, and then hydrophobized by treatment with OTS. In the second approach, the catalysts, TiO_2/$mSiO_2$ + OTS, was synthesized by impregnating TiO_2 onto mesoporous silica, and then hydrophobized by treatment with OTS. Both approaches use mesoporous silica to protect the hydrophobic functional groups as well as to significantly increase the surface area of the catalyst. Mesoporous silica was used in order to guarantee good accessibility of the molecules to the active site (TiO_2). As thoroughly explained in the results and discussion section, the catalyst TiO_2/$mSiO_2$ + OTS significantly outperform the catalytic behavior of TiO_2@$mSiO_2$ + OTS.

In order to provide fairly detailed information about the structure and functionality of the catalysts, several characterization techniques were employed including transmission electron microscopy (TEM), scanning electron microscopy (SEM), Brunauer, Emmett and Teller (BET) surface analysis, Fourier transform infrared spectroscopy (FTIR), thermogravimetric and mass spectrometer analysis (TG-MS), diffuse reflectance UV-Vis spectroscopy (DR UV-Vis), and x-ray diffraction analysis

(XRD). The results from the characterization techniques applied to TiO_2@mSiO_2 + OTS are discussed in the appendix.

Further work was initiated with m-cresol and furfural as model reaction compounds of bio-oil obtained from biomass. The main goal was to study the feasibility of using photocatalytic partial oxidation reactions with oxygenated molecules that would lead to the formation of functional groups, offering alternative routes for coupling reaction and further upgrading to fuels and fine chemicals.

CHAPTER 1: FUNDAMENTAL ELEMENTS IN PHOTOCATALYSIS

1.1. Introduction

Pollution levels, global warming, and abnormal climatic changes are the most consequential threats currently being faced by humanity. The development of environmentally friendly, clean, sustainable, and safe energy chemical technologies such as photocatalysis will lead humankind towards the solution of these problems. In the last three decades, research studies about photocatalysis on semiconductor surfaces have become much more abundant. Photocatalysis has a high potential for a wide range of industrial applications such as air and water purification. Also, photocatalysis has been found to be a promising route for production of fuels from water and atmospheric gases, as well as selective organic synthesis.

Titanium dioxide, TiO_2, is a very well-known semiconductor that has been proven to be a promising and low cost catalyst for photocatalytic reactions.[3,4,5] Moreover, TiO_2 exhibits chemical stability, nontoxicity, and high reactivity; making it an ideal and powerful photocatalyst for various chemical processes.[6]

The selective oxidation of aromatics and alkanes is an attractive topic of research since higher-valuable products can be obtained from reasonably inexpensive feedstocks. However, there are few studies concentrated on the application of photocatalysis for synthesis and production of valuable products via selective oxidation.[7,8,9,10] The main focus of the photocatalytic studies using semiconductor materials has been the total oxidation of organic molecules with application on

degradation of contaminants present in water and air.[11,12,13,14,15,16,17] There is a high potential to use photocatalysis as an innovative approach for the synthesis of fine and specialty chemicals via selective partial oxidation.

1.2. Principles of Heterogeneous photocatalysis

Photocatalysis is defined as the catalytic process in which the catalyst is activated by light. The process involves four fundamental steps photon absorption, electron-hole pair generation, charge transport, and surface reactions.[18] Figure 1 shows the overall photocatalytic reaction process. A semiconductor aggregate of nanoparticles is illustrated with the respective conduction and valence band edges.

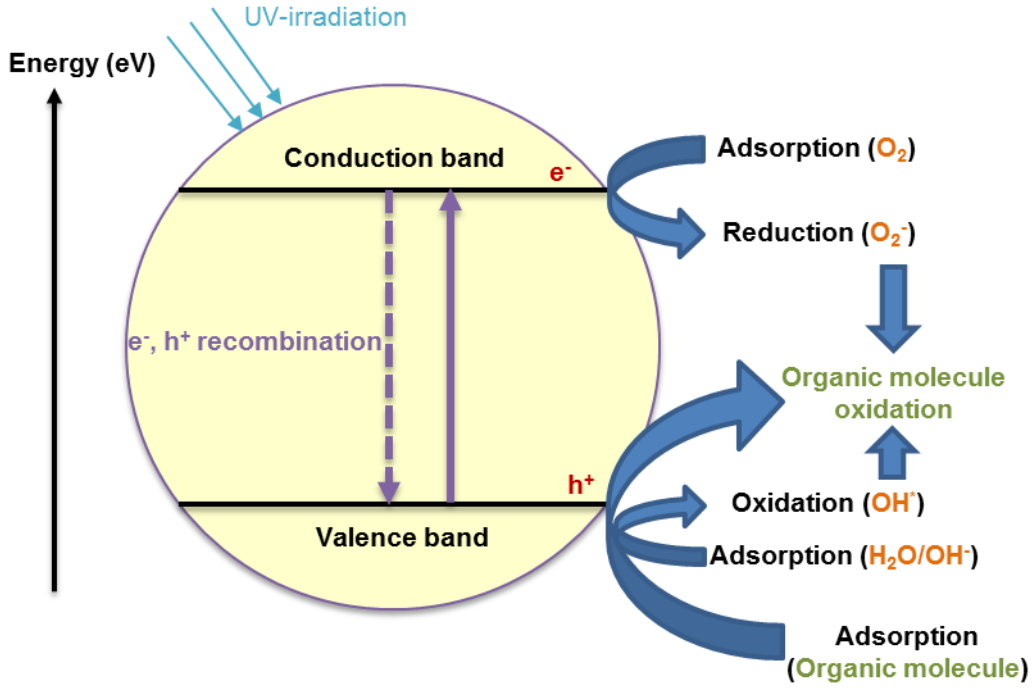

Figure 1. Electron energy band diagram of titania.[19]

As heterogeneous catalysts, a photocatalyst can be used in gas and liquid phases (with both, pure organic solvents or aqueous solutions). The only difference between conventional heterogeneous catalysis and photocatalysis is the mode of activation of the

catalyst. Heterogeneous catalysts, e.g., metals, acids, and oxides are thermally activated whereas photocatalysts are activated by light.[20, 19, 21, 22] According to Herrmann, the photocatalytic process can be broken down into four steps:[20, 19, 21]

1. The semiconductor (SC) absorbs photons whose energy (*hv*) is equal to or higher than its bandgap energy. The term "bandgap" refers to the energy difference between the top of the valence band (VB) to the bottom of the conduction band (CB) in the semiconductor material. In order to guarantee a true photocatalytic regime, the light must be absorbed by the semiconductor catalyst and not by the reactants or intermediate products. This ensures the absence of photolysis in the reactive system.

2. Creation of electron-hole pairs. The absorption of photons induces the excitation of electrons (e^-) from the VB to the CB, leaving holes (h^+) (which are electron vacancies or virtual positive electrical charges), behind in the VB.[23, 24]

3. Migration of the electron-hole pairs to the surface. Once the electron-hole pair has been generated, there are different pathways that will define their fate. Figure 2 shows the possible paths that electrons and holes can follow within a semiconductor particle. The e^- or h^+ charge carriers may not transport all the way to the surface and recombine at the bulk of the semiconductor (Path B). Additionally, the e^- or h^+ charge carriers can migrate from the bulk to the surface and undergo recombination at the surface of the semiconductor in the absence of adsorbed species that act as scavengers (Path A_1/A_2). A third path can be followed when adsorbed species are available to initiate electron transfer reactions (Path C_1/C_2). The efficiency of the photocatalytic

reaction can be reduced by the rate of electron-hole recombination. When electron-hole recombination occurs the photoelectronic energy is degraded into heat.[20, 19,21]

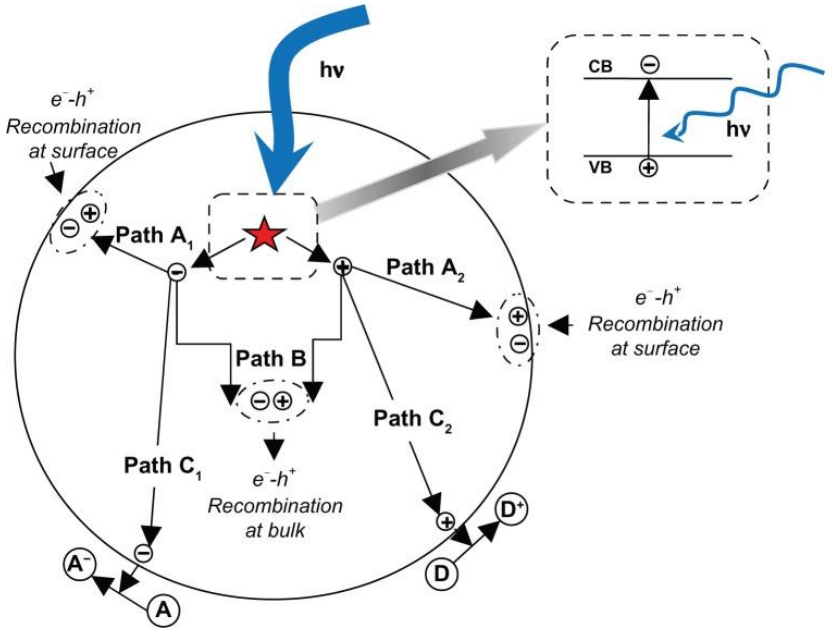

Figure 2. Schematic representation of pathways for electron and holes within the spherical particle of TiO_2.[25]

4. Electron transfer reactions at the surface such as charge neutralization, radical formation, surface reactions, etc. This step is also known as surface electrocatalysis.[18] Due to the existence of both e^- and h^+ electrical charges, the adsorption of the reactants is followed by redox reactions. An adsorbed chemical specie (A_{ads}) is reduced when it gains electrons (A_{ads}^-). On the other hand, a compound (D_{ads}) is oxidized when it loses electrons (D_{ads}^+). Thus, depending on the redox potential (energy level) of each adsorbed specie, the following reactions occur:

$$hv + SC \rightarrow e^- + h^+$$

$$A_{ads} + e^- \rightarrow A_{ads}^-$$

$$D_{ads} + h^+ \rightarrow D_{ads}^+$$

The electron-hole pairs generated are transferred to acceptor and donor molecules at the surface, forming ions and radicals that then react to yield the intermediates and final products.

1.3. TiO_2 as photocatalyst

The development of highly active heterogeneous photocatalysts has gained great attention in recent years, putting effort on the use of semiconductors such as TiO_2, ZnO, CeO_2, ZrO_2, SnO_2, CdS, and ZnS for photocatalytic applications.[26] Among these materials, titanium oxide (TiO_2) has been proven to be the most promising material because of its convenient valence and conduction band positions as well as its long term stability, non-toxicity, easy availability, and low cost.

Figure 3 shows the valence band and conduction band edge positions, light absorption onsets, and band gap energies of some semiconductors. A high oxidation potential is desired in order to increase the electron affinity of the hole (bearing a positive charge). A high reducing potential is desired with the aim of facilitating the electron transfer to an acceptor molecule. TiO_2 has convenient band edge positions, generating electrons that have moderate reducing power (maximum of -0.5 V) and holes with very high oxidizing power (maximum of +2.7 V).[26]

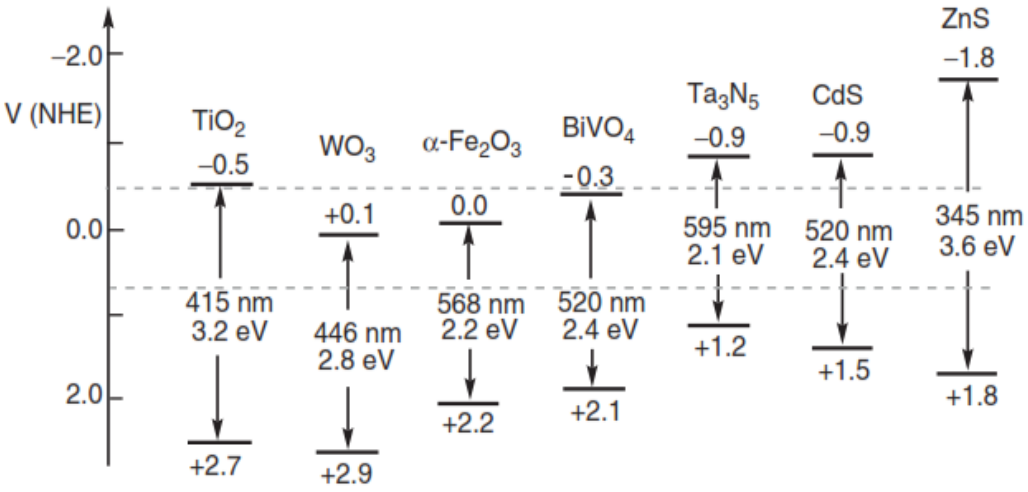

Figure 3. Valence band and conduction band edge positions, light absorption onsets, and band gap energies of some semiconductors. NHE (normal hydrogen electrode).[26]

There are three crystal modifications of TiO_2, (anatase, rutile, and brookite). These polymorphs exhibit different photocatalytic performances. Although anatase has a higher band gap energy (3.2 eV) than (3.03 eV) of rutile, the photocatalytic activity of anatase is greater. Brookite is difficult to synthesize compared to anatase and rutile so it is hardly ever reported as photocatalyst. The reasons for the observed differences in photocatalytic activity are still a matter of debate. Some explanations include:

1. *Type of band gap*: Density functional calculations conducted by Zhang *et al*. indicated that anatase exhibits an indirect band gap while rutile and brookite have a direct band gap,[27] which is illustrated in Figure 4. In a direct band gap, the momentum of electrons and holes is the same in the conduction band and the valence band. This is not desired since the photogenerated electron in the conduction band can directly emit a photon and recombine with a hole in the valence band. On the other hand, in an indirect band gap, a photon cannot be emitted because the electron must pass through an intermediate state and transfer momentum to the crystal lattice. Consequently, the

photoexcited electrons and holes have a longer lifetime in an indirect band gap because photogenerated electrons cannot move directly from the conduction band to the valence band of TiO_2 anatase. This results in a lower recombination rate in anatase compared to rutile and brookite. Hence, enhancing the availability of photoexcited electrons and holes to participate in surface chemical reactions.[27]

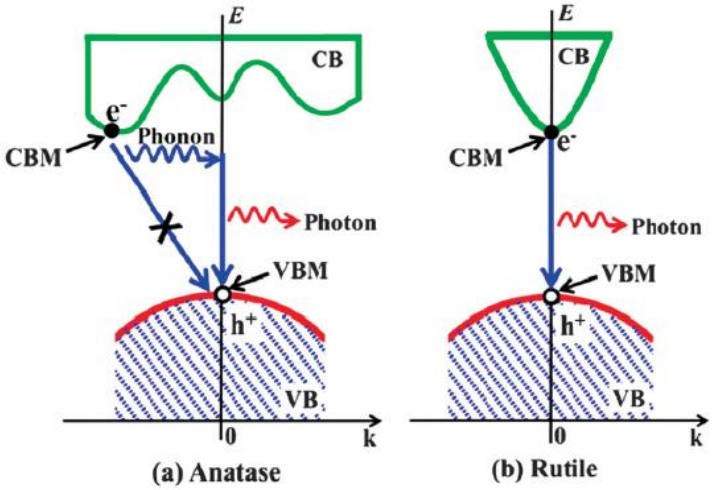

Figure 4. Electron-hole recombination processes in anatase (indirect band gap) and rutile (direct band gap).[27]

2. *Different specific surface area:* Anatase and brookite are metastable phases while rutile is the stable phase.[28] Although, anatase is thermodynamically less stable than rutile, its formation is kinetically favored at temperatures lower than 600 °C.[21] At higher temperatures, anatase transforms irreversibly to rutile. According to Herrmann, the lower temperature needed for the formation of anatase could be responsible for its higher surface area.[20, 19, 21] The superior photocatalytic activity of anatase compared to rutile has been correlated by the higher surface area as well as the larger surface adsorption capacity to hydroxyl groups.[29, 30]

3. *Grain size*: As portrayed in Figure 5, anatase has a smaller grain size than rutile. Accordingly, the distance from the bulk to the surface is smaller in anatase than in rutile. Therefore, the charge carriers of anatase migrate more easily to the surface. This implies that a higher number of e^--h^+ pairs can participate in photocatalytic reactions in the case of anatase.[27]

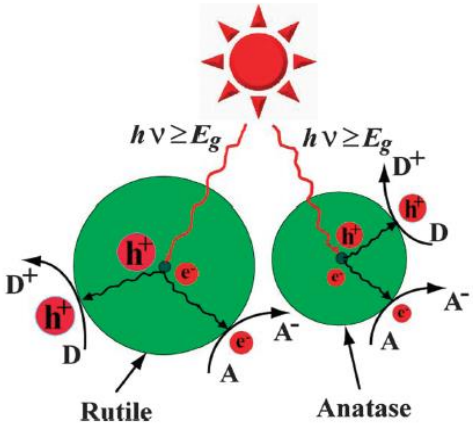

Figure 5. Diagram illustrating the photogenerated electrons and holes for rutile and anatase particles.[27]

It is also stated that mixed-phase samples of anatase and rutile outperform the individual polymorphs. However, the possible explanations are still being debated. In general, the band gap energy of anatase and rutile are specified as 3.20 eV and 3.03 eV, respectively. According to recent photoemission experiments, the conduction band of anatase lies 0.2 eV below that of rutile.[31] By combination of theory and experiments (XPS measurements), Scanlon *et al*. concluded that the electron affinity or work function of rutile is 0.2 eV lower than that of anatase (Figure 6.b). The opposite case has been also proposed (Figure 6.a).[32] The authors claim that a type-II (anatase) band alignment considerably lowers the effective band gap energy but at the same time, it facilitates an efficient electron hole separation.[33]

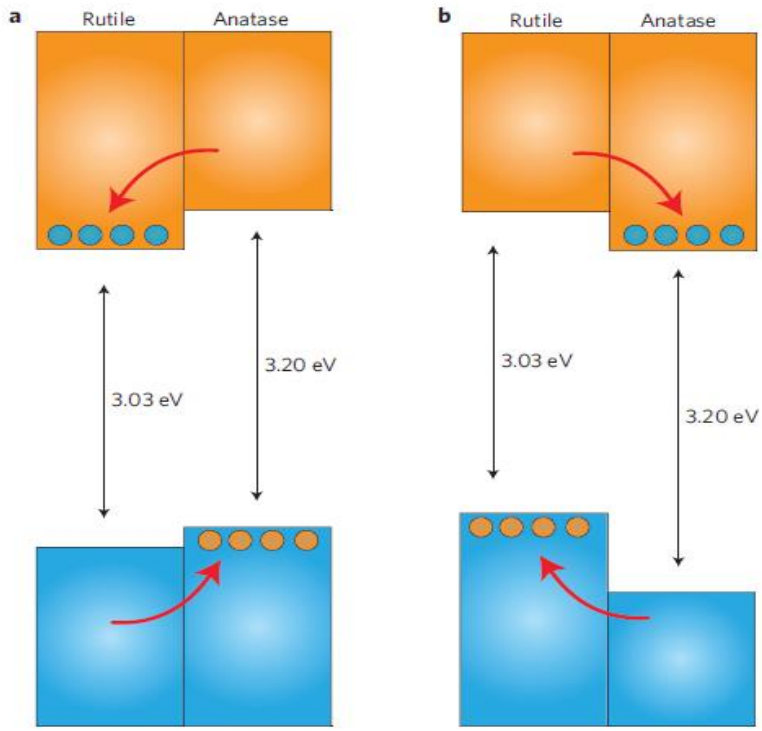

Figure 6. Proposed valence and conduction band alignment mechanisms for the anatase/rutile interface. a. Type-II (rutile). b. Type II (anatase). Red arrows indicate the flow of electrons in the conduction band and holes in the valence band.[33]

1.4. Influence of operational parameters in photocatalysis

The identification of the oxidant in photocatalytic reactions on TiO_2 has been one of the major mechanistic issues. There are many debates about the relative role of VB holes for direct oxidation (electron transfer between the organic molecule to the hole), versus hydroxyl radicals ($OH^{\bullet}$) for 'indirect' oxidation (e.g. homolytic hydrogen abstraction from the organic molecule by the $OH^{\bullet}$).[34] There has been also discussion about how $OH^{\bullet}$ are formed, which can be either by direct hole oxidation of adsorbed H_2O and/or hydroxyls ions, or via electron scavenging reactions involving O_2.[34-35] Reaction conditions can also play a role in deciding which oxidant is available and most useful. According to Henderson, at high organic coverage the VB holes are the key oxidizer because of the inability of water or O_2 to gain access to the surface.[34] The

amount of oxygen, type of solvent, light wavelength, radiant flux, reactor material, mass of catalyst, pH, and reactant initial concentration are some important parameters that need to be taken into account in photocatalysis and are briefly discussed in the next pages.

1.4.1. Oxygen role in photocatalysis

Photo-oxidation can happen by electron transfer between the hole generated in the VB or the $OH^{\bullet}$ radicals and the substrate. On the other hand, photo-reduction involves coupling of an electron in the CB with an acceptor adsorbed specie. However, in order to prevent back-electron transfer to the TiO_2 CB, the coupling has to be strong,[34] i.e., the charge transfer from the reduced surface to the adsorbate occurs if the electronegativity of the adsorbate exceeds the surface electronegativity of TiO_2 (e.g., O_2, O, Cl, and F have a higher electronegativity than TiO_2). In such cases there is no back-electron transfer to the TiO_2 CB. On the other hand, upon adsorption of species with low electronegativity (e.g., H_2O, NH_3, and H_2S), there is no net electron transfer to the TiO_2 CB.[23] Consequently, the O_2 molecule has been found to be a good e^- scavenger and it has been widely used in photocatalytic reactions. Nonetheless, the electron transfer dynamics of the reaction between the O_2 molecule and an excited electron in the TiO_2 CB is not yet well-understood.

The sources of oxygen in photocatalytic reactions on TiO_2 include molecular oxygen, water, surface hydroxyls, and the involvement of lattice oxygen. According to Henderson, lattice oxygen is not really recognized but should also be taken into consideration in order to understand photocatalysis over TiO_2.[34] However, some studies concluded that lattice oxygen does not play a role in photocatalysis.[36] By means of

photoluminescence (PL) studies, Stevanovic *et al*. found that the O_2 molecule can behave two ways. One way, as a reversibly adsorbed electron-acceptor molecule, and the second way as an irreversibly adsorbed molecule that reduces the concentration of natural oxygen vacancy defects in the near-surface region of TiO_2.[37]

1.4.2. Solvent and wavelength

Solvent choice is also an important factor. The solvent must be able to dissolve the substrates but must not be a strong UV absorber itself. Also, the solvent should not undergo hydrogen atom abstraction or other reactions with the excited state.[38] Acetonitrile is commonly used as a solvent for photocatalytic reactions because it is relatively inexpensive, good at dissolving polar substrates, does not absorb UV light at wavelenghts higher than 190 nm, and it is stable under photocatalytic conditions toward redox reactions.[15,9-10, 38] Photocatalytic reactions are often performed in solvents such as benzene, acetonitrile, carbon tetrachloride or methanol.[39] However, safety precautions need to be taken because these are hazardous solvents. Also, it is important to make sure that the solvent does not absorb UV light in order to conserve the exclusive photoactivation of the catalyst for a true heterogeneous catalytic regime. Table 1 shows the different solvents commonly used and their corresponding threshold for UV light absorption.

Table 1. UV absorption onset for different solvents.[40]

Solvent	**λ (nm)**
Acetonitrile	190
Water	191
Cyclohexane	195
Hexane	201
Methanol	203
Dichloromethane	220

When having water as solvent, the TiO_2 surface is completely hydrated and hydroxylated due to its amphoteric hydroxyls groups. Hence, the adsorbed H_2O or OH^- anions are oxidized by h^+ to form OH radicals. These OH radicals are strong unselective oxidizing agents that can oxidize organic compounds.[20]

$$OH^-_{(\text{ads})} + h^+ \rightarrow OH^*_{(\text{ads})}$$

According to Fu *et al*., water can either promote the $OH^\bullet$ radicals formation or block the surface sites needed for reactants. Water can be a promoter or inhibitor depending on the following aspects: the relative binding of water versus organic molecule to the surface, concentration of water and organic present, and mechanism by which the organic is photochemically activated (e.g., $OH^\bullet$ radicals versus direct hole oxidation).[41]

Regarding the promoter role, Muggli and Falconer stated that the oxygen atom in water can be incorporated into the products and intermediates of a typical photooxidation reaction.[42] Furthermore, the surfaces coverages of reactants, intermediates, and products can be moderated and redistributed by water assistance.[43] Nonetheless, the most important benefit attributed by water to the photochemical processes on TiO_2 is the generation of reactive radicals, such as $OH^\bullet$, responsible for the photooxidation reactions.[44]

In regard to the inhibiting role, water can act as a blocker of surface sites. Organic molecules that bind weakly to oxide surfaces and prefer oxidation by holes, the initial photooxidation step decreases greatly at higher relative humidity values where water dominates the chemisorbed layer and occupies important adsorption and/or reaction sites on the surface.[34] On the other hand, a strongly bound organic molecule

that oxidizes by $OH^{\bullet}$ will have a low rate of photooxidation at very low relative humidity, and will see a rate increase with increasing relative humidity.[34] Moreover, it has been suggested that the destabilization or access of reactants such as O_2 to the TiO_2 surface can be limited by water layers (formed by hydrogen-bonded networks at room temperature) situated above TiO_2 surfaces.[31] These effects could be partially mitigated by increasing the reaction temperature (to ~50-100 °C), and therefore lowering the water coverage on the surface.[12] Higher temperature might have the opposite effect when water is a promoter.

1.4.3. Radiant flux

In photocatalytic reactions the catalyst is activated by light with the participation of photo-induced electrical charges (e^- and h^+). At high radiant fluxes, the instantaneous concentrations of e^- and h^+ increase. However, the rate of reaction is proportional to the radiant flux only up to a certain value. Above this point, the rate of generation of e^- and h^+ becomes greater than the photocatalytic reaction rate, leading to electron-hole recombination.[20]

1.4.4. Mass of catalyst

In photo-reactors the initial rate of reaction has been found to be directly proportional to the mass of catalyst, indicating a true heterogeneous catalytic regime. However, this behavior is only observed until a certain catalyst loading. At some point, the reaction rate levels off and becomes independent of the photocatalyst concentration. When solutions are highly concentrated, light scattering occurs decreasing the amount of light penetrated. Therefore, the catalyst concentration has to be optimized in order to

ensure a complete absorption of photons. In general, the concentration of photocatalyst goes from 0.2 to 2.5 g L^{-1}.

1.4.5. pH

In heterogeneous photocatalysis pH is another important parameter because it can either affect or enhance the rate of adsorption of the reactants on the catalyst surface. TiO_2 is an amphoteric compound that can react both as an acid and as a base. The isoelectric point of zero charge (PZC) refers to the pH at which a molecule carries no net electrical charge, e.g. the PZC of TiO_2 is 6.3.[45] Thus, the net charge on the TiO_2 surface is affected by the pH of its surrounding environment. As shown in the equations below, at $pH < PZC$, the TiO_2 surface becomes more positively charged due to the gains of protons (H^+), which favors electrostatic attraction forces with anionic compounds, improving the rate of adsorption. At $pH > PZC$, the TiO_2 surface becomes more negatively charged and anionic compounds are now repulsed, decreasing the rate of adsorption. When $pH = PZC$, moderate adsorption of anions and cations can be expected.[46]

$$\text{At } pH < PZC\text{: } TiOH_2^+ \leftrightarrow TiOH + H^+$$

$$\text{At } pH > PZC\text{: } TiOH + OH^- \leftrightarrow TiO^- + H_2O$$

1.4.6. Initial concentration of reactant

Generally, the rate of photocatalytic reactions is affected by the initial concentration of organic compounds. A longer irradiation time is required for high concentrations of organic compounds in order to reach a certain level of conversion. If the concentration is too high, the organic molecule can saturate the surface of TiO_2 decreasing the photonic efficiency.

1.4.7 Photocatalytic Quantum Yield

The efficiency of photocatalytic reactions can be evaluated by the measuring of the photonic efficiency (ζ), which is the rate of formation of reaction products divided by the incident photon flux. Unfortunately, ζ is usually found to be rather small. One the reasons for the relatively low ζ values (<10%) of most semiconductor-based photocatalytic reactions is that most of the photogenerated e^{-}/h^{+} pairs (~90%) recombine rapidly after excitation.[47,48] The electron-hole recombination is a highly exothermic process that restitutes most of the band gap energy absorbed by the semiconductor. Many factors such as sample preparation, reaction temperature, charge trapping, interfacial charge transfer, excitation, and radiant flux have been found to affect the electron−hole recombination process.[23, 49]

CHAPTER 2: KEY CONCEPTS IN RADICAL REACTIONS

David Klein devotes an entire chapter of his book, Organic Chemistry, to describe radical reactions.[50] A brief summary of the main concepts related to radicals is given in this section. As shown in Figure 7, radicals are formed as a result of homolytic bond cleavage. Homolytic cleavage is the breaking of a bond in such a way that each fragment gets one of the shared electrons.

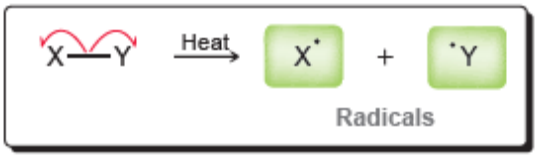

Figure 7. Homolytic bond cleavage.[50]

Some bonds are easier to cleave than others. Figure 8 illustrates the stability of primary, secondary, and tertiary radicals. As in the case of carbocations, tertiary radicals are the most stable and have the lowest bonding dissociation energy (BDE) for the C-H bond (406 kJ/mol), see Figure 9. This implies that it is easier to cleave homolytically the C-H bond in a tertiary carbon. However, resonance-stabilized radicals are even more stable than tertiary radicals. As shown in Figure 10, the C-H bond at an allylic (364 kJ/mol) or benzylic position (356 kJ/mol) have lower BDE than a tertiary carbon.[50]

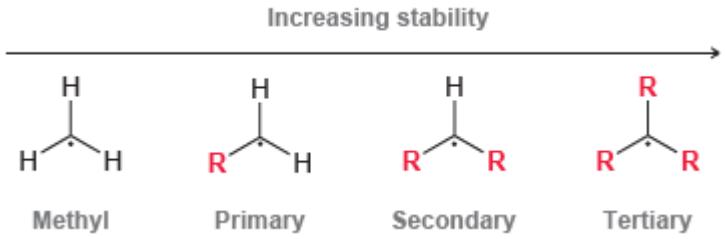

Figure 8. Order of stability for carbon radicals.[50]

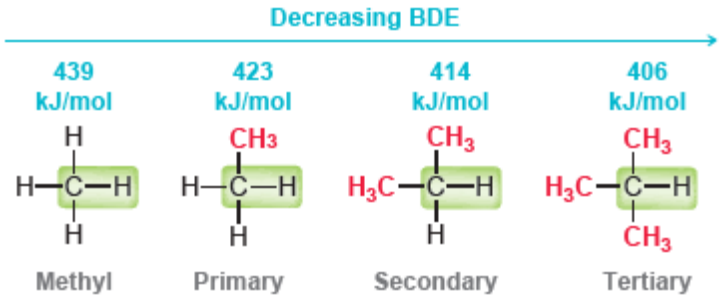

Figure 9. Bond dissociation energies for various C-H bonds.[50]

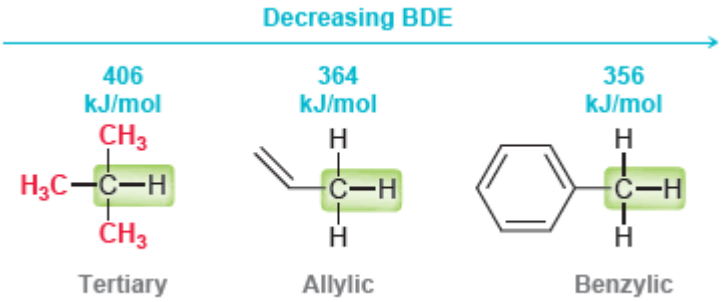

Figure 10. Comparison of bond dissociation energies for several C-H bonds.[50]

It is also important to point out the difference between an allylic and a vinylic position. A vinylic position does not have a resonance structure and it is not resonance stabilized. Additionally, as observed in Figure 11, the BDE for a vinylic position (464 kJ/mol) is even higher than the one for a primary carbon (423 kJ/mol), this means that more energy is needed to cleave a C-H at a vinylic position than all the other cases previously mentioned.[50]

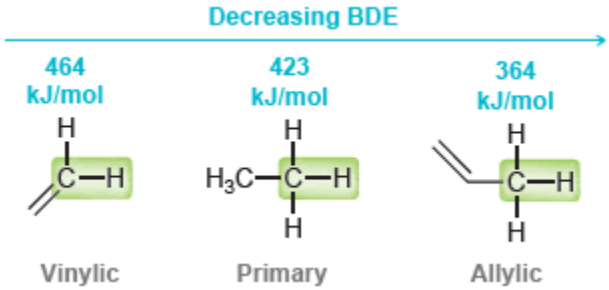

Figure 11. Comparison of bond dissociation energies for several C-H bonds.[50]

Figure 12 displays the common patterns in radical mechanisms including: hemolytic cleavage which is the opposite of coupling; addition to a π bond which is opposite to elimination; and hydrogen abstraction which is similar to halogen abstraction.

Homolytic bond cleavage (a) requires a large input of energy in the form of heat or light. Photolytic reactions are in general carried out at room temperature, therefore, the energy necessary to cause hemolytic bond cleavage would be supplied by light. Coupling (f) happens when two radicals join together and form a bond.[50]

In a radical molecule, there are two relevant positions, α and β positions. The α position is the carbon bearing the unpaired electron. The β position is the adjacent carbon to the α position. A radical can add to a π bond (b), break it and form a new radical. In elimination (e) a double bond forms after the cleavage of a single bond at the β position.[50]

Finally, a radical can abstract a hydrogen atom (proton and electron, H•) or a halogen atom from a compound and form a new radical, patterns (c) and (d), respectively.[50]

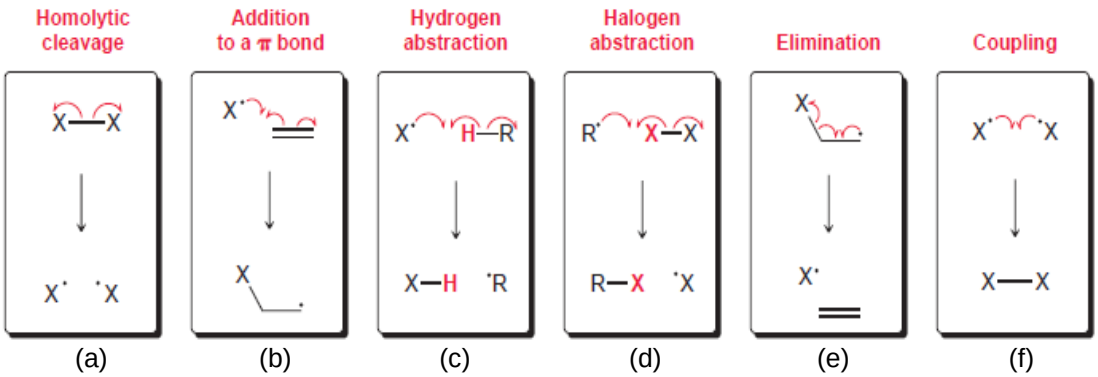

Figure 12. Common patterns in radical mechanisms.[50]

Radical initiators and inhibitors

Radical reactions can be initiated by radical initiators but can also be restricted by radical inhibitors. Radical initiators are compounds containing a weak bond that requires a lower amount of energy in order to undergo homolytic cleavage. For instance, peroxides are radical initiators containing an O-O bond that is weak and only requires 159 kJ/mol of energy to break, see Figure 13.[50]

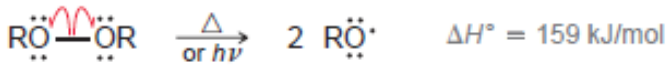

Figure 13. Formation of radical initiators from a peroxide.[50]

Additionally, radical's inhibitors (radical scavengers) destroy radicals by coupling with other radicals. One example is the diradical oxygen molecule (O_2). Each oxygen atom is able to couple with other radicals, thereby destroying them. Generally, all of the available oxygen has to be consumed first so the radical chain reactions occur fast. As shown in Figure 14, hydroquinone is another radical inhibitor that can undergo hydrogen abstraction when meeting another radical and therefore producing a less reactive resonance-stabilized radical. This resonance-stabilized radical can meet another radical and undergo another hydrogen abstraction forming benzoquinone.[50]

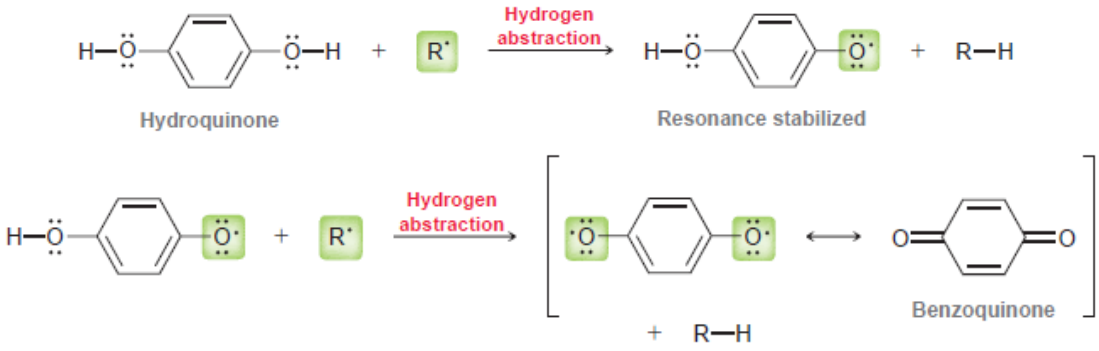

Figure 14. Benzoquinone as radical inhibitor.[50]

CHAPTER 3: PHOTOCATALYTIC SELECTIVE OXIDATION OF CYCLOHEXANE

3.1. Overview

Among the selective oxidation reactions, the photocatalytic partial oxidation of cyclohexane in liquid phase using TiO_2 as catalyst, has been widely studied.[51, 52, 53, 54, 55, 2] This reaction is important because cyclohexanone can yield ε-caprolactam which is the precursor to Nylon 6, a popular synthetic polymer.[51] As illustrated in Figure 15, cyclohexane can undergo partial oxidation to either cyclohexanol or cyclohexanone, and then further oxidation reactions lead to the formation of CO_2.

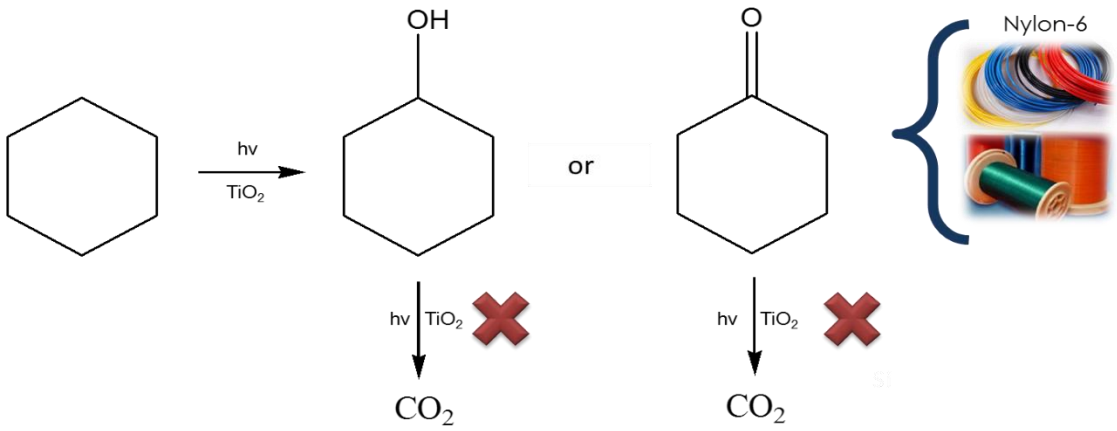

Figure 15. Photocatalytic oxidation of cyclohexane.

Carneiro *et al.* proposed a simplified scheme illustrated in Figure 16, for the photocatalytic oxidation of cyclohexane using TiO_2.[53] The left side of Figure 16 illustrates the formation of an electron-hole (e^-, h^+) pair that occurs as a result of light excitation of the semiconductor. Subsequently, surface reactions occur between the holes that reach the surface of the catalyst and the surface hydroxyl group (OH_{ads}) or adsorbed water (H_2O_{ads}). This results in the formation of surface hydroxyl radicals

(OH•) which are known to be the primary oxidizing species in photocatalytic oxidation reactions.[53] Next, the surface adsorbed cyclohexane undergoes hydrogen abstraction by the surface OH• making cylclohexyl radicals and water.

As shown in the right side of Figure 16, once the electrons generated reach the surface, they interact and reduce the Ti^{IV} center. The molecular oxygen bubbled throughout the reaction reacts with the reduced Ti^{III} center producing superoxide anions (O^{2-}) which play an important role in the selective generation of cyclohexanone, as discussed below.[53]

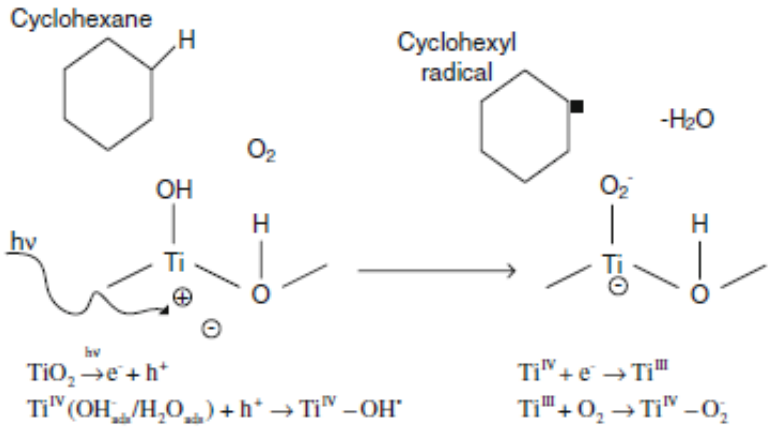

Figure 16. Simplified scheme of the photocatalytic oxidation of cyclohexane using TiO_2.[53]

3.2. Mechanism of photocatalytic oxidation of cyclohexane

In the following year, Carneiro *et al*. proposed the mechanism for the cyclohexane selective photocatalytic oxidation to cyclohexanone (mechanism A in Figure 17), and cyclohexanol (mechanism B in Figure 17).[55] It can be observed that peroxide intermediates are formed from the reaction between the cyclohexyl radicals

and the superoxide anions. According to mechanism (A), cyclohexanone is formed as a result of the acid-catalyzed peroxide decomposition and regeneration of the surface hydroxyl group. Once cyclohexanone is formed at the surface, it can either desorb to the reaction medium or further oxidize to carboxylates, carbonates and finally to CO_2/H_2O. According to mechanism (B), the combination of two cyclohexylperoxy radicals at the catalyst surface produces cyclohexanol and cyclohexanone simultaneously. Strongly adsorbed reaction intermediates can also be responsible for the carboxylates and carbonates formation that cause the deactivation of OH groups on the TiO_2 surface.[55]

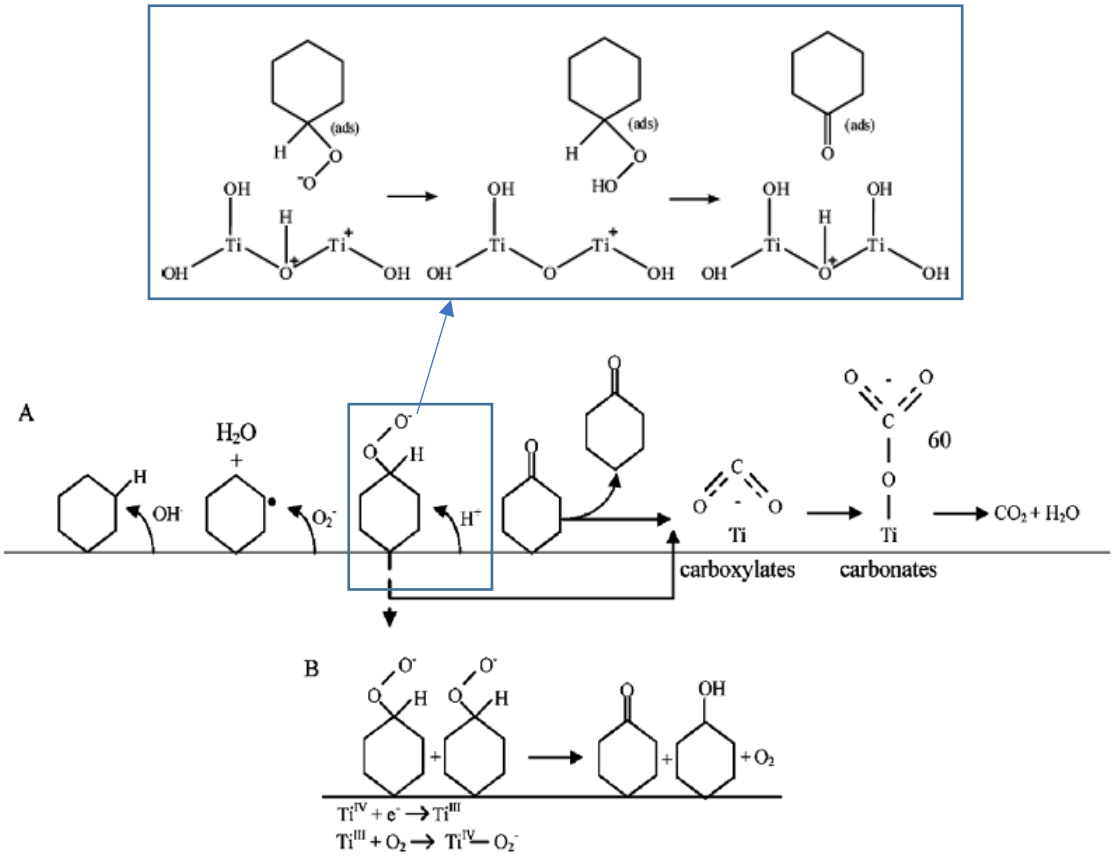

Figure 17. Top: Acid-catalyzed peroxide decomposition and formation of cyclohexanone, with regeneration of the hydroxyl group.[52] Bottom: Illustration of the mechanism for the photocatalytic selective oxidation of cyclohexane. Path (A) indicates the formation of cyclohexanone, and path (B), the formation of cyclohexanol.[55]

3.3. Research objective

The influence of several factors on the mechanism and selectivity of the reaction has been widely investigated. Some factors include, solvent,[56, 57, 58] oxygen flow, light wavelength,[51, 59] crystal phase[30, 60] and particle size of the catalyst,[55] ion doping,[38] surface silylation,[2] and catalyst deactivation and regeneration.[52, 54] The use of TiO_2 to selectively oxidize cyclohexane to cyclohexanol and cyclohexanone is of great interest. However, fast deactivation and therefore low conversion have been found to be two potential problems of using TiO_2 as catalyst.[2] Attenuated total reflection Fourier transform infrared (ATR-FTIR) studies carried out by Almeida and Carneiro *et al*. stated that strongly adsorbed intermediates and products such as cyclohexylperoxides, cyclohexanol, and especially cyclohexanone are further oxidized to carboxylates and carbonates, which are responsible for the fast deactivation of the TiO_2 surface.[52, 54]

The rate of desorption of intermediates and products can be promoted by tailoring the chemical nature of the solvent, reaction temperature, and catalyst surfaces. Almeida *et al*. showed that the selective photo-catalytic oxidation of cyclohexane can be enhanced by increasing the rate of desorption through surface silylation of TiO_2.[2] Due to the improved desorption, the silylation helps to reduce the rate of formation of surface deactivating carbonate and carboxylate species on TiO_2. Consequently, the rate of catalyst deactivation also decreases. However, the hydrophobic catalyst was found to be unstable under UV light conditions.[2]

In this work, it is attempted to synthesize a more stable hydrophobic catalyst that conserves its hydrophobic nature at the reaction conditions with the aim of achieving a more selective oxidation process. In order to accomplish this, two different photostable

catalysts (TiO_2@$mSiO_2$ core-shell + OTS and TiO_2/$mSiO_2$ + OTS) were synthesized and their photocatalytic performance was evaluated. The photocatalytic activity and selectivity of the most promising catalyst, TiO_2/$mSiO_2$ + OTS, is discussed, as well as the photocatalytic performance of the commercially available catalysts, TiO_2 and TiO_2 T805.

In order to provide fairly detailed information about the structure and functionality of the catalysts, the following characterization techniques were employed for the most promising catalyst: transmission electron microscopy (TEM), scanning electron microscopy (SEM), Brunauer, Emmett and Teller (BET) surface analysis, Fourier transform infrared spectroscopy (FTIR), thermogravimetric and mass spectrometer analysis (TG-MS), diffuse reflectance UV-Vis spectroscopy (DR UV-Vis), and x-ray diffraction analysis (XRD).

CHAPTER 4. EXPERIMENTAL METHODS AND PROCEDURES

4.1. Chemicals and materials

TiO_2, anatase 99.9% (metal basis) was purchased and used as received from Alfa Aesar. AEROXIDE® TiO_2 T805 (3.2 wt% of C content) was purchased from Evonik. Octadecyltrichlorosilane 95% (OTS), barium hydroxide anhydrous 94-98% $Ba(OH)_2$ were purchased from Alfa Aesar, and ammonium hydroxide 28.8% (NH_4OH), from Fisher Chemical. Tetraethyl orthosilicate 99.999% (TEOS), titanium (IV) isopropoxide ≥97%, hexadecyltrimethylammonium bromide ≥99% (CTAB), and pure ethanol 99% (C_2H_5OH) were purchased from Sigma-Aldrich. Cyclohexane 99.9% was purchased from Sigma-Aldrich and used without any purification. Distilled water was used for catalysis synthesis and reactions experiments.

4.2. Catalyst preparation

4.2.1. Synthesis of TiO_2@mSiO_2 core-shell

Synthesis of TiO_2@mSiO_2 core-shell was performed following a procedure adapted from the ones suggested by Yoon *et al*.[61] and Deng *et al*.[62] 2 g of TiO_2, anatase, 99.9% were dispersed in 40 ml of distilled H_2O and 4 mL NH_4OH solution (50 % aq. Soln.). Then, 6 ml of CTAB surfactant solution (100 mM, dissolved in a 2:1 mixture of H_2O and EtOH) was quickly added under vigorous stirring. After stirring 30 minutes, 1 mL of TEOS was added in 0.1 mL increments while stirring the vial in between doses. The mixture was allowed to stir overnight. The particle suspension was centrifuged and washed with 200 ml of ethanol in order to remove the CTAB selectively and led to the formation of TiO_2 cores with a mesoporous silica shell of ~ 4

nm. The sample was further dried at 80^0C overnight and calcined at 400°C during 6 hours.

4.2.2. Synthesis of $mSiO_2$

The widely used surfactant (CTAB) was utilized for the synthesis of the mesoporous silica, identified as $mSiO_2$. 2.5g of CTAB were dissolved in 50 mL of distilled H_2O. After stirring, 35 mL of C_2H_5OH and 14.8 mL of aqueous NH_4OH were added to the CTAB solution. These amounts were chosen so the CTAB concentration is higher than its critical micelle concentration (CMC_{CTAB} ~ 1 mM)[63] in order to form rod-like micelles in the synthesis solution. The solution was stirred until transparent, allowing the micelles to align into hexagonal arrays. Then, 5 mL of TEOS were added dropwise under vigorous stirring, letting the silica species cover the rods. Stirring was provided for three more hours and then the solution was left to rest at room conditions for one hour. The obtained sample was centrifuged, washed with ethanol, and then dried at 80 °C overnight. Finally, the resulting powder was calcined at 500 °C in static air for 5 hours, leading to the oxidation of the organic template (or CTAB).

4.2.3. Synthesis of $TiO_2/mSiO_2$

For the synthesis of the $TiO_2/mSiO_2$, 1.946 mL of titanium (IV) isopropoxide were impregnated onto 0.975 g of $mSiO_2$ via incipient wetness method. After impregnation, the sample was left for two days in ambient air to slowly hydrolyze by normal humidity of the room. The resulting sample was dried at 100 °C overnight and then calcined in static air at 400 °C for 4 hours.

4.2.4. Functionalization with OTS

Functionalization of the external surfaces of the nanoparticles was carried out following an adapted procedure reported for zeolites silylation that uses OTS as a silylation agent.[64] In this procedure, 0.45 mL of water were added to 1 g of TiO_2@$mSiO_2$ core-shell or TiO_2/$mSiO_2$. The sample was shaken until the added water soaked into the aggregates. Then, 10 mL of toluene containing 0.197 mL of OTS were added to the sample. This solution was shaken for another 10 minutes using a vortex mixer and then allowed to react overnight at 500 rpm under magnetic stirring. After reaction with OTS, the particles were removed from solution via centrifugation and washed with C_2H_5OH to remove excess silane/toluene. The resulting material was then dried overnight at 110 °C. The synthesis approach for these catalysts are schematically represented in Figure 18 and Figure 19, respectively.

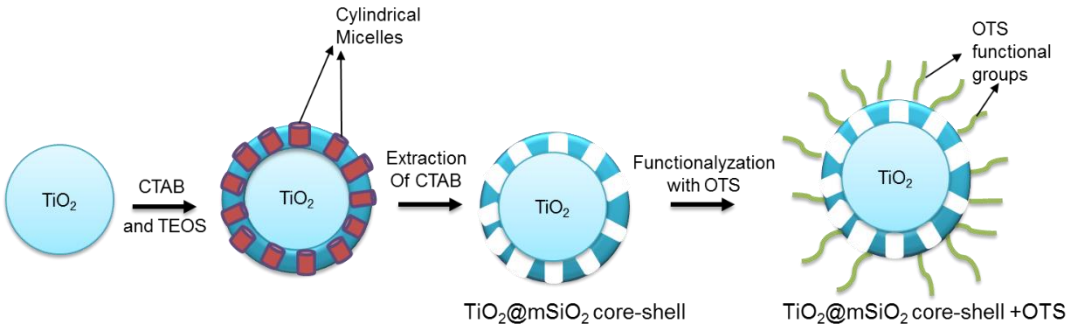

Figure 18. Schematic formation of TiO_2@$mSiO_2$ core-shell + OTS

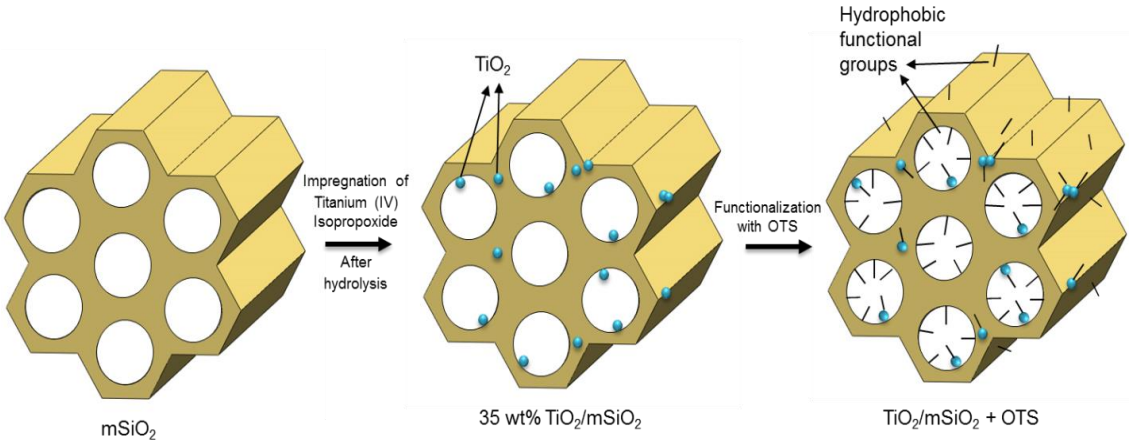

Figure 19. Schematic formation of $TiO_2/mSiO_2$ + OTS.

4.3. Catalyst characterization: Equipment and procedures

4.3.1. Transmission and scanning electron microscopy (TEM and SEM)

TEM analysis was carried out on a JEOL 2000FX field emission microscope operating at an acceleration voltage of 200 kV. SEM images were obtained on a Zeiss NEON FEG-SEM dual beam high resolution scanning electron microscope.

4.3.2. Brunauer, Emmett and Teller (BET) surface area

The BET surface areas were measured by N_2 physisorption at liquid nitrogen temperature on a Micromeritics ASAP 2020 surface and porosity analyzer instrument. Degassing process of catalysts was performed at 200 °C for 4 hours prior to the analysis. The BJH model was used to calculate the pore size distribution.

4.3.3. Fourier transform infrared spectroscopy (FTIR)

The FTIR spectra were recorded between 500 and 4000 cm^{-1} using a Spectrum 100 FT-IR spectrometer, the catalyst powders were introduced into a cell and dried

under flowing He (15 sccm) for 30 minutes at 140 °C. All absorbance and spectra were collected with 128 averaged scans.

4.3.4. Thermogravimetric and mass spectrometer analysis (TG-MS)

TG-MS analysis was performed using STA 449 F1 Jupiter®, Netzsch and Quadrupole Mass Spectrometer (QMS) 403 C Aëolos®. The fresh catalysts were heated in air from 40 to 750 °C at a heating rate of 2 K min^{-1}. The catalysts collected after reaction were pre-treated in argon at 100 °C for one hour to remove adsorbed hydrocarbons on the surface and then heated in air from 40 to 750 °C at a heating rate of 2 K min^{-1}.

4.3.5. X-ray diffraction analysis (XRD)

The X-ray diffraction data were collected in reflection configuration using a Bruker AXS D8 instrument with a GADDS area detector of 15 cm. The instrument primary beam was deflected by Goebel mirror to give a parallel beam of Cu Kα radiation (1.54059 Å) that subsequently passes through a 0.3 mm slit and a 0.3 mm collimator tube. The patterns were recorded in the range 10-70° (2θ) with a step size 0.02°.

4.3.6. Diffuse reflectance UV-Vis spectroscopy (DR UV-Vis)

The optical properties of the catalysts and reactants were investigated by means of DR UV-Vis technique using a UV-2450 UV-VIS spectrophotometer.

4.3.7. Contact angle

The degree of hydrophobicity of the nanoparticles was confirmed by measuring the contact angle. Sessile drops of water were analyzed with an Attension Theta optical tensiometer manufactured by Biolin Scientific. After fitting the drop shape with a

Young−Laplace contact angle model the static contact angle for water was obtained. The procedure described by Weston *et al*. was followed for the preparation of the solid surface.[65] Microscope glass slides were coated with a layer of nanoparticles by placing 2 mL of a 1.0 wt% dispersion of nanoparticles in isopropyl alcohol on a 76 × 26 × 1 mm glass slide. Then, the glass slides were dried in a vacuum oven at 120 °C for 12 hours to remove the alcohol and adsorbed water, and were kept in the vacuum oven until immediately prior to the experiments. The static contact angle was measured by placing an 8 - 12 μL droplet of water on the surface of the nanoparticle-coated slide. Each measurement was repeated three times and the average was calculated. Sessile drop method assumes that the particles form a smooth, flat, nonporous surface, as required by the Young−Laplace equation, which is a false assumption when having a deposited layer.[65] However, this simple technique was used for having an idea of the degree of hydrophobicity.

4.4. Photocatalytic activity measurements

The photocatalytic reactions were carried out in a laboratory UV liquid phase reactor system that consists of a 500 mL Pyrex glass reactor and a 150 W medium-pressure mercury UV lamp. Figure 20 displays a picture of the reactor system. The UV lamp goes inside a Pyrex glass immersion well that is located in the center of the reactor. The inlet port of the reactor is used to feed low pressure air (ultra-zero grade from Airgas). The system consists of a back pressure regulator that reduces the input pressure of air to a desired value at its output while constant air flow passes through the unit. The outlet port of the reactor connects to a bottle gas trap containing 250 ml of an aqueous solution containing $Ba(OH)_2$ (0.0152 g mL^{-1}). The $Ba(OH)_2$ dissolved in water reacts with CO_2 to

precipitate $BaCO_3$. The particles of $BaCO_3$ (with extremely low solubility in water ~ 0.024 mg mL^{-1}) obtained were filtered using a Pyrex crucible, and the corresponding weight was measured. The moles of CO_2 produced throughout the reaction were calculated from the moles of $BaCO_3$ by stoichiometry. The radiant flux was measured using a UVA/B light meter UV513AB purchased from General ®.

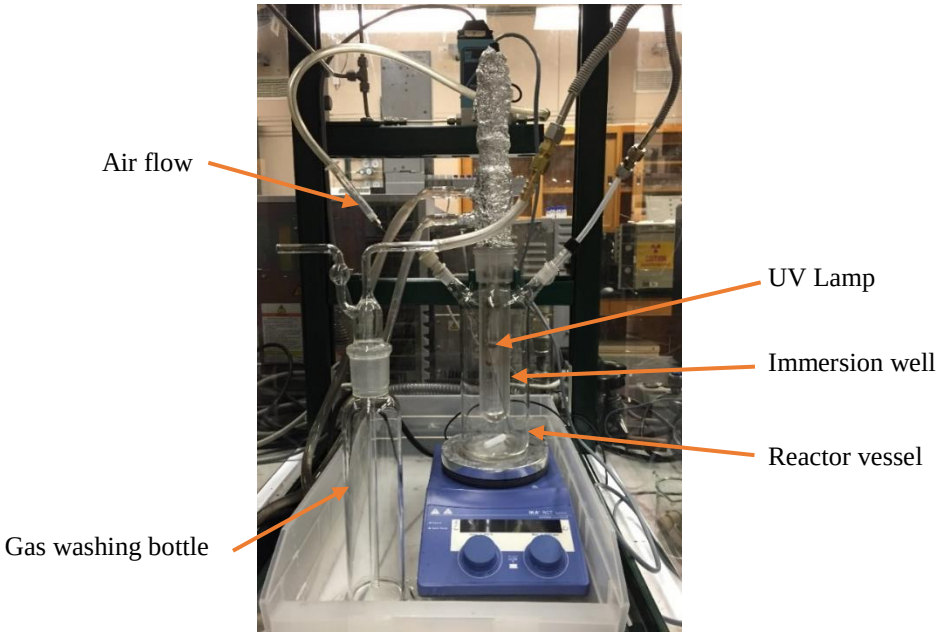

Figure 20. Picture of reaction system used to carry out the photocatalytic activity tests.

Prior to the reaction, the hydrophobic catalysts were dispersed in the organic phase for 20 minutes using bath sonication. Air was continuously bubbled through the TiO_2 suspension (0.1 g TiO_2 L^{-1}) at a rate of 18 mL min^{-1} throughout the reaction. Stirring of 500 rpm was provided. When working in single phase system, 500 mL of pure cyclohexane were used. In biphasic system, 250 mL of cyclohexane and 250 mL of water. Liquid product samples taken from the organic and aqueous phases were filtered and then analyzed. GC–FID with column ZB-5 from Phenomenex ® was used for quantification. Hexadecane and 1,4 dioxane were utilized as chemical standards to

obtain the response factors for the organic and aqueous phase, respectively. Because of the small changes in the reactant concentration, the conversion can only be calculated precisely based on product formation, and since the formation of surface carboxylates and carbonates is not quantified, calculation of the mass balance was not performed.

4.5. Safety precautions

Material safety data sheets (MSDS) of all the chemicals utilized were acquired in order to identify the chemical hazards, possible risk, and danger to which one might be exposed to while working with chemical compounds. Table 2 summarizes the chemical hazards and the safety precautions for cyclohexane. The safety precautions for all the other chemical components used can be found in the appendix. Safety precautions were taken before carrying out the experiments. Personal protective equipment, appropriate gloves, goggles, face mask, and lab coat were always worn while executing the experiments.

Table 2. Chemical hazards of cyclohexane and safety precautions.

Compound	Chemical Hazard	Hazard Code	Safety precautions
Cyclohexane	Highly flammable liquid and vapor. May be fatal if swallowed and enters airways. Causes skin irritation. May cause drowsiness or dizziness. Very toxic to aquatic life.		Keep away from heat/sparks/open flames/hot surfaces. Keep container tightly closed. Avoid breathing dust/ fume/ gas/ mist/ vapors/ spray. Wash skin thoroughly after handling. Use only in a well-ventilated area. Avoid release to the environment.

The UV radiation emitted by the UV lamp is harmful to eyes and skin. Hence, specific protective measure against direct exposure to UV irradiation needs to be taken (e.g. personal protective equipment, signposting of working area). The reactor system does not have to operate in an explosion risk atmosphere, since the UV lamp may cause combustion. It is important to mention that the temperature at the surface of the lamp tube is approximately 700°C during operation and the immersion tube wall temperature near the lamp tube is approximately 450°C without cooling. Therefore, the reactor system is not intended for the purpose of heating liquids and cooling should always be provided to dissipate the radiant heat produced during operation. Over-cooling causes the tungsten from the electrode to combine with mercury, when condensing onto the inside of the lamp ends, giving it a mirror coated effect that results in UV emitter intensity loss. Hence, the temperature of the inflowing cooling water should not be below 10°C. Further details regarding the safety instructions to operate the UV lamp can be found in the Laboratory-UV-Reactor system manual provided by Heraeus Noblelight.

CHAPTER 5: RESULTS AND DISCUSSION

5.1. Catalyst characterization

5.1.1. Transmission and scanning electron microscopy (TEM and SEM)

Figure 21 and Figure 22 display the TEM, SEM micrographs, and Energy Dispersive Spectroscopy (EDS) elemental mapping of $TiO_2/mSiO_2$ + OTS. It can be observed that TiO_2 is located on the inside and outside of the mesoporous silica.

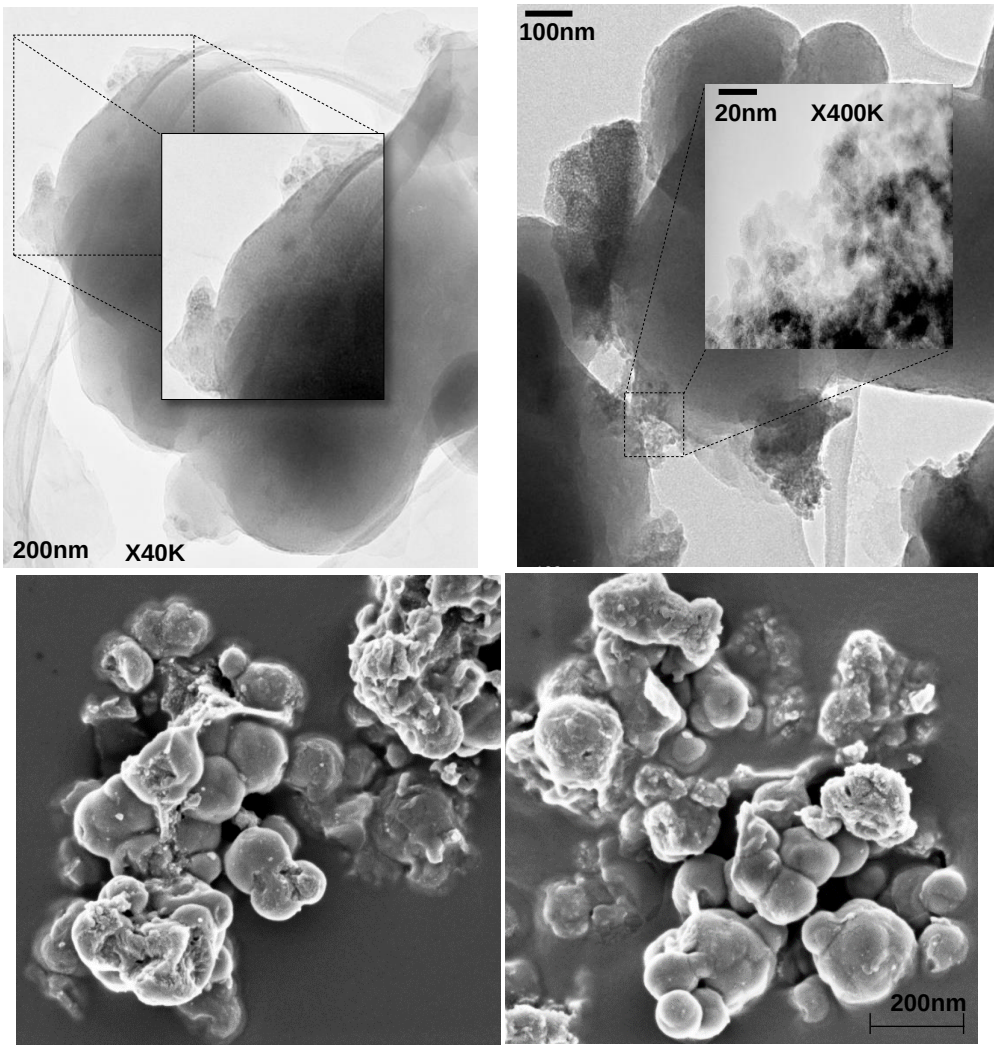

Figure 21. Top: TEM; Bottom: SEM micrographs of $TiO_2/mSiO_2$ + OTS catalyst.

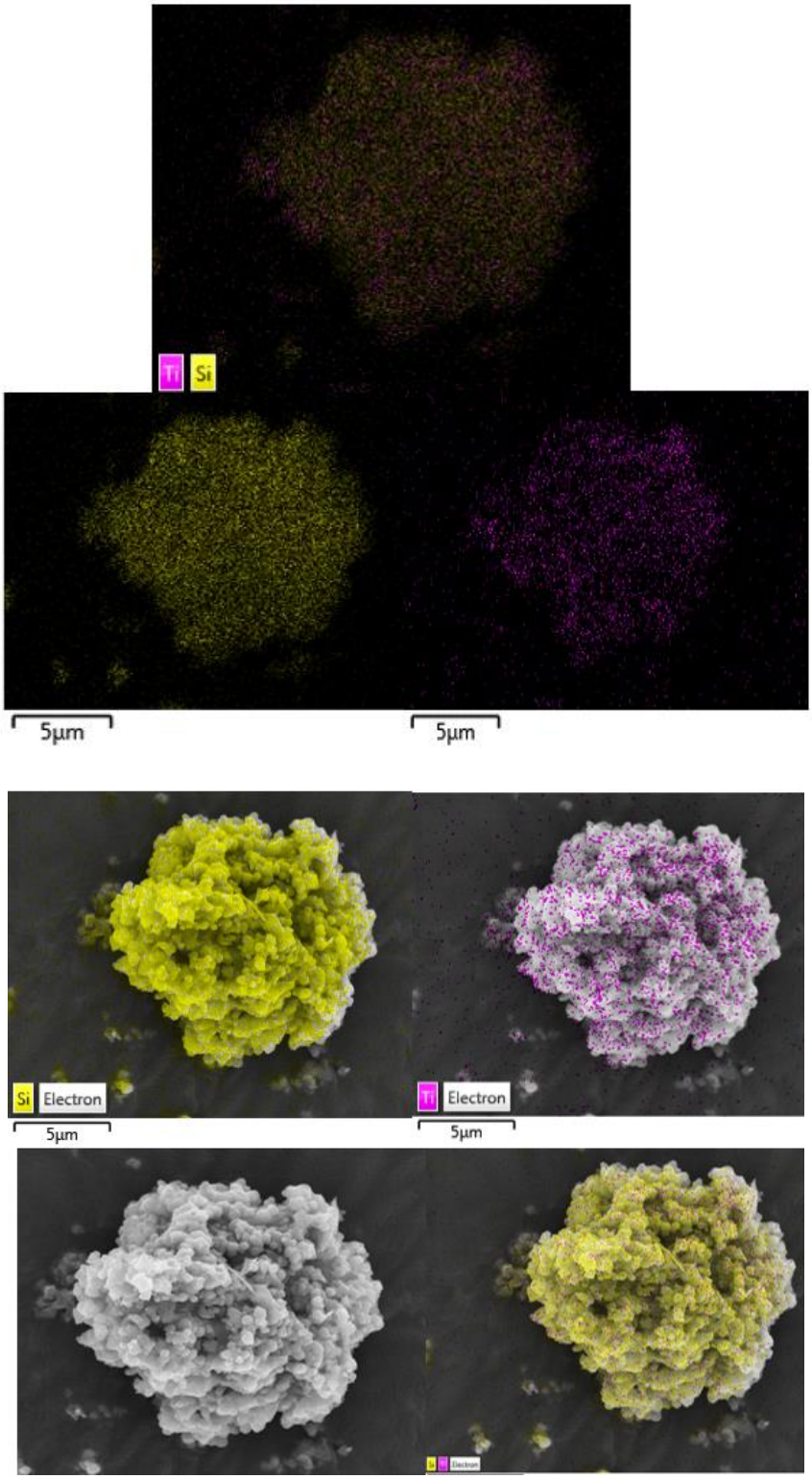

Figure 22. EDS element mapping of $TiO_2/mSiO_2$ + OTS catalyst.

5.1.2. Brunauer, Emmett and Teller (BET) surface area

Specific surface areas were determined by the classical BET procedure. The values obtained were 51 for TiO_2 and 48 $m^2\ g^{-1}$ for TiO_2 T805. In regard to the $TiO_2/mSiO_2$ + OTS catalyst, the surface area calculated after each step of preparation is shown in Table 3. It can be observed that the mesoporous SiO_2 decreases after the impregnation of TiO_2 and that the surface area markedly drop off after the OTS functionalization because the mesoporous SiO_2 may become partially blocked by the silane. The isotherms for $TiO_2/mSiO_2$ + OTS are depicted in Figure 23. The pore size distribution is not so well defined and is very broad with a maximum at less than 10 nm in size. Therefore, the catalyst can be considered as micro and mesoporous which is in agreement with the presence of hysteresis.

Table 3. BET surface area of the catalysts.

Catalyst	BET Surface area ± 5 (m^2/g)
$mSiO_2$	936.86
$TiO_2/mSiO_2$	696.6
$TiO_2/mSiO_2$ + OTS	490.78

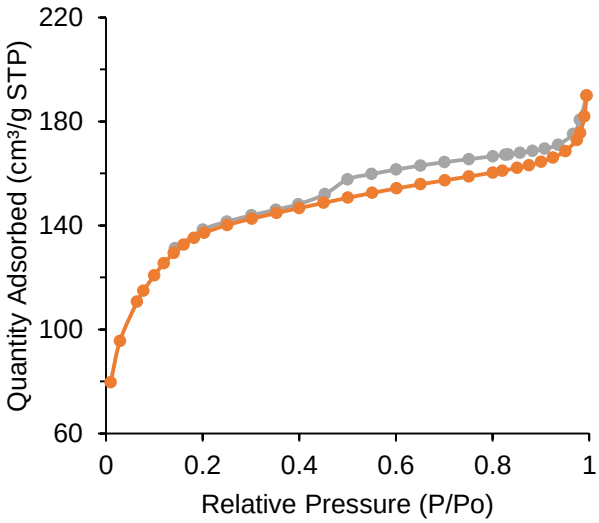

Figure 23. N_2-physisorption isotherms of $TiO_2/mSiO_2$ + OTS.

5.1.3. Fourier transform infrared spectroscopy (FTIR)

Figure 24 depicts the FTIR spectra of the catalysts. The presence of water causes the broad band at 3250-3600 cm^{-1} and the band at 1620 cm^{-1}. The hydrophobic functional groups cause the antisymmetric and symmetric CH_2 stretching band positions occurring at 2919 and 2849 cm^{-1}, respectively (green line).[66] As expected, these CH_2 stretching bands are absent in both the $mSiO_2$ and $TiO_2/mSiO_2$. The characteristic bands of the surface hydroxyl (OH) groups are located at 3744 cm^{-1} for $mSiO_2$, 3731 cm^{-1} for $TiO_2/mSiO_2$, and 3731 cm^{-1} for $TiO_2/mSiO_2$ + OTS.[55] While the $mSiO_2$ (blue line) shows an intense and rather narrow band of OH groups, the OH vibrational frequency is much weaker after functionalization due to interaction with the OTS molecules (green line). Also, the bands at 3661 cm^{-1} and 3640 cm^{-1} assigned to bridging OH groups, Ti–OH, of titania anatase can also be observed. The complete removal of the CTAB micelles can be corroborated by the absence of the CH_2 vibration frequency in the spectra for $TiO_2/mSiO_2$ (red line).

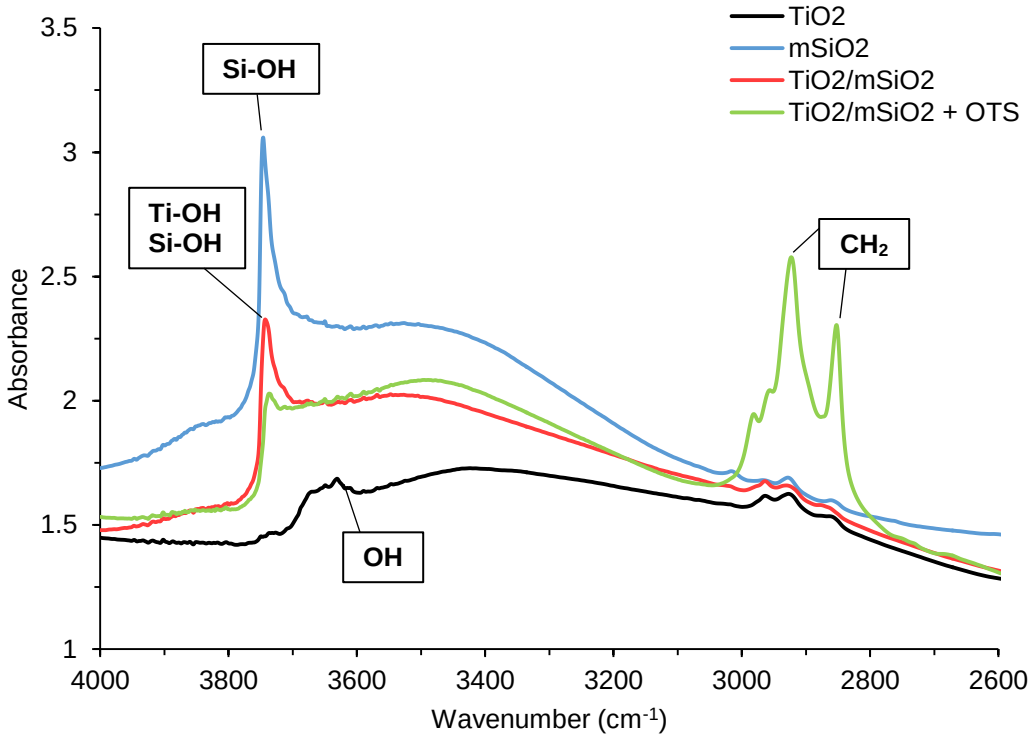

Figure 24. FTIR spectra on $mSiO_2$, TiO_2, $TiO_2/mSiO_2$, and $TiO_2/mSiO_2$ + OTS. Top: Full range spectrum, wavenumber range from 500 to 4000 cm^{-1}. Bottom: Wavenumber range from 2600 to 4000 cm^{-1}.

5.1.4. Thermogravimetric and mass spectrometer (TG-MS) measurement

A TG-MS experiment was carried out in order to study the behavior of $TiO_2/mSiO_2$ + OTS and TiO_2 T 805 catalysts as a function of temperature. The weight percent of carbon anchored on the $TiO_2/mSiO_2$ surface during the silylation process was also obtained. The TG-MS results of the fresh and used catalyst are shown in Figure 25.

The top graph displays the weight loss of the catalysts with temperature and the bottom graph shows the results from the MS measurement. The total weight loss for the fresh catalyst (before reaction) is 17.4 wt% in two stages. First, a loss of 3.6 wt% was observed at the beginning of the heating ramp from 40 °C to about 198 °C, and a final more pronounced loss of about 13.8 wt% was seen in the range 198 – 570 °C. In the

first stage only a small peak is observed for water and in the second stage two pronounced peaks are observed for water and CO_2. From the combined variation of weight and MS results, it can be concluded that the initial mass loss (3.6 wt%) is mostly due to water moisture desorbed from the surface. However, in the range 198 – 570 °C, there is simultaneous desorption of water and CO_2 consistent with the combustion of the hydrocarbon functional groups. The carbon content of the fresh catalyst, $TiO_2/mSiO_2$ + OTS, was found to be around 11.8 wt%.

The total weight loss for the used catalyst (after 3 hours reaction) is approximately 11.1 wt% in only one stage, in the range 172 – 570 °C. Simultaneous desorption of water and CO_2 is observed consistent with the combustion of the hydrocarbon functional groups. The desorption of water moisture is not observed since the catalyst was pre-treated in argon at 100 °C in order to remove any adsorbed reactant, reaction product, and water. The carbon content of the catalyst, $TiO_2/mSiO_2$ + OTS collected after three hours of reaction is 9.5 wt%. This implies that only around 2.3 wt% of carbon is lost throughout the reaction. Since the catalyst is approximately 29 wt% TiO_2 and 54 wt% SiO_2, we believe that, the 2.3 wt% of the carbon lost is a result of the oxidation of hydrophobic functional groups anchored to the surface of the TiO_2 particles. However, the hydrophobic functional groups anchored to the mesoporous silica (which is about 55 wt% of the catalyst) do not get oxidized, and that is the reason why the catalyst keeps its hydrophobic nature.

Figure 26Figure 26 shows the TG-MS analysis performed to the commercially available hydrophobic titania, TiO_2 T805, before and after reaction. The carbon content

obtained for the catalyst before reaction was 3.1 wt% which is very similar to the carbon content specified by Evonik (3.2 wt%). The catalyst collected after 3 hours of reaction had a carbon content equal to 1.1 wt%. This implies that around 2.0 wt% of carbon is lost throughout the reaction.

Figure 25. Top: Thermogravimetric analysis. Bottom: Mass Spectrometer of the $TiO_2/mSiO_2$ + OTS catalyst before and after reaction time 3 hours.

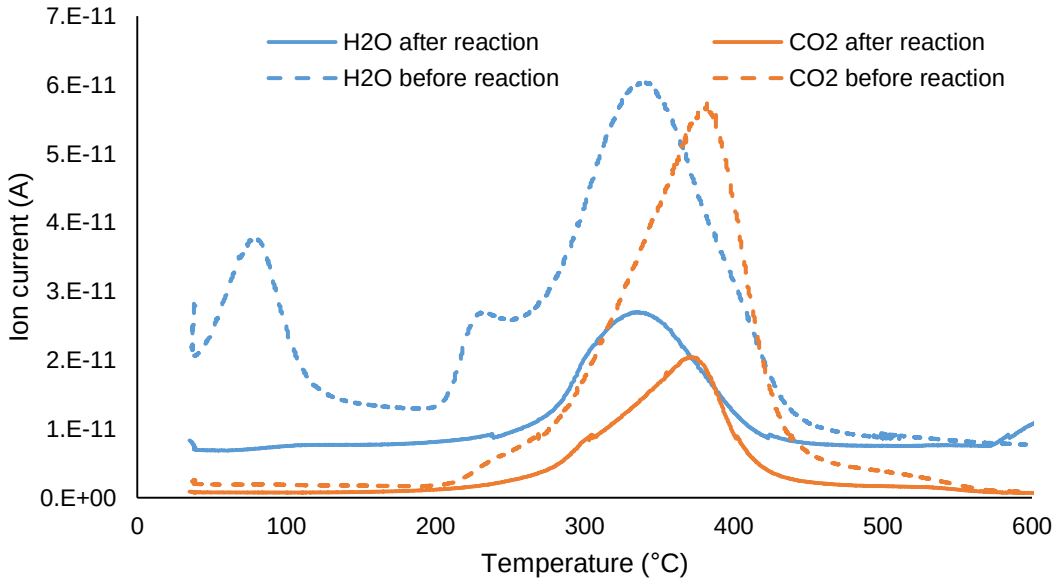

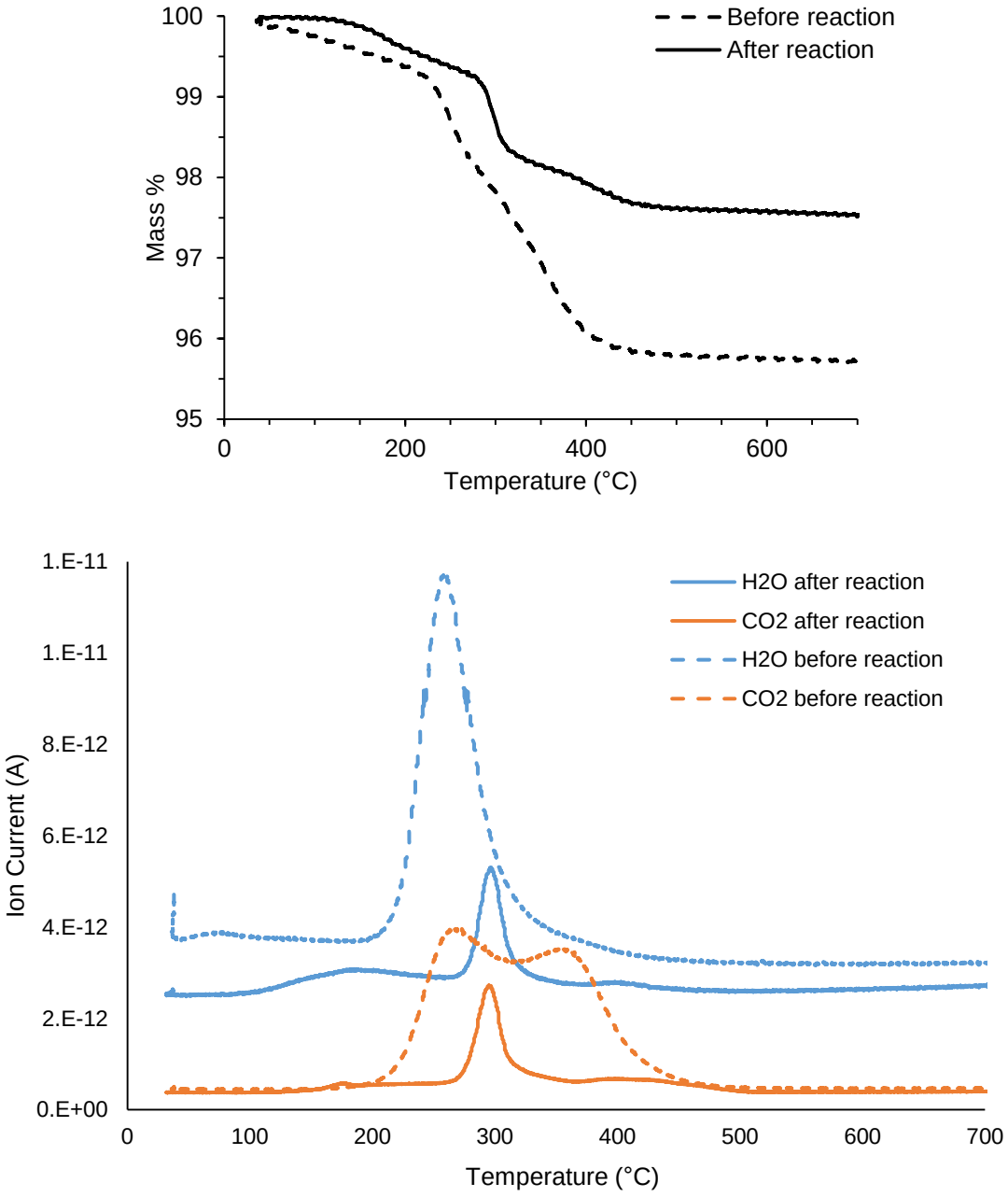

Figure 26. Top: Thermogravimetric analysis. Bottom: Mass Spectrometer of the TiO_2 T805 catalyst before and after reaction time 3 hours.

5.1.5. X-ray Diffraction analysis (XRD)

Cendrowski *et al*. studied the crystallographic composition of $mSiO_2$, $mSiO_2$/TiO2 core-shell, and TiO_2-Degussa P25 via XRD. The diffraction pattern in Figure 27 shows five peaks corresponding to the presence of TiO_2 in anatase phase (red line) and a broad peak at ~22.5° corresponding to the amorphous silica (black line). The XRD of the TiO_2-Degussa P25 is also illustrated with the respective peaks for both anatase and rutile (green line).

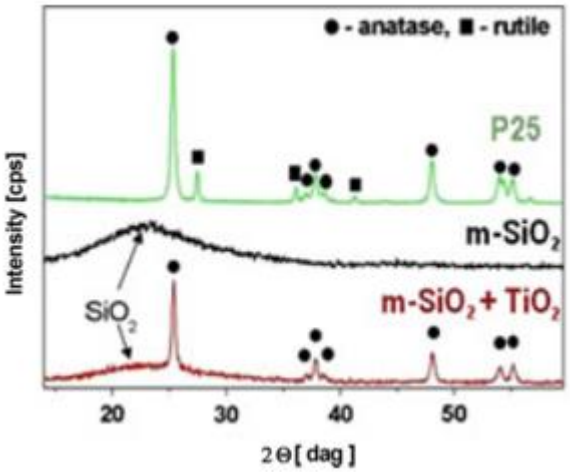

Figure 27. XRD patterns of P25 (green line), m-SiO_2 (black line), and m-SiO_2/TiO_2 (red line).[67]

In this work' the crystallographic composition of TiO_2/$mSiO_2$ + OTS was also studied via XRD. The results obtained are in accordance with the literature. The diffraction pattern in Figure 28 shows strong diffraction peaks at 25° and 48° indicating the presence of TiO_2 in anatase phase. A broad peak at 21° is also observed corresponding to the amorphous silica.

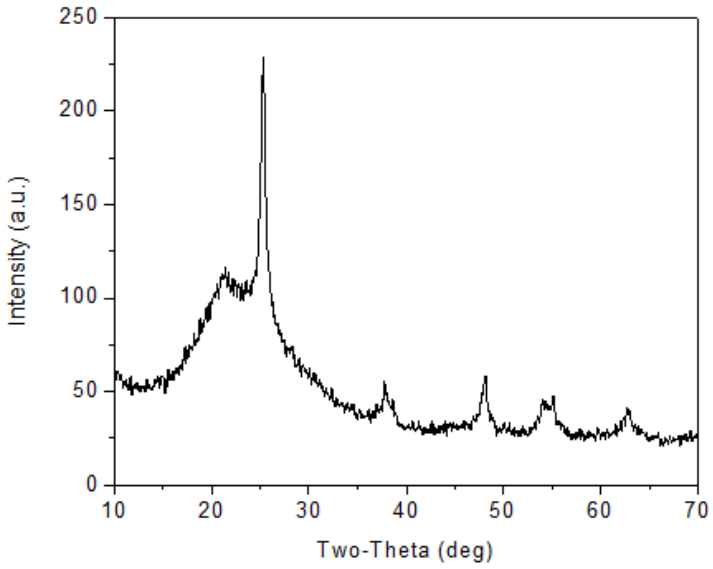

Figure 28. XRD pattern of $TiO_2/mSiO_2$ + OTS.

5.1.6. Diffuse Reflectance UV-Vis Spectroscopy (DR UV-Vis)

The UV-Vis diffuse reflectance spectrum and the Tauc plot of the catalysts studied are depicted in

Figure 29, top and bottom, respectively. The Tauc plot has a distinct linear regime which denotes the onset of absorption. The optical band gap of the catalysts was obtained by extrapolating this linear region to the abscissa. It can be observed that the optical bandgap energy is approximately 3.05 eV for TiO_2 and 3.14 eV for $TiO_2/mSiO_2$ + OTS. Additionally, the UV spectrum shows that light with more energy ($\lambda < 395$ nm) is needed to activate $TiO_2/mSiO_2$ + OTS (i.e., 3.14 eV is the threshold for creating an electron–hole pair that is not bound together) and that none of the catalysts absorb photons in the visible light region ($\lambda > 400$ nm).

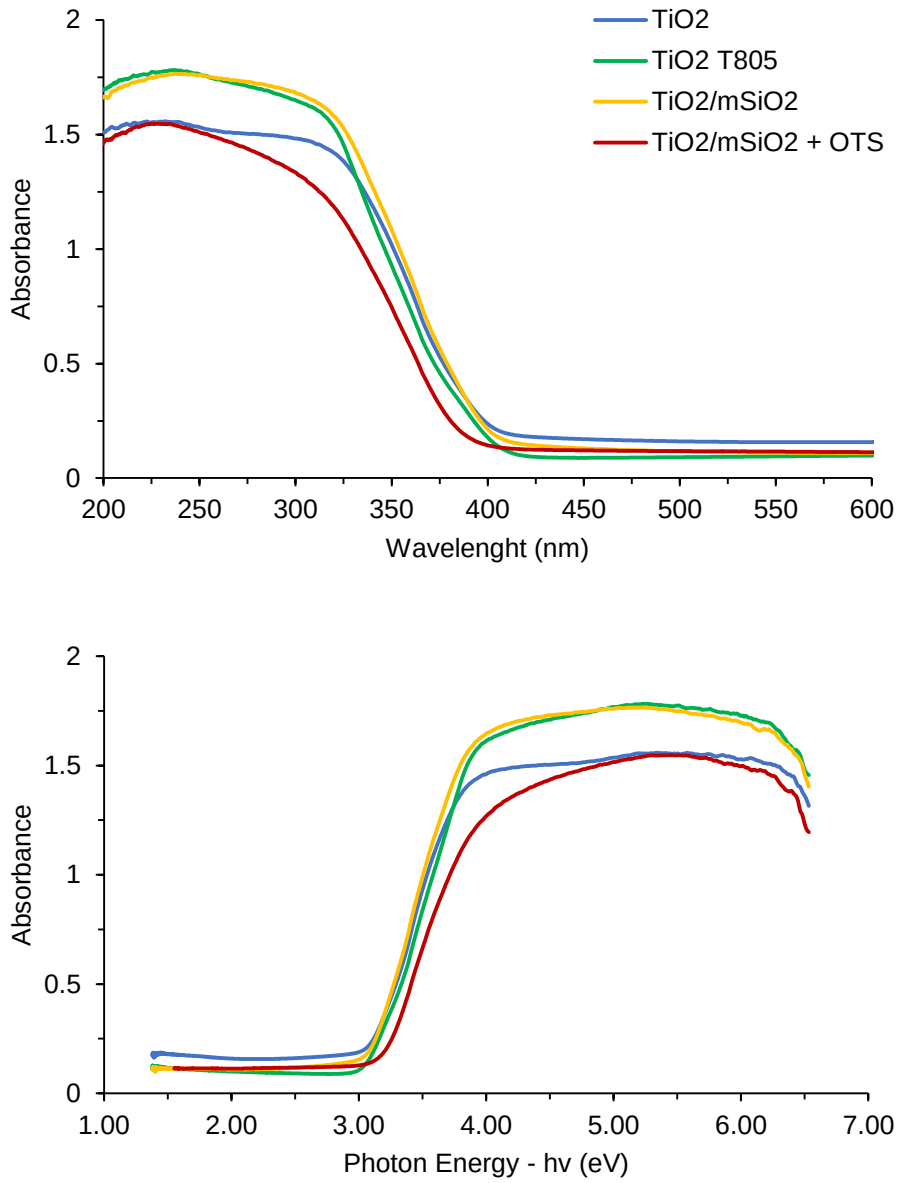

Figure 29. Top: UV-Vis diffuse reflectance spectrum. Bottom: Tauc Plot for TiO_2, TiO_2 T805, and TiO_2/$mSiO_2$ + OTS.

5.1.7. Contact angle measurement

The sessile drop method which is a well-known technique, was used for the contact angle measurement. This method requires a thin film of particles on a substrate or a compressed pellet of particles upon which a static and dynamic liquid drop can be placed.[65,68] The high static contact angles obtained, 164° for TiO_2 T805 and 156° for $TiO_2/mSiO_2$ + OTS, imply that their surface is hydrophobic and has poor wetting property.[69] Figure 30 contains images illustrating the glass slide coated with TiO_2 T805. The picture on the left shows the droplet about to be deposited on the surface and the picture on the right shows the droplet deposited on the surface.

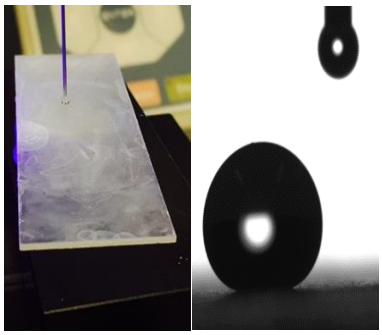

Figure 30. Images illustrating the glass slide coated with TiO_2 T805. Left: Immediately prior to the droplet being deposited on the surface; Right: Immediately after the droplet has been deposited on the surface.

5.2. Photolysis vs. Photocatalysis

The glassware material used for the immersion-well is particularly important as it functions as a filter of high radiation that would lead to photolysis (photochemical reactions).[70] Figure 31 shows the UV-Vis spectrum of cyclohexane and also the transmittance of different types of glass such as Quartz, Vycor, and Pyrex. The reactor material of this work was chosen to be Pyrex which transmits UV light at λ higher than 280 nm. This implies that photochemical reactions of molecules that absorb UV light at wavelength lower than 280 nm are prevented. For instance, the cut-off wavelength of cyclohexane is around 250 nm. Therefore any photochemical reaction of cyclohexane should be negligible.[51]

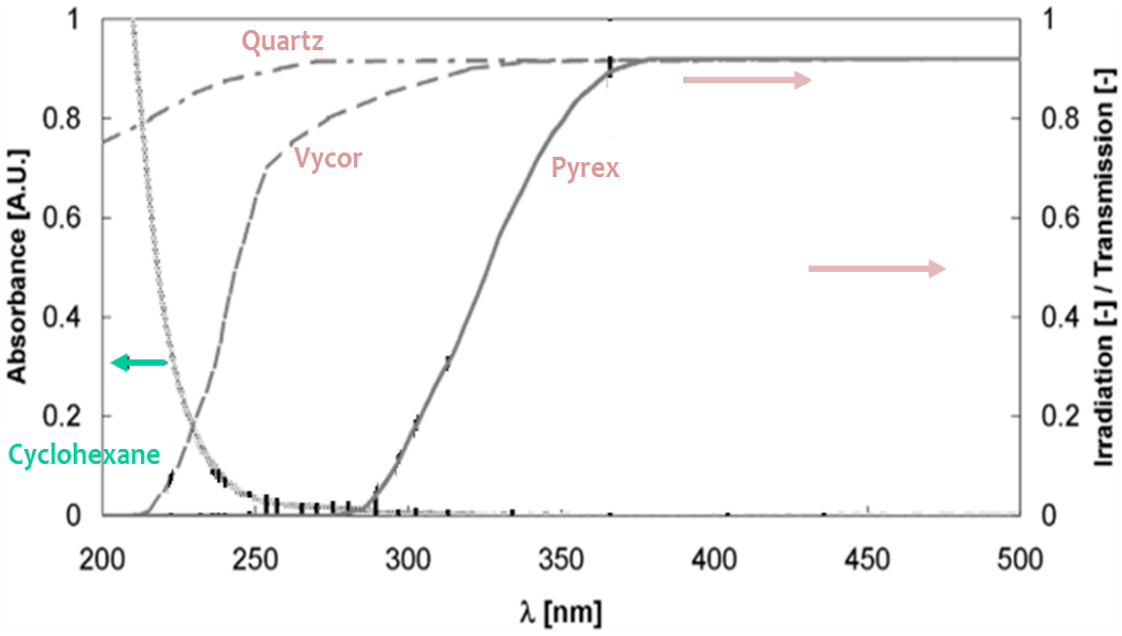

Figure 31. Comparison of the absorption spectrum of liquid cyclohexane and the UV transmittance of different glass types. From left to right, Quartz, Vycor, and Pyrex.[51]

In order to know that the reactions are photocatalytic, i.e., a reaction where only the photocatalyst is activated by light and oxidizes the molecules, or photolytic, i.e. reaction where photons break down a chemical compound in the absence of catalyst, the UV spectra of the intermediates was also measured. The UV absorption spectra measured for liquid cyclohexanol, cyclohexanone, and cyclohexane is illustrated in Figure 32. It can be observed that cyclohexanone absorbs UV light from 190 to 320 nm, and that both cyclohexane and cyclohexanol absorb UV light at wavelengths below 250 nm only. The UV transmittance of the reactor material is negligible below 280 nm. Consequently, cyclohexanone is the only reaction molecule than undergoes photolysis. Therefore, no comparisons of cyclohexanone/cyclohexanol ratio obtained with the different catalyst are performed in section 5.3.

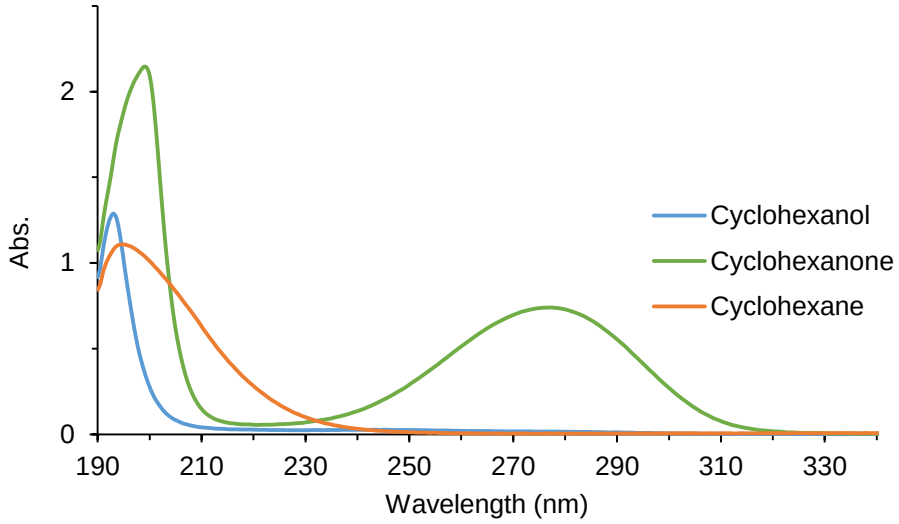

Figure 32. UV absorption spectra of liquid cyclohexanol, cyclohexanone, and cyclohexane.

5.3. Photocatalytic performance of catalysts

The photocatalytic activity and selectivity of the catalyst $TiO_2/mSiO_2$ + OTS (171 mg) prepared in this work were evaluated through the selective oxidation of cyclohexane in a biphasic and single phase system. For comparison purposes, the reaction was also carried out using the commercially available, hydrophobic and hydrophilic catalysts, TiO_2 T805 and TiO_2, respectively. The mass of catalyst was chosen so the TiO_2 loading was the same 50 mg for all the experiments. Figure 33 shows the results of the reaction carried out with no catalyst. The amount of oxidation products after 3 hours of reaction is very small which confirms that there is negligible photolytic oxidation of cyclohexane.

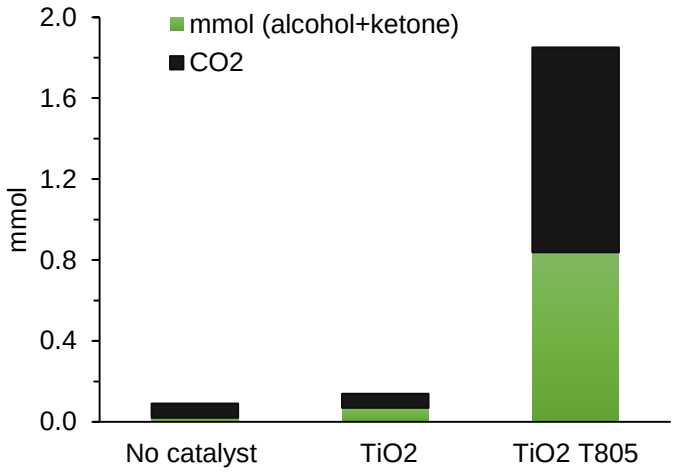

Figure 33. Resulting cyclohexanol, cyclohexanone, and CO_2 yield with no catalyst, and with TiO_2 and TiO_2 T805 as catalysts. Reaction time: 3 hours.

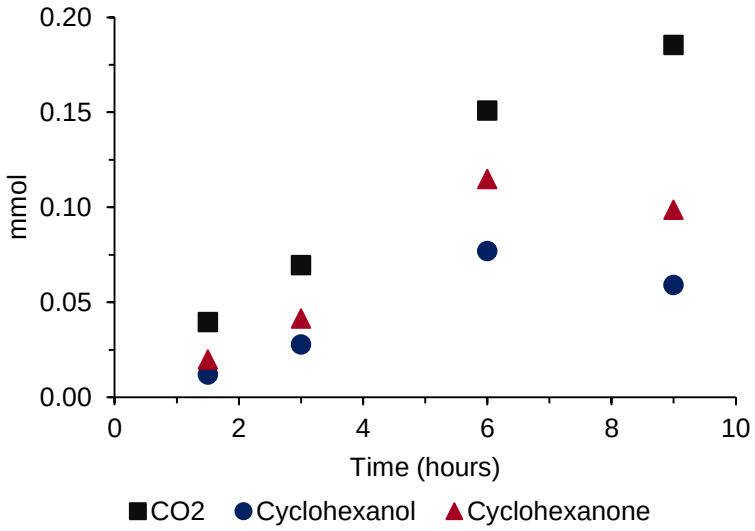

Figure 34. Cyclohexanol, cyclohexanone, and CO_2 yield as a function of time using TiO_2.

Figure 33 and Figure 34 clearly show that TiO_2 is not a promising catalyst in terms of conversion. Even after 6 hours of reaction the activity is still low, and there is not significant improvement compared to the blank reaction. According to ATR-FTIR studies performed by Almeida and Carneiro *et al*., this low activity is a result of fast deactivation of the TiO_2 catalyst caused by the strongly adsorbed intermediates and products that are further oxidized to carboxylates and carbonates.[55, 52, 54]

Carneiro *et al*. also showed that in order to improve the selectivity of the desired products, cyclohexanol and cyclohexanone, a hydrophobic catalyst is needed to enhance desorption of products, and hence avoid their further oxidation to carboxylates and carbonates.[54] In order to confirm this hypothesis, the reaction was carried out using commercially available hydrophobic catalyst, TiO_2 T 805. As observed in Figure 33, the photocatalytic activity of TiO_2 T 805 is significantly higher than the activity of TiO_2. However, TiO_2 T805 was not photo-stable.

Figure 35 illustrates the reactor glass vessel after reaction at different periods of time. Before reaction, the TiO_2 T805 catalyst was hydrophobic and preferentially located in the organic phase. After 0.5 hours of reaction, the catalyst started to become hydrophilic due to photocatalytic degradation of the hydrophobic groups on the TiO_2 surface. Something interesting is that TiO_2 T805 catalyst was found to be very active even after the loss of its hydrophobic nature. This behavior could be attributed to the formation of a coating on the top walls of the reactor, which became more stable and thicker as the reaction time increased. The initial location of TiO_2 T805 and the stirring provided could prompt the coating formation.

It is believed that the formation of the coating is the reason why the conversion keeps increasing after 3 hours of reaction. In order to confirm this hypothesis, the reaction was carried out using the TiO_2 T805 catalyst but this time, the reactor was washed after 1.5 and after 4 hours of reaction, thereby minimizing the coating effect in the reaction conversion profile. Figure 36 shows that when the coating is present, the rate of formation of cyclohexane and cyclohexanol increased up to 6 hours of reaction but then reaches a plateau. On the other hand, when the coating was washed out, the rate of formation of cyclohexane and cyclohexanol reached a maximum after 3 hours of reaction and then decreased.

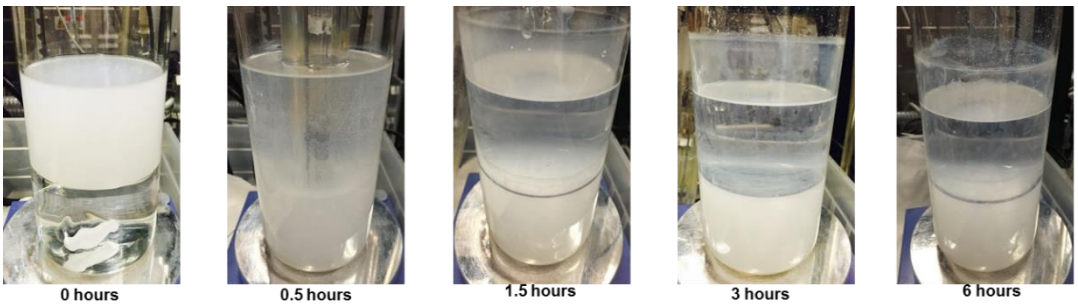

Figure 35. Images of reactor glass vessel taken as a function of time when using the catalyst TiO_2 T805.

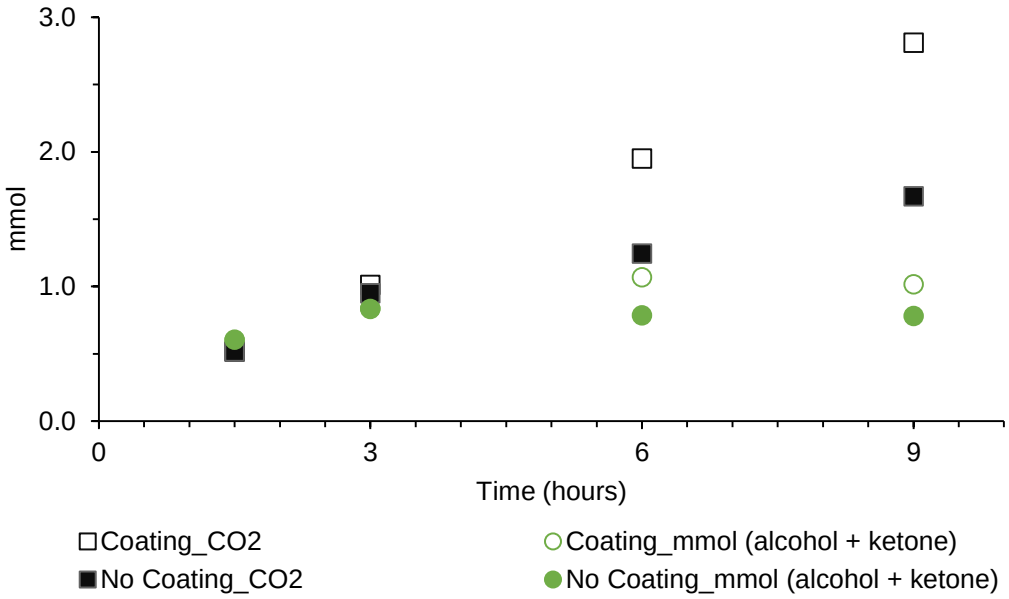

Figure 36. millimoles (cyclohexanol + cyclohexanone) and millimoles of CO_2, as a function of time using the catalyst TiO_2 T805, with coating and no coating in the top phase of the reactor vessel.

Since the hydrophobic catalyst, TiO_2 T805, was confirmed to be more active, the next step was to synthesize a catalyst that is active and selective but also photo-stable throughout the reaction. If the catalyst retains its hydrophobic nature, the rate of desorption of products could be favorable even after long reaction times. Studies conducted by Ikeda *et al.* revealed that silica can protect the hydrophobic functional

groups on the TiO_2 surface avoiding their decomposition.[71] Siliceous materials are good because they are known to be chemically inert and transparent to UV radiation.

In the present work, mesoporous silica is utilized to protect the hydrophobic functional groups as well as to significantly increase the surface area of the catalyst. As stated before, two catalysts were synthesized, (TiO_2@$mSiO_2$ + OTS and TiO_2/$mSiO_2$ + OTS), and their catalytic performance was studied.

As observed in Figure 37, TiO_2@$mSiO_2$ + OTS was found to be photostable, keeping their hydrophobicity nature after 3 hours of reaction. This indicates the good photo-stability of the hydrophobic functional groups anchored to the catalyst. The hydrophobic functional groups were protected by the silica and did not get oxidized as the reaction proceeded.

Figure 37. Images illustrating the reactor glass vessel containing the organic phase, aqueous phase, and TiO_2@$mSiO_2$ + OTS. The left and right images were taken before and after 3 hours of reaction, respectively.

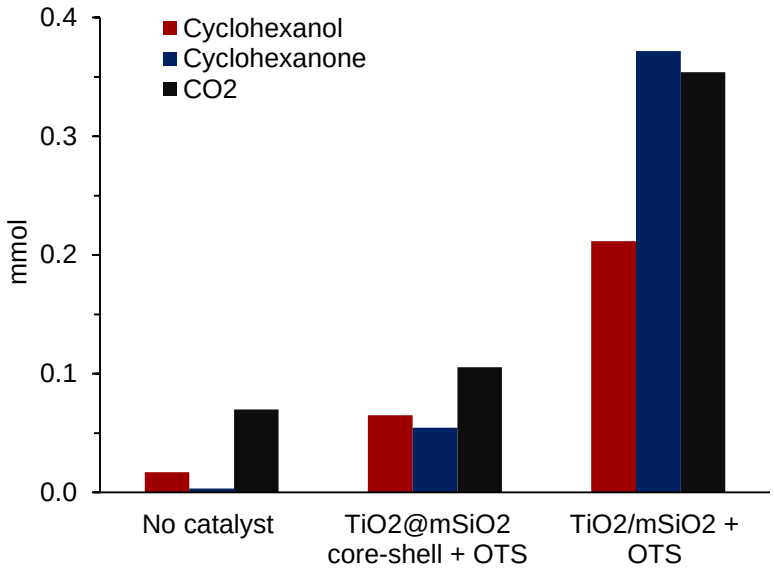

Figure 38. Resulting yield to cyclohexanol and cyclohexanone (mmol), in absence of catalyst; using TiO_2@$mSiO_2$ core-shell + OTS and TiO_2/$mSiO_2$ as catalysts. Reaction time: 3 hours. Biphasic system.

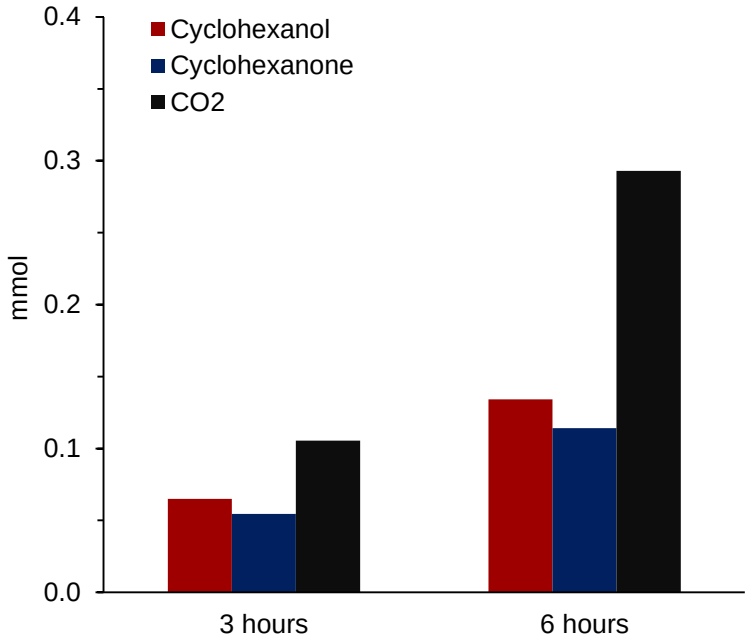

Figure 39. Resulting yield to cyclohexanol and cyclohexanone (mmol) when using TiO_2@$mSiO_2$ core-shell + OTS as catalyst. Reaction time: 3 and 6 hours. Biphasic system.

Figure 38 displays the millimoles of cyclohexanol, cyclohexanone, and CO_2 obtained when using the hydrophobic catalysts proposed in this work (TiO_2@$mSiO_2$ core-shell + OTS and TiO_2/$mSiO_2$ + OTS). Figure 39 shows the results increasing the reaction time from 3 to 6 hours of reaction, although the formation of desired products (cyclohexanol and cyclohexanone) slightly increased, the amount of CO_2 increased considerably. From these results it can be concluded that TiO_2/$mSiO_2$ + OTS is significantly more active and selective than TiO_2@$mSiO_2$ + OTS. One explanation could be that the TiO_2 active sites were not completely accessible because of possible nucleation of SiO_2 particles around the TiO_2 cores, formed during the synthesis procedure. Moreover, according to the results from BET analysis presented in the appendix Table 9, the surface area of TiO_2@$mSiO_2$ core-shell + OTS (67.46 m^2 g^{-1}) is significantly smaller than the surface area of TiO_2/$mSiO_2$ + OTS (490.78 m^2 g^{-1}). Thus, the accessibility and adsorption of cyclohexane onto the TiO_2@$mSiO_2$ core-shell + OTS surface was not as feasible as in the case TiO_2/$mSiO_2$ + OTS. As a result, decreasing the efficiency of interfacial electron transfer reactions and thereby decreasing the rate of reaction.

TiO_2/$mSiO_2$ + OTS exhibited a better photocatalytic performance, therefore its photocatalytic behavior was compared to the one exhibited by the commercially available catalysts.

Figure 40 shows the reactor vessel containing water and the catalyst, TiO_2/$mSiO_2$ + OTS, dispersed in cyclohexane. The pictures were taken right after the reactions at different periods of time were completed. It is clearly observed that the catalyst TiO_2/$mSiO_2$ + OTS is also photostable and retains its hydrophobic nature even

after 9 hours of reaction. As concluded in the TGA results, the catalyst is stable after reaction because the hydrophobic groups anchored to the mesoporous silica (which is about 55 wt% of the catalyst) do not undergo photocatalytic oxidation, only the hydrophobic groups anchored to the TiO_2 are oxidized.

Figure 41 illustrates that $TiO_2/mSiO_2$ has a slight higher activity than TiO_2 which could be attributed to the higher surface area. TiO_2 shows the poorer catalytic activity possibly because its fast deactivation. On the other hand, $TiO_2/mSiO_2$ + OTS is significantly more active, which could be due to its high surface area. Also, as previously confirmed by Almeida *et. al*., the hydrophobicity enhances the desorption rate of oxygenated products, thereby decreasing the rate of catalyst deactivation.[2]

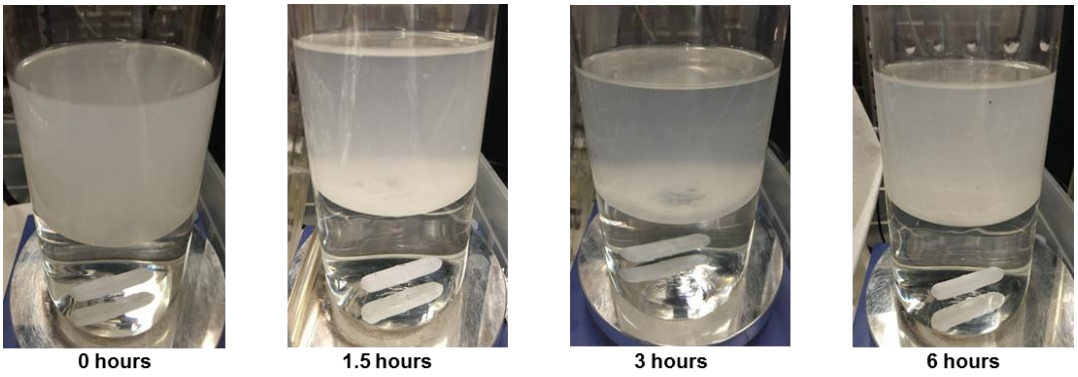

Figure 40. Images of reactor vessel taken after reaction as a function of time when using the catalyst $TiO_2/mSiO_2$ + OTS.

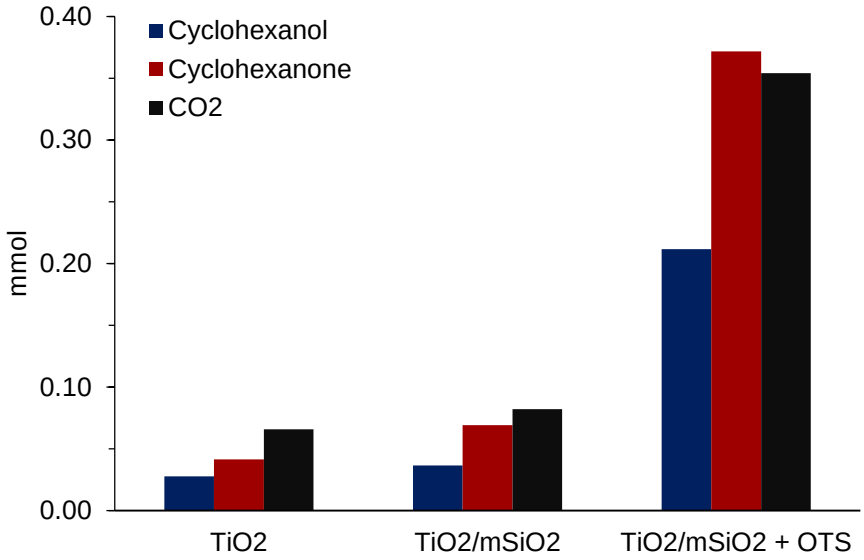

Figure 41. Product formation using TiO_2, $TiO_2/mSiO_2$, and $TiO_2/mSiO_2$ + OTS as catalysts after 3 hours of reaction.

The photocatalytic performance of the catalysts: TiO_2, $TiO_2/mSiO_2$ + OTS, and TiO_2 T805 is discussed and compared below. For the TiO_2 T805 catalyst, the results obtained washing the coating formed on the walls of the reactor are the only ones taken into account. This is done in order to study how the location of the catalyst, either aqueous or organic phase, affects the activity of the photocatalytic oxidation of cyclohexane.

Figure 42 and Figure 43 illustrate the reaction profiles for the formation of cyclohexanol and cyclohexanone using TiO_2, $TiO_2/mSiO_2$ + OTS, and TiO_2 805 as catalysts. Initially, TiO_2 T805 exhibits a slightly higher initial rate of product formation than $TiO_2/mSiO_2$ + OTS. However, when using TiO_2 T805 as catalyst, the rate of cyclohexanone formation reaches a plateau and the rate of cyclohexanol formation starts to gradually decrease after 3 hours of reaction. This behavior can be attributed to

the instability of the silane groups on the surface under UV photocatalytic conditions, causing the hydrophobic catalyst to become completely hydrophilic after 3 hours of reaction, and therefore decreasing the desorption constant of cyclohexanone and promoting total oxidation to CO_2. Figure 44 shows that the rate of CO_2 formation as a function of time is highest for TiO_2 T805.

The opposite behavior is found using $TiO_2/mSiO_2$ + OTS, this catalyst retains its activity and the rate of both cyclohexanol and cyclohexanone formation continuously increase up to 9 hours of reaction. The maximum productivity towards cyclohexanone is obtained using $TiO_2/mSiO_2$ + OTS after 9 hours of reaction. As mentioned previously, the reaction rate can also be affected by the specific surface area of the catalyst. $TiO_2/mSiO_2$ + OTS has the largest specific surface area which leads to a higher concentration of adsorbed substrates per unit volume. This enhances the interfacial electron transfer rate, and thereby increases the reaction rate.

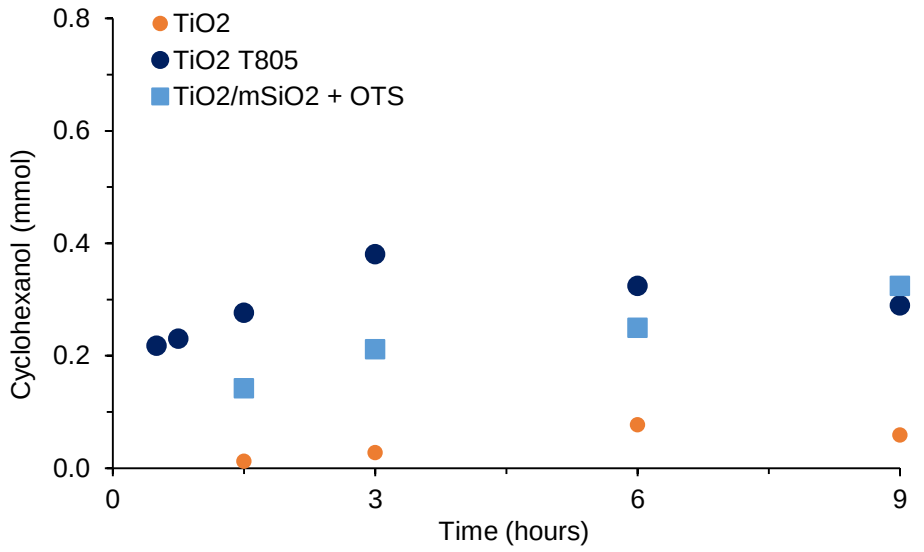

Figure 42. Cyclohexanol formation as a function of time using TiO_2 T805, $TiO_2/mSiO_2$ + OTS, and TiO_2 as catalyst.

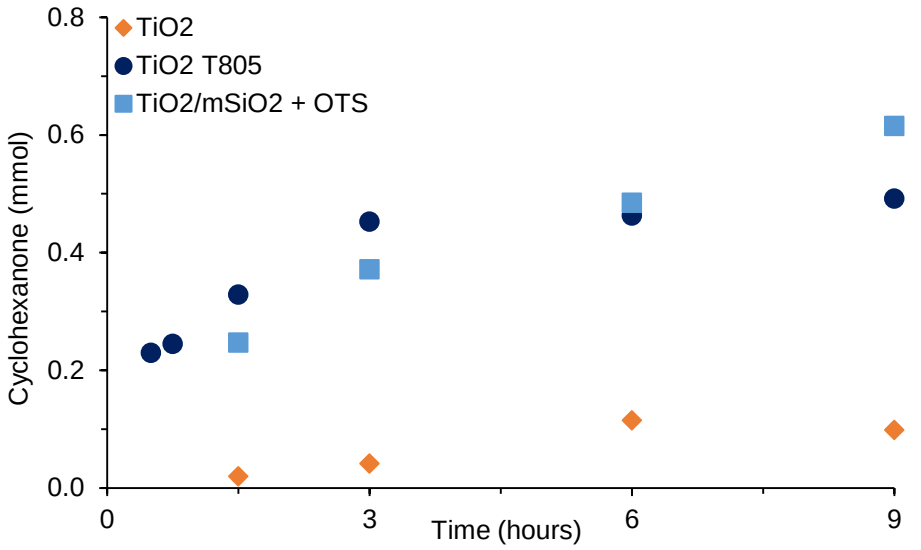

Figure 43. Cyclohexanone formation as a function of time using TiO_2 T805, $TiO_2/mSiO_2$ + OTS, and TiO_2 as catalyst.

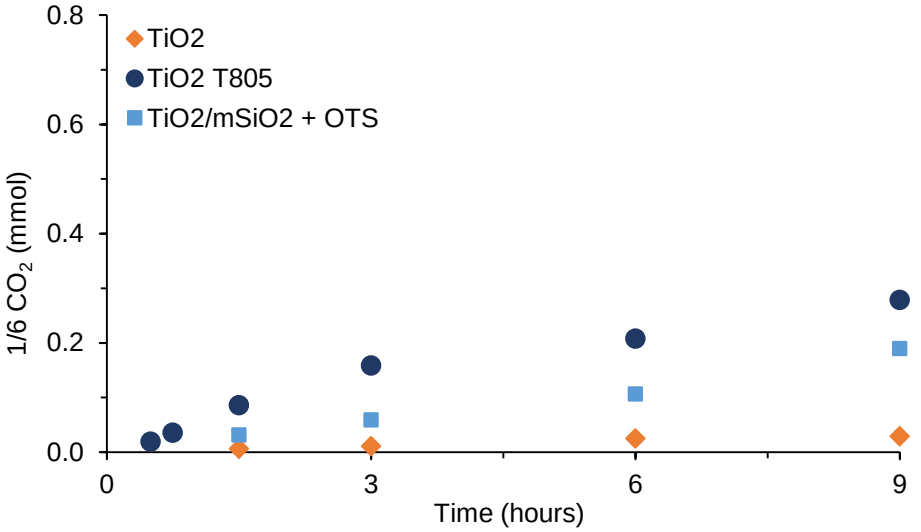

Figure 44. CO_2 formation as a function of time using TiO_2 T805, $TiO_2/mSiO_2$ + OTS, and TiO_2 as catalyst.

Figure 45 and Figure 46 illustrate the catalytic behavior of TiO_2, TiO2 $T80_5$, and $TiO_2/mSiO_2$ + OTS, obtained after 3 hours of reaction in biphasic and single (pure cyclohexane) phase systems, respectively. It is clearly shown that all the catalysts are more active in single phase system than in a biphasic system. One possible explanation could be that water acts inhibitor role by blocking important surface sites and reducing

the amount of reactant adsorbed on the surface. $TiO_2/mSiO_2$ + OTS shows the higher selectivity towards the desired products, cyclohexanol and cyclohexanone, over CO_2 in both, single and biphasic system.

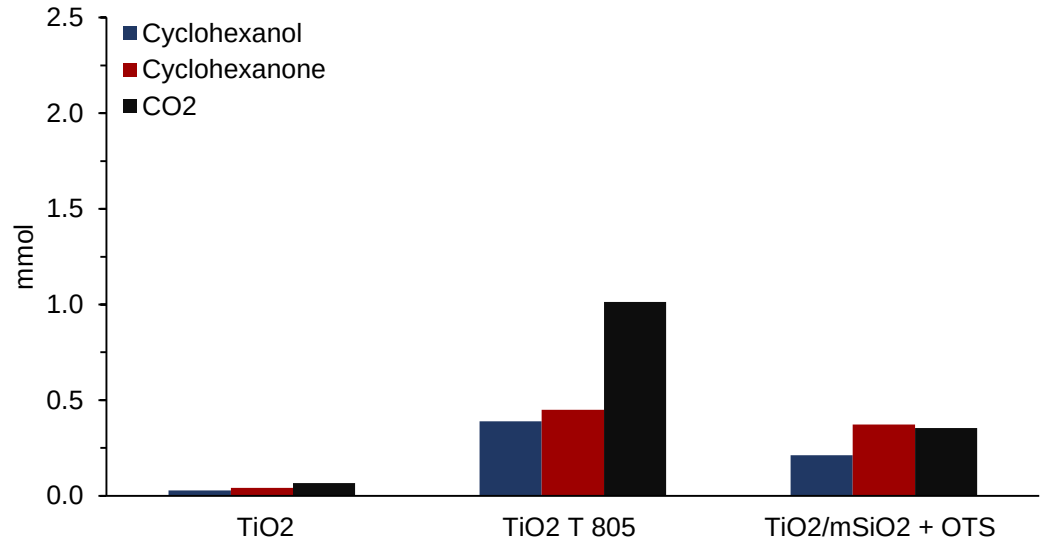

Figure 45. Cyclohexanol, cyclohexanone, and CO_2 formation using TiO_2, $TiO_2/mSiO_2$ + OTS, and TiO_2 T805 after 3 hours of reaction in biphasic system.

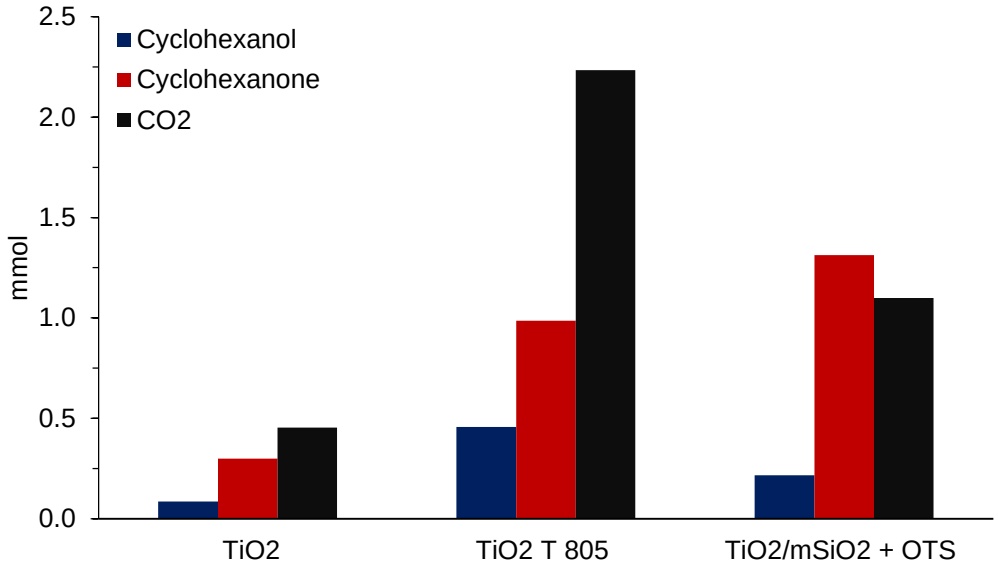

Figure 46. Cyclohexanol, cyclohexanone, and CO_2 formation using TiO_2, $TiO_2/mSiO_2$ + OTS, and TiO_2 T805 after 3 hours of reaction in pure cyclohexane.

A good photocatalyst must combine excellent photon absorption as well as excellent reactant adsorption. It is clear that superior reactant adsorption occurs when the catalyst is surrounded by cyclohexane molecules, that is when the reaction is carried out in single phase system or when the catalyst is preferentially located in the organic phase.

The poor photocatalytic performance of TiO_2 in biphasic system can be explained by the low rate of reactant adsorption. Due to the hydrophilicity of the catalyst, TiO_2 is located in the water phase and since the solubility of cyclohexane in water is extremely low (around ~ 0.00005 g/ml), there is limited accessibility of cyclohexane to the surface of the catalyst. Figure 47 shows that the photocatalytic activity of TiO_2 increases when the catalyst is dispersed in the organic phase. However, the photocatalytic activity is still lower than the activity of the hydrophobic catalysts. This could be because hydrophilic TiO_2 undergoes fast catalyst deactivation due to the high affinity to polar molecules and thereby very small rate of desorption of products. Besides, the excellent photocatalytic performance of $TiO_2/mSiO_2$ + OTS can be attributed to the high stability under UV conditions but also to the largest surface area.

Figure 48 illustrates the radiant flux profile along the reactor. Due to the design of the UV lamp, the radiant flux varied depending on the position. The radiant flux or light intensity was measured using a UVA/B light meter UV513AB. The highest radiant flux, > 9.9 mW cm^{-2} was obtained at the center of the reactor, around 6.4 mW cm^{-2} at the top, and 1 mW cm^{-2} at the bottom of the reactor. In the experiments conducted in biphasic system, the hydrophilic TiO_2 was located in the aqueous and therefore it was exposed to low radiant flux.

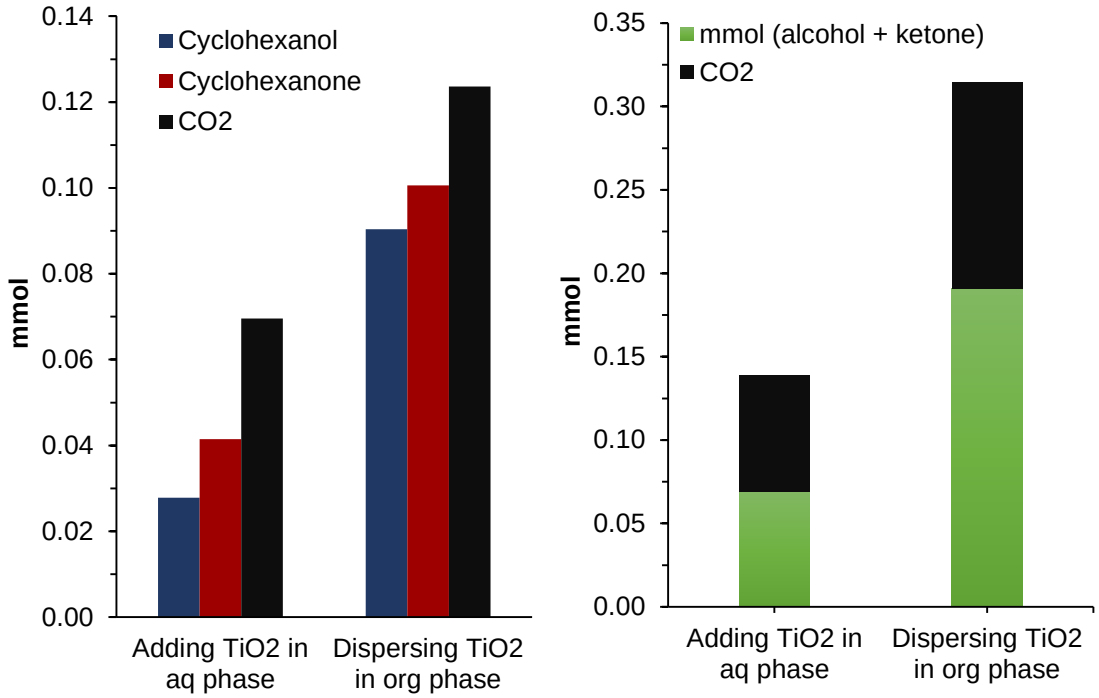

Figure 47. Reaction results varying the location of the catalyst. Biphasic system; reaction time: 3 hours; catalyst: 50 mg of TiO_2.

In order to evaluate the effect of radiant flux in the photocatalytic performance of TiO_2, the reaction was carried out varying the volume percent of water. The first experiment was conducted with 50 v/v% of water and the second one with 80 v/v% so the TiO_2 can be exposed to the high light intensity. The results obtained are displayed in Figure 49, when the reaction is carried out with 80 v/v% of water, the activity of TiO_2 increases by 23% and the photocatalytic activity of TiO_2 is still significantly low compared to the activity of hydrophobic catalysts.

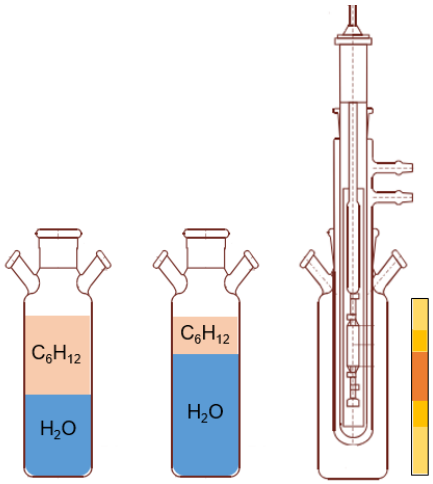

Figure 48. Left: Biphasic system 250 ml of cyclohexane + 250 ml water. Center: Biphasic system 100 ml cyclohexane + 400 ml water. Right: Light intensity profile in the reactor system.

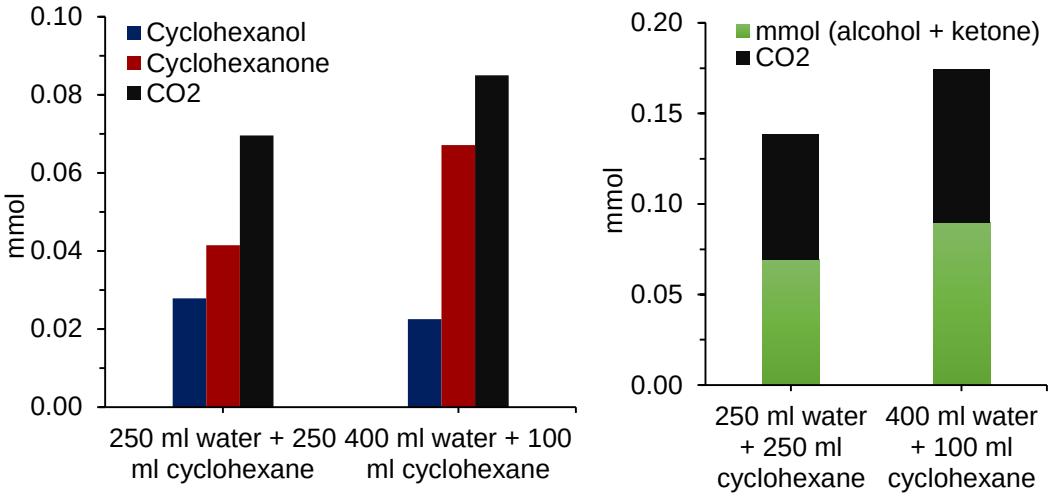

Figure 49. Photocatalytic performance of hydrophilic TiO_2 varying the amount of cyclohexane and water present in biphasic system.

Figure 50 shows the effect of the stirring speed on the photocatalytic performance of TiO_2 in biphasic system. It is clearly observed that the activity of TiO_2 is independent of the stirring speed. This confirms that the extremely poor activity showed by TiO_2 is caused by the low solubility of cyclohexane in water.

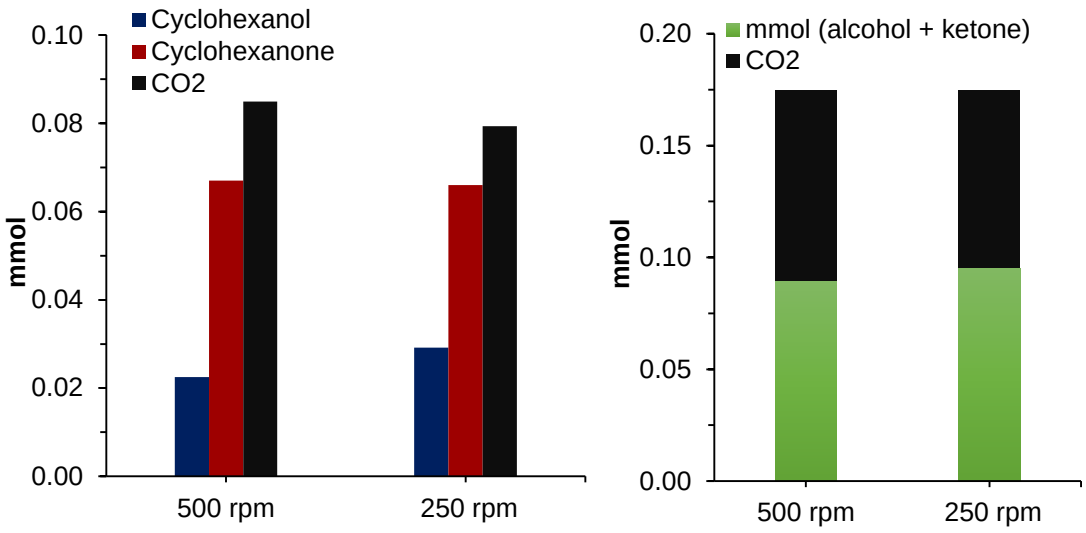

Figure 50. Photocatalytic performance of hydrophilic TiO_2 varying the stirring speed in biphasic system.

CHAPTER 6: FURTHER WORK

Additional work was initiated with m-cresol and furfural as model reaction compounds of bio-oil obtained from biomass. The main goal was to study the feasibility of using photocatalytic partial oxidation reactions to selectively oxidize these oxygenated molecules for the production of molecules with functional groups that offer alternative routes for coupling reaction and further upgrading to fuels and fine chemicals.

6.1. Photocatalytic oxidation of Furfural

6.1.1. Overview

Regarding sustainable chemistry, biomass is a renewable resource that plays a substantial role in the production of biofuels and value added bio-based chemicals. Furfural has gained a lot of attention from academic researches. Some of the industrial applications of furfural include its use as a fungicide and weed killer, production of tetrahydrofuran, and use as a solvent for refining lubricating oils. In addition, furfural can be used a building block for the synthesis of green fuels and chemicals.

Multistage torrefaction of biomass has been extensively used for the thermal conversion and fractionation of lignocellulosic biomass (i.e. hemicellulose, cellulose, and lignin) into three different bio-oil streams comprised primarily of light oxygenates, furan derivatives, and phenolic species, respectively. Furfural is a well-known and highly flexible starting material that can be obtained from the stage two of the torrefaction process. The oxidation of furfural has been one of the chemical reactions studied for the catalytic upgrading of thermally fractionated bio-oils. Figure 51 illustrates the liquid phase technique, developed by Vann *et al*. to upgrade furfural. In

this work, furfural was oxidized via photocatalysis but the same upgrading technique was utilized.

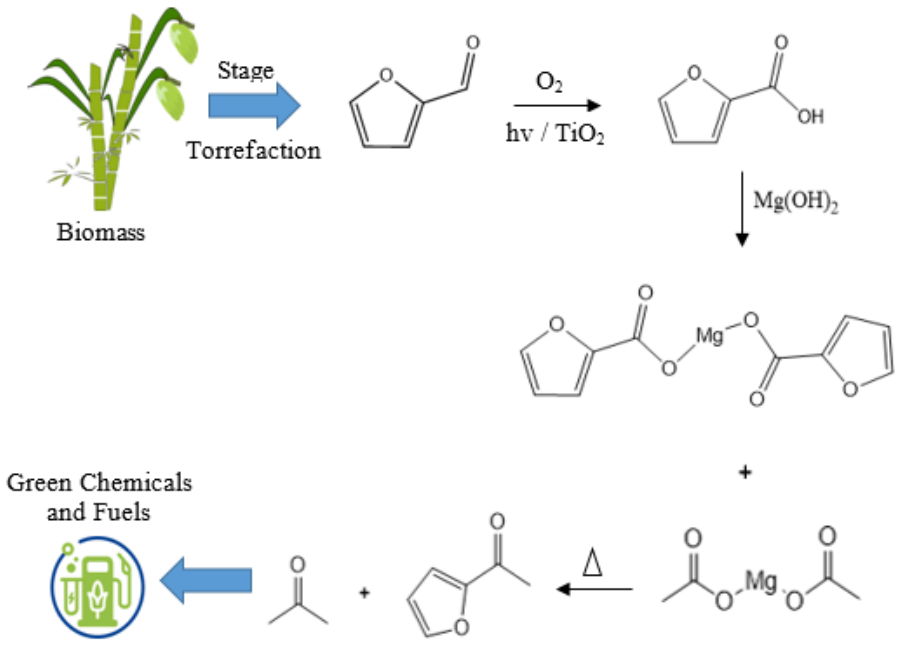

Figure 51. Reaction pathway of furfural upgrading to 2-acetylfuran.

Figure 51 shows the upgrading strategy starting with the photocatalytic oxidation of furfural to furoic acid, followed by the formation of the magnesium furoate salt, magnesium furan-2-carboxylate. Since a significant amount of acetic acid is also obtained after the torrefaction process, magnesium acetate can be obtained from the reaction of acetic acid and additional $Mg(OH)_2$. Then, magnesium furan-2-carboxylate and magnesium acetate can be exposed to high temperatures in inert atmospheres and undergo ketonization to yield 2-acetylfuran. The ketone obtained is a bio-based building block for the production of specialty chemicals and also fuels. The same approach is expected when maleic acid is used to form the magnesium salt.

There are no studies reported in the literature that focus on photocatalytic selective oxidation of furfural, only photocatalytic degradation of furfural has been reported.[72, 73] Ahmadi *et al*. investigated the degradation of furfural using TiO2 immobilized on a glass support and proposed a reaction scheme by using LC-Mass technique. The authors suggested that furfural degradation involves three steps; aldehyde group oxidation, photo-oxidation of aromatic ring and ring cleavage. The reaction scheme depicted in Figure 52 illustrates the intermediates obtained after two hours of reaction, including maleic and tartaric acid.[72]

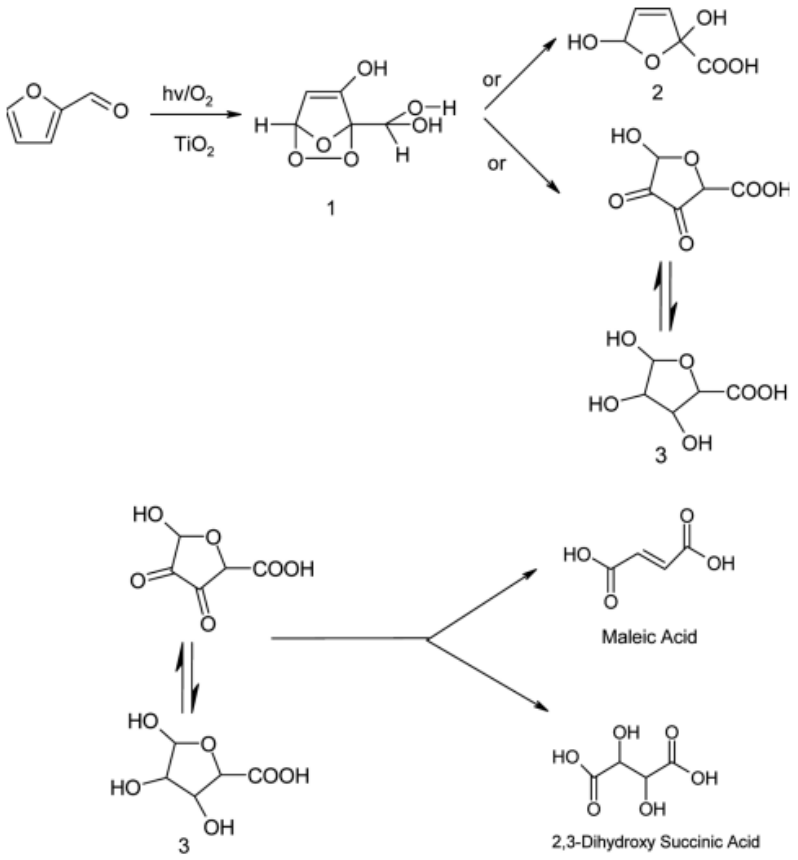

Figure 52. Reaction scheme for the photo-oxidation of furfural.[72]

6.1.2. Methods and procedures

AEROXIDE® TiO_2 T805 (3.2 wt% of C content) was purchased from Evonik. Barium hydroxide anhydrous 94-98% $Ba(OH)_2$ was purchased from Alfa Aesar. Furfural 99%, 2-Furoic acid 98%, and maleic acid ≥99.0% (HPLC), were purchased from Sigma-Aldrich and purified by distillation prior to use. Distilled water was used in the reaction experiments

The photocatalytic reactions were carried out in the laboratory UV reactor system described previously in section 4.4. The only difference is the volume capacity of the reactor vessel, which is now 200 mL. A short reaction time of 1 hour was chosen in order to minimize furfural polymerization when exposed to UV light. The furfural and products concentration in all samples were analyzed by HPLC equipped with a Waters 486 Tunable Absorbance Detector at 210 nm and a Waters 410 refractometer. The separation was done by an Aminex HPX-87H column from Bio-Rad Laboratories. The flow rate of eluant (5mM sulfuric acid) was fixed to 0.6 mL/min and the temperature was 45 °C.

The photocatalytic selective oxidation of furfural to furoic acid and maleic acid was carried out in aqueous phase using the commercially available hydrophobic titania, TiO_2 T805 as catalyst. MgO was added in order to titrate the furoic acid and maleic acid formed throughout the reaction. Both, the hydrophobic surface of the catalyst and the base, help to avoid fast catalyst deactivation. The hydrophobic surface promotes the desorption of the hydrophilic products and the base is used for neutralization of the acids that would otherwise adsorb strongly onto the metal. The acid products can react

with $Mg(OH)_2$ to form magnesium salts. After the reaction is complete, the reaction solvent is evaporated at low temperatures so that the salts can precipitate.

The thermal decomposition experiments were carried out by Tyler Vann. A physical mixture of 2.6/1 mg of magnesium acetate to solid was heated at 400 °C via an analytical pyroprobe in inert helium. The vapor products were quantified by flame ionization detection and identified by mass spectral analysis.

6.1.3. Results and discussion

Reactions were carried out in an aqueous solution at room temperature with an initial furfural concentration of 0.024 M and 100 milligrams of catalyst. A furfural conversion of 23.3 % was obtained after 1 hour of reaction. The three larger peaks observed on the chromatogram were identified as maleic acid, furoic acid, and a third product that could not be identified. In addition, two small peaks were detected and identified as 2(5H)-furanone and succinic acid. The reaction yields obtained were 12.5% to maleic acid and 0.9% to furoic acid. The yield to CO_2 was found to be 0.7%, meaning that the reaction is selective towards maleic acid. Therefore, the remaining 9.2% yield could be attributed to the unknown product that is also predominant, and 2(5H)-furanone and succinic acid.

A reaction with no catalyst present was carried out in order to confirm whether the reaction is photocatalytic or photolytic. Similar results were obtained implying that there is negligible photocatalytic oxidation. The reaction carried out in the absence of the catalyst gave a slight higher conversion of furfural, 30% after 1 hour of reaction. The reaction yields were 18.1% to maleic acid, 0.5% to furoic acid, and 0.7% to CO_2. Since the furfural absorbs the light, the exclusive photoactivation of the catalyst was not

conserved, and therefore there was no true heterogeneous catalytic regime. In order to verify this hypothesis, the UV-spectrum of furfural was obtained and it is shown in Figure 53. The green dashed line is located at 270 nm to indicate that only UV light at wavelengths higher than 270 nm is transmitted through the Pyrex immersion well. The UV-spectrum shows that furfural absorbs UV light from 190 to 320 nm and that higher absorption occurs above 270 nm. As a result, the furfural molecule can absorb light and therefore, it can undergo oxidation via photolysis.

As illustrated in Figure 54, the formation of dark brown solids or humins along with the salt crystals while evaporating the solvent was one of the biggest challenges faced during the evaporation of the solvent for the separation of the salts.

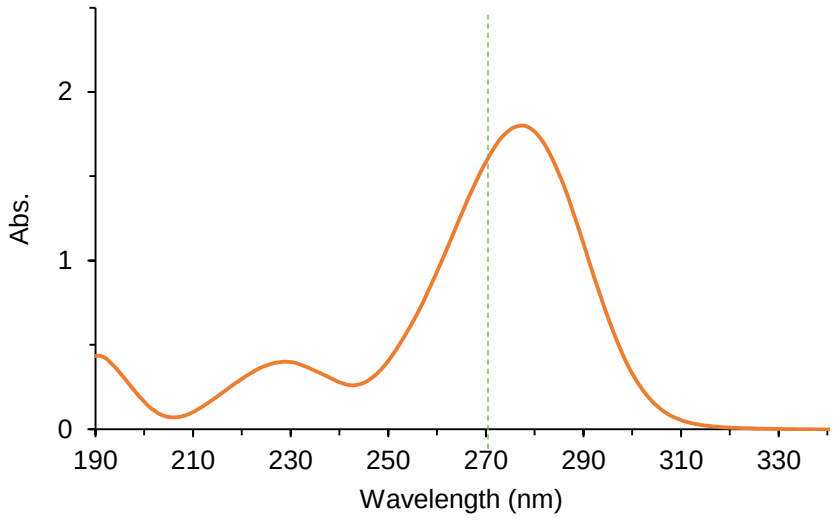

Figure 53. UV absorption spectrum of liquid furfural.

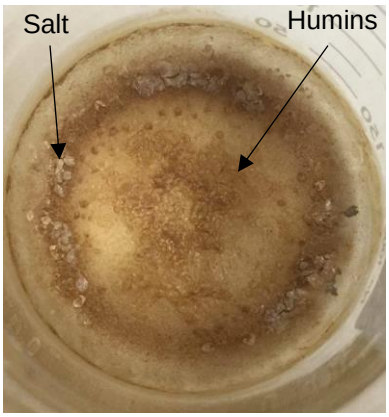

Figure 54. Image of salt and possible humins formed after evaporation of the water solvent.

From the thermal decomposition experiments, the presence of 2-acetylfuran was able to be confirmed. However, the amount of acetone obtained ($3.36x10^{-3}$ mmol/mg of solid) was considerably larger than the amout of 2-acetylfuran ($2.37x10^{-5}$ mmol/mg of solid). This could be explained by the fact that, there is only a small amount of furoic acid obtained. However, when using acetonitrile as solvent, the amount to furoic acid and especially to maleic increased significantly. Unfortunately, the thermal decomposition experiments of this sample were not carried out since the equipment broke but it could be done in the future.

6.2. Photocatalytic selective oxidation of m-cresol

6.2.1. Overview

A lot of attention has been focused on the removal of dangerous compounds in wastewater. Photocatalysis uses semiconductors that are stable and non-toxic, to oxidize molecules in a suitable reaction time and atmospheric conditions.

m-Cresol is a harmful and toxic chemical compound, therefore, its photocatalytic degradation to less harmful products such as CO_2 and H_2O has been focus of attention in several research studies.[74, 75, 76, 77] m-Cresol is widely used as a solvent, and as a precursor in the pesticide and pharmaceutical industries. Total oxidation of m-cresol has been investigated due to the large amount of m-cresol present in industrial wastewater.

However, to the best of our knowledge, studies targeting selective oxidation of m-cresol for the production of specialty chemical compounds have not yet been reported. In this work, the main motivation for the use of cresol is that it can be obtained from the third stage of the torrefaction process applied to lignocellulosic biomass. This stage is reach in phenolic compound such as (cresol, anisole, guaiacol, catechol, etc.). The photocatalytic oxidation of these molecules is a great alternative for the production of fine chemicals. For instance, o-cresol can be selectively oxidized to 2-hydroxybenzoic acid, also known as salicylic acid.

Salicylic acid has abundant industrial applications, it is used as an anti-inflammatory drug, as food preservative, as bactericidal, as antiseptic, etc. Also, it is a key ingredient in many skin-care products and it can be used for production of other pharmaceuticals, etc. In this study, m-Cresol was chosen as the model compound

because it is liquid at room conditions facilitating the conduction of the reaction experiments.

Abdollahi *et al.* studied the photocatalytic degradation of m-cresol under visible and UV light using ZnO as photocatalyst.[74] Although, the use of visible light is certainly convenient, the concentration of m-cresol removed was insignificant. In order to remove higher concentrations of m-cresol, the authors also studied the reaction under UV conditions.[75] Figure 55Figure 55 depicts the reaction intermediates detected were (b) 2-methyl-1,4-benzodiol. (c) 2-methyl-para-benzoquinone, (e) 3,5-dihydroxytoluene and (f) 2,5-dihydroxy-benzaldehyde. However, the authors did not focus on partial oxidation and therefore, a detailed and quantitative study of the yield to reaction intermediates was not provided.

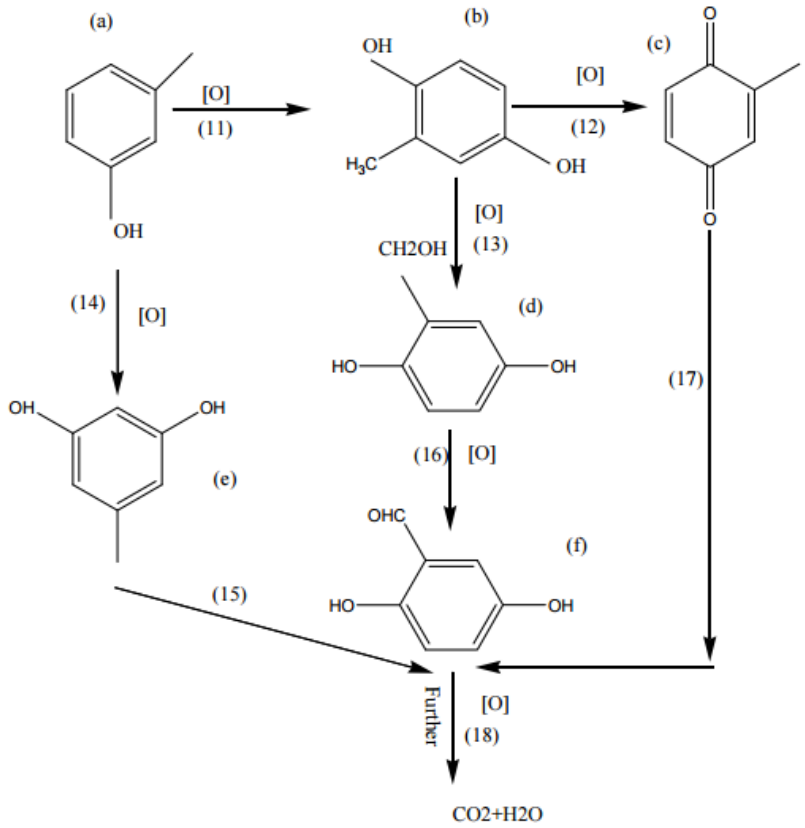

Figure 55. Reaction scheme showing the reaction intermediates from the photocatalytic degradation of m-cresol.[75]

In this work, the photocatalytic selective oxidation of m-cresol in aqueous phase was studied using TiO_2 as photocatalyst. For comparison purposes, the commercially available hydrophobic TiO_2 was also used. The reaction products identified from lower to higher concentration are 3-methylcatechol, 4-methylcatechol, 3-hydroxybenzaldehyde, and methyl-p-benzoquinone.

6.2.2. Experimental methods and procedures

TiO_2, anatase 99.9% (metal basis) was purchased and used as received from Alfa Aesar. AEROXIDE® TiO_2 T805 (3.2 wt% of C content) was purchased from Evonik. Barium hydroxide anhydrous 94-98% $Ba(OH)_2$ was purchased from Alfa Aesar. Methyl-p-benzoquinone 98%, 3-hydroxybenzaldehyde ≥99%, 3-hydroxybenzoic acid ReagentPlus® 99%, 3-methylcatechol 98%, and 4-methylcatechol ≥95% were purchased from Sigma-Aldrich and used without any purification. Distilled water was used in the reaction experiments. Table 4 summarizes the chemical hazards and the safety precautions for the different compounds employed in the reaction system.

The reactor system used for the photocatalytic selective oxidation of furfural is the same used for the photocatalytic selective oxidation of furfural. Air was continuously bubbled through the reaction suspension at a rate of 18 mL/min. The concentration of catalyst (TiO_2 T 805) was varied from 0.25 to 0.75 g L^{-1}. Stirring of 500 rpm was provided to avoid external mass transfer limitations. Liquid product samples were filtered and then analyzed. GC-MS and GC–FID with column ZB-1701 (from Phenomenex ®) were used for product identification and quantification.

Table 4. Chemical hazards and safety precautions of the different compounds used.

Compounds	Chemical Hazard	Hazard Code	Safety precautions
m-cresol US health exposure limits (NIOSH): IDLH (Immediate danger) 250 ppm	May cause serious burns. Harmful if inhaled. Toxic in contact with the skin or if swallowed.		Use full-face supplied air respirators, compatible chemical-resistant gloves, and safety goggles. Wash skin thoroughly after handling.
3-hydroxybenzaldehyde *3-hydroxybenzoic acid* *Methyl-p-benzoquinone*	Harmful if swallowed. Causes skin irritation, serious eye irritation. May cause respiratory irritation.		Avoid breathing dust/ fume/ gas/ mist/ vapors/ spray. Wash skin thoroughly after handling. Use only in a well-ventilated area. Wear eye protection/ face protection and protective gloves.

6.2.3. Results and discussion

As previously mentioned, and as shown in Figure 56, m-cresol absorbs a smaller amount of UV light above 270 nm than furfural. As expected, the reaction carried out in absence of catalyst showed negligible photolysis present.

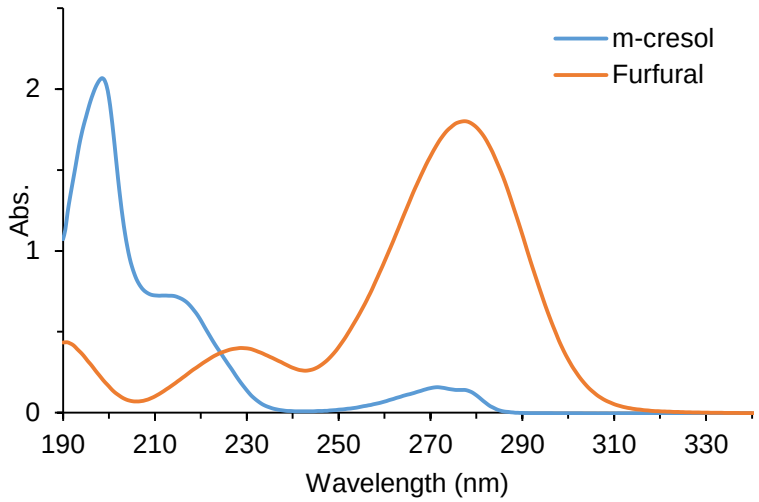

Figure 56. UV absorption spectrum of liquid m-cresol and furfural.

Due to the low concentration of m-cresol used, the samples obtained after reaction were concentrated in order to perform the identification and quantification of the reaction products. A rotary evaporator was used for the gentle removal of solvent (water) by evaporation under reduced pressure. The reduction of the pressure was done by means of a vacuum system. The initial sample volume was 20 mL of sample and the temperature of the fluid bath was fixed at 60 °C. After 45 min, 2 mL of sample were collected. However, the concentration of m-cresol did not increase which implies that some m-cresol was lost during the rotary evaporation process (the concentration of m-cresol after reaction was 0.0062 M and after rotary evaporation the concentration decreased to 0.0014 M). One possible explanation could be that the vacuum applied was so high at a certain point that it suddenly sucked the liquid from the flask containing the sample. As observed in Figure 57, the vapor pressure of m-cresol is significantly smaller than the vapor pressure of water at 60 °C. Hence, evaporation of m-cresol cannot be considered as a cause of the reduced concentration of m-cresol.

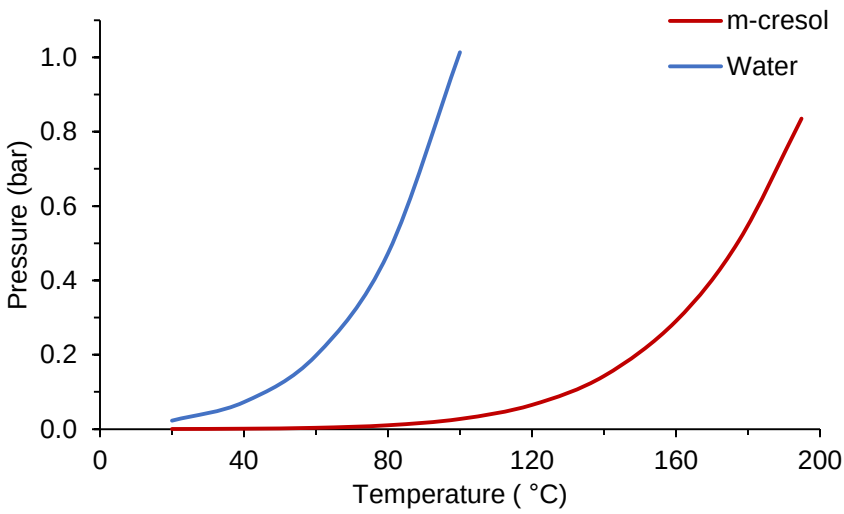

Figure 57. Pressure and temperature diagram for m-cresol and water.

Unfortunately, a precise quantification of the carbon balance of the reaction was not able to be obtained since the amount of the reaction products was uncertain. Nevertheless, an approximation of the results obtained is given in Table 5 and Table 6. As shown in Table 5, 0.131 mmol of CO_2 are formed when the reaction is carried out without reactant. This implies that not all the CO_2 obtained from the experiments is a result of total oxidation of m-cresol. Therefore, it can be concluded that a certain amount of CO_2 is actually coming from the oxidation of the hydrophobic groups anchored to the catalyst. The amount of CO_2 obtained when using the TiO_2 (0.123 mmol) as catalyst is relatively higher than the amount of CO_2 obtained when using TiO_2 T805 (0.076 mmol). One reason can be the strong affinity of the oxygenated products to the hydrophilic surface, which results in a low desorption rate of the products and further oxidation to CO_2. Table 6 shows that after 1 hour of reaction, only 3-hydroxybenzaldehyde is obtained as reaction product. After 2 hours of reaction, the amount of aldehyde increases and a considerable yield to 2-methyl-p-benzoquinone is obtained. It can also be concluded that, the selectivity towards 2-methyl-p-benzoquinone is significantly higher than 3-hydroxybenzaldehyde.

Table 5. CO_2 formation (mmol) in the photocatalytic oxidation of m-cresol using TiO_2 T805 and TiO_2 as catalysts; in absence of catalyst; and when no reactant is present.

Rxn time: 60 min	m-cresol (M)	Catalyst: 100 mg	CO_2 (mmol)
Rxn10	0	TiO2 T805	0.131
Rxn5	0.01	TiO2 T805	0.076
Rxn11	0.01	TiO2 hydrophilic	0.123
Rxn6	0.01	No catalyst	0.081

Table 6. Results of the photocatalytic reactions (samples analyzed after concentration using the rotary evaporator)

		Yield (mmol)		
Catalyst loading: 100 mg	**Rxn time (min)**	**1/7 CO_2**	**3-hydroxybenzaldehyde**	**2-methyl-p-benzoquinone**
Rxn5	60	0.002	1.97E-04	0
Rxn9	120	0.020	6.05E-04	0.088

Liquid-liquid extraction was also used in order to concentrate the sample avoiding polymerization and loss of the products. 5 mL of m-cresol were added to 113 mL of sample obtained after reaction in order to extract the products. Although products were not completely soluble in m-cresol, the respective peaks were able to be identified in GC-FID. The results obtained can be observed in Figure 58. It can be observed that above 50 mg of catalyst (0.25 g L^{-1}), the reaction rate decreases. This case is particular since the catalyst is not dispersed in the aqueous phase. The catalyst is located at the interface, and therefore as the concentration of catalyst increases, light scattering occurs, thereby decreasing the amount of light penetrated. This results in a lower conversion and lower yield to 3-hydroxybenzaldehyde and methyl-p-benzoquinone. The higher CO_2 concentration obtained as the catalyst loading increases can be explained by the fact that, some of the CO_2 produced comes from the hydrophobic catalyst as a result of the oxidation of the hydrophobic groups after exposure to UV light.

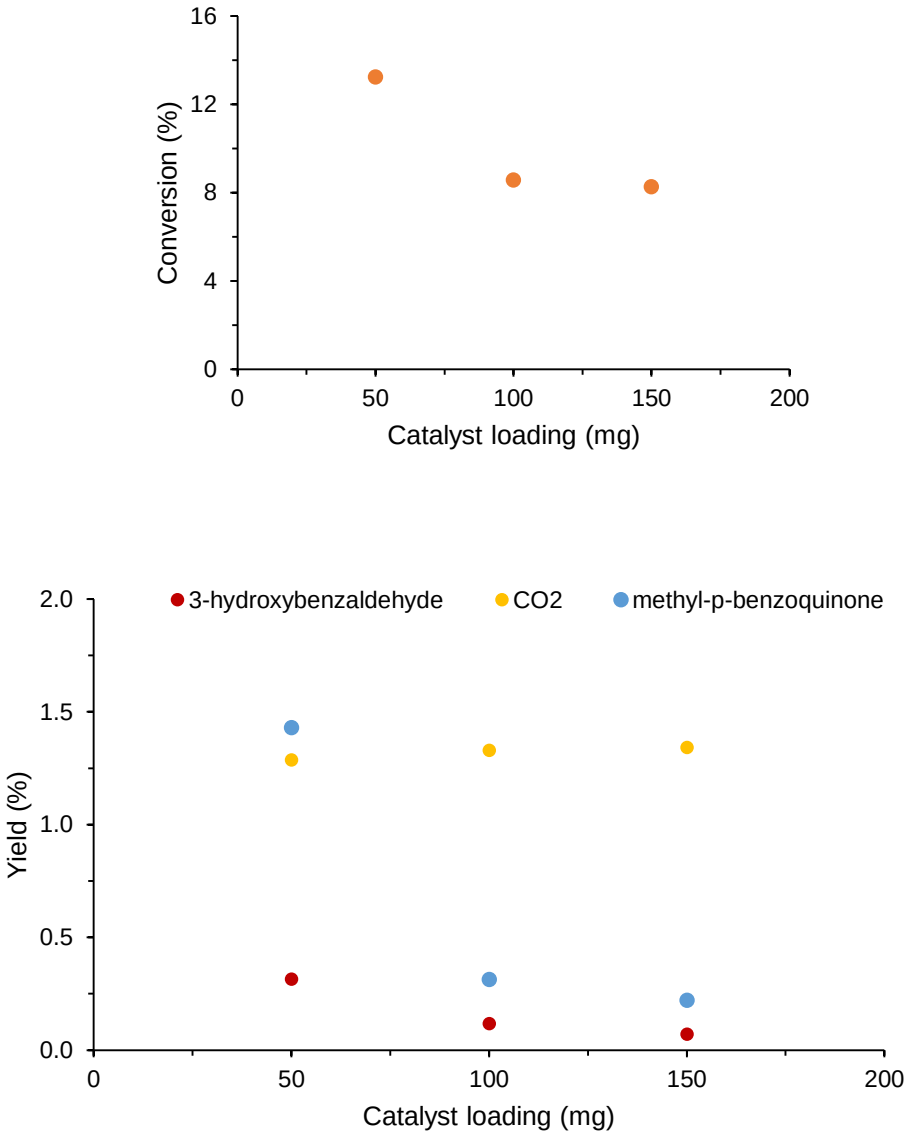

Figure 58. Conversion profile and yield to 3-hydroxybenzaldehyde, methyl-p-benzoquinone, and CO_2 obtained as the catalyst (TiO_2 T805) loading increases.

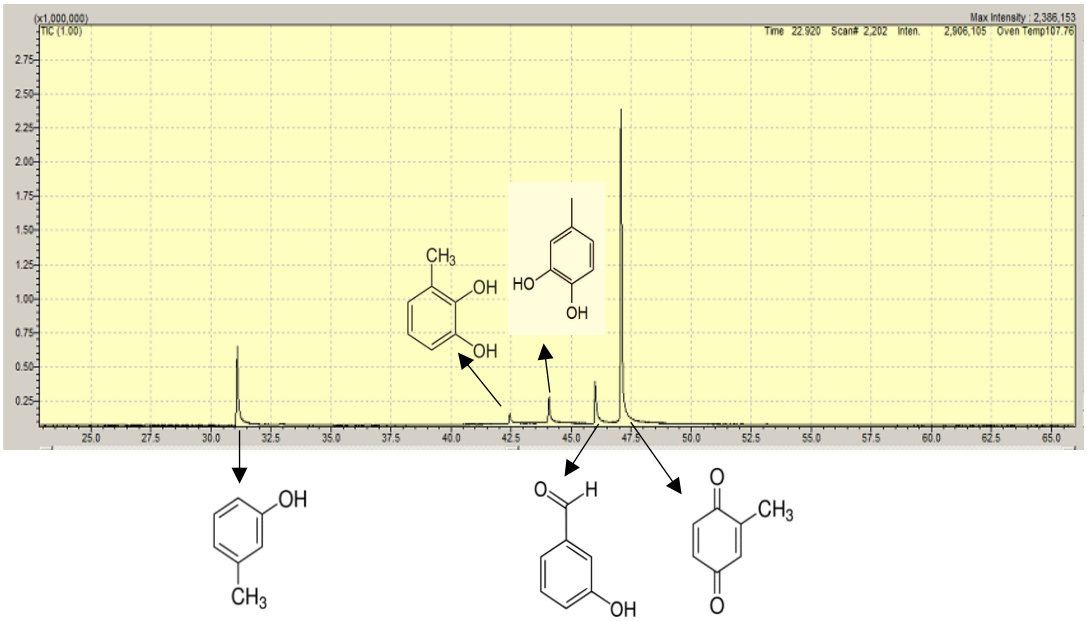

Figure 59. GC-MS chromatogram showing the presence of m-cresol, 3-methylcatechol, 4-methylcatechol, 3-hydroxybenzaldehyde, and methyl-p-benzoquinone.

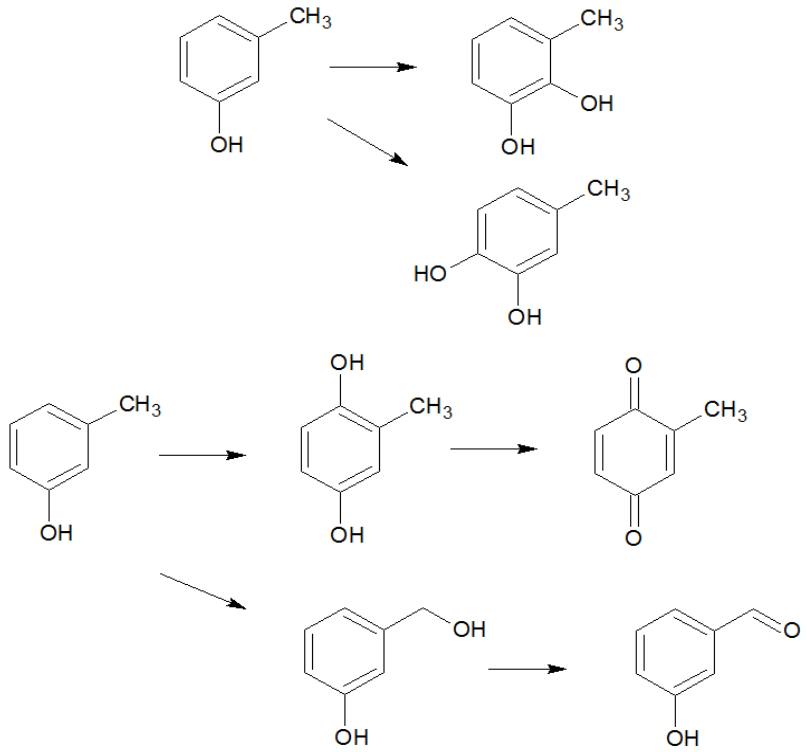

Figure 60. Reaction scheme showing the reaction intermediates from the photocatalytic selective oxidation of m-cresol using TiO_2.

Figure 59 shows the chromatogram obtained from the GC-MS analysis of the concentrated sample. The reaction products identified including m-cresol, 3-methylcatechol, 4-methylcatechol, 3-hydroxybenzaldehyde, and methyl-p-benzoquinone suggest the reaction scheme displayed in Figure 60. Although, 3-hydroxybenzoic acid was not identified in GC analysis possibly because its high boiling point, it could also be present. The intermediate hydroquinone was not detected perhaps because it is a radical inhibitor that can quickly undergo hydrogen abstraction forming the benzoquinone.

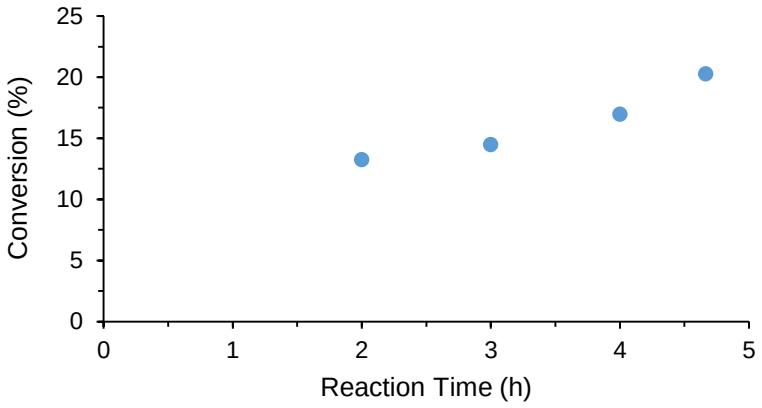

Figure 61. Conversion profile as the reaction time increases using TiO_2 T805 as catalyst. Catalyst mass: 50 mg.

The reaction profile showed in Figure 61 shows that the catalyst is active even after 4 hours of reaction.

Figure 62 shows the reactor vessel after 4 hours of reaction, it can clearly be observed that some catalyst particles remain hydrophobic, explaining the observed remaining positive effects in m-cresol conversion.

Figure 62. Reaction vessel after 4 hours of reaction.

However, as observed in Table 7, the amount of 3-hydroxybenzaldehyde and 2-methyl-p-benzoquinone decreases as the reaction time increases from 2 to 4.7 hours. On the contrary, the formation of CO_2 increases. This can be the result of 3-hydroxybenzaldehyde oxidation to 3-hydroxybenzoic acid as well as total oxidation of the reaction intermediates to CO_2.

Table 7. Resulting yield to 3-hydroxybenzaldehyde, methyl-p-benzoquinone, and CO_2 obtained as the reaction time increases using TiO_2 T805 as catalyst.

Catalyst loading: 50 mg	Rxn time (h)	1/7 CO_2	3-hydroxybenzaldehyde (mmol)	2-methyl-p-benzoquinone (mmol)
Rxn12	2	0.019	0.00468	0.02128
Rxn16	4.7	0.029	0.00295	0.00502

For future studies, the amount of 3-hydroxybenzoic acid produced throughout the reaction could be obtained by calculating the modified acid number (MAN). The MAN is the amount of potassium hydroxide (KOH) that is required to neutralize the acids that are present in 1 gram of sample. The instrument used to determine the MAN is the titrator 798 MPT Titrino from Metrohm.

The reaction conditions can be optimized so that the rate of formation of 3-hydroxybenzaldehyde increases, and a higher production of 3-hydroxybenzoic acid can be achieved. Additional experiments can be carried to evaluate the feasibility of converting p-cresol to salicylic acid via photocatalytic selective oxidation reactions.

CHAPTER 7: CONCLUSIONS

7.1. Photocatalytic selective oxidation of cyclohexane

A key challenge to the photocatalytic research field is the identification and improvement of the slow and inefficient steps. In the liquid-phase photocatalytic oxidation of cyclohexane to cyclohexanol and cyclohexanone, TiO_2 T805 was found to be photostable, active and selective by enhancing product desorption. The idea presented here is the use of mesoporous SiO_2 to protect the hydrophobic groups from being attacked by the radicals that are formed throughout the course of the photocatalytic reaction. Hence, the catalyst hydrophobicity keeps practically unaltered when used in reactions under UV light conditions. This greatly enhances the photo-stability and therefore the catalytic activity and selectivity of the solid catalysts in biphasic and single systems. The best catalyst in terms of activity, selectivity to the desired products over CO_2, as well as photo stability was found to be TiO_2/SiO_2 + OTS. These results lead us to conclude that the effectiveness of the photocatalytic selective oxidation of cyclohexane can be greatly improved by surface modification of the catalyst.

It is difficult to compare the photocatalytic activities achieved in this contribution with the ones obtained by others research groups since different reactor systems are employed. Moreover, the fraction of light absorbed is unlikely to be the same in each experiment because of the significant changes in the amount of scattered and reflected light from one experiment to another. In this work, the same reactor was used and the standard deviation of the mean was calculated to be less than 10%.

7.2. Photocatalytic selective oxidation of furfural and m-cresol

The photocatalytic selective oxidation of furfural and m-cresol was carried out using the commercially available hydrophobic catalyst (TiO_2 $T80_5$). The results obtained can be considered preliminary since more detailed work is required to allow a deeper understanding of the effect of using a hydrophobic catalyst on the reaction selectivity and activity. However, it provides a good starting point for further investigation and potential use of the catalyst proposed previously, $TiO_2/mSiO_2$ + OTS, which exhibited great photostability, selectivity, and activity in the photocatalytic selective oxidation of cyclohexane.

7.2.1. Furfural

The oxidation of furfural seems to happen as result of photochemical reactions rather than photocatalytic reactions. It is believed that furfural absorbed UV light and therefore underwent oxidation through a photolytic process. In order to evaluate the catalytic activity of TiO_2, another molecule that does not absorb UV light above 270 nm had be to chosen in order to avoid the presence of photolysis. Cresol was chosen since it absorbs a negligible amount of UV light in that region of the spectrum.

It was also found that the selectivity of the reaction under UV light conditions can be tuned by manipulating the solvent environment. When water was used as solvent, CO_2 was the main reaction product. The use of acetonitrile as solvent resulted in a lower production of CO_2 and a higher yield to more valuable chemical compounds such as maleic acid and furoic acid. These acids could potentially be used to form a salt that can subsequently be used to do cross-ketonization reactions to finally obtain a

ketone product. This ketone product can be used as building block for the production of biofuels.

7.2.2. m-cresol

The selective oxidation of m-cresol was found to be feasible via photocatalytic partial oxidation reactions. The reaction intermediates identified from lower to higher concentration were 3-methylcatechol, 4-methylcatechol, 3-hydroxybenzaldehyde, and methyl-p-benzoquinone.

This study evaluated the applicability of hydrophilic and hydrophobic TiO_2, by far the most used photocatalyst, to selectively oxidize m-cresol. The photocatalytic of m-cresol was investigated in aqueous phase and no oxidation products were observed when the reaction was carried out in the absence of catalyst. A reaction time of 2 hours was clearly sufficient for a significant amount of products to be detected by GC-FID and GC-MS. The concentration of CO_2 formed from the m-cresol oxidation is very low, especially when using the commercially hydrophobic catalyst (TiO_2 $T80_5$). This indicates that the reaction is selective towards the formation of the desired products.

REFERENCES

1. Musser, M. T., Cyclohexanol and Cyclohexanone. In *Ullmann's Encyclopedia of Industrial Chemistry*, Wiley-VCH Verlag GmbH & Co. KGaA: 2000.

2. Almeida, A. R.; Carneiro, J. T.; Moulijn, J. A.; Mul, G., Improved performance of TiO2 in the selective photo-catalytic oxidation of cyclohexane by increasing the rate of desorption through surface silylation. *Journal of Catalysis* **2010,** *273* (2), 116-124.

3. Hashimoto, K., Irie, H., and Akira Fujishima, A., TiO2 Photocatalysis: A Historical Overview and Future Prospects. *AAPPS Bulletin* **2007,** *17* (6), 12-28.

4. Khataee, A. R.; Kasiri, M. B., Photocatalytic degradation of organic dyes in the presence of nanostructured titanium dioxide: Influence of the chemical structure of dyes. *Journal of Molecular Catalysis a-Chemical* **2010,** *328* (1-2), 8-26.

5. Somasundaran, P., Encyclopedia of Surface and Colloid Science. Second ed.; Taylor & Francis Group: **2006**. https://books.google.com/books?id=n4luwcdQWv4C&pg=PA4526&lpg=PA4526&dq=why+is+tio2+a+good+photocatalysis&source=bl&ots=-PGzynf8C6&sig=Ssearhtw6X_D5n-CV4pW1U1gpdI&hl=es&sa=X&ved=0CG8Q6AEwCGoVChMIhei45MfJxwIVgQ-SCh00oAyT#v=onepage&q=why%20is%20tio2%20a%20good%20photocatalysis&f=false.

6. Munusamy, S., Aparna, R., Prasad, R., Photocatalytic effect of TiO2 and the effect of dopants on degradation of brilliant green. *Sustainable Chemical processes* **2013,** *1* (4), 8.

7. Cermenati, L.; Albini, A.; Cermenati, L.; Richter, C.; Albini, A., Solar light induced carbon-carbon bond formation via TiO2 photocatalysis. *Chemical Communications* **1998,** (7), 805-806.

8. Sokmen, M.; Allen, D. W.; Hewson, A. T.; Clench, M. R., Photocatalytic oxidative degradation of 2-methylthiophene in suspensions of TiO2: identification of intermediates and degradation pathways. *Journal of Photochemistry and Photobiology A: Chemistry* **2001,** *141* (1), 63-67.

9. Ohno, T.; Masaki, Y.; Hirayama, S.; Matsumura, M., TiO2-Photocatalyzed Epoxidation of 1-Decene by H2O2 under Visible Light. *Journal of Catalysis* **2001,** *204* (1), 163-168.

10. Ohno, T.; Tokieda, K.; Higashida, S.; Matsumura, M., Synergism between rutile and anatase TiO2 particles in photocatalytic oxidation of naphthalene. *Applied Catalysis A: General* **2003,** *244* (2), 383-391.

11. Zhu, X.; Wang, Y.; Zhou, D., TiO2 photocatalytic degradation of tetracycline as affected by a series of environmental factors. *J Soils Sediments* **2014,** *14* (8), 1350-1358.

12. Kim S.B., J. H. T., Hong S.C. , Photodegradation of gas-phase methanol and toluene using thin-film TiO2 photocatalyst. 1. Influence of water vapor, molecular oxygen and temperature. . *J. Ind. Eng. Chem* **2002,** *8*, 156–161.

13. Kim, J.; Kim, J., Arsenite Oxidation-Enhanced Photocatalytic Degradation of Phenolic Pollutants on Platinized TiO2. *Environmental Science & Technology* **2014,** *48* (22), 13384-13391.

14. Minero, C.; Catozzo, F.; Pelizzetti, E., Role of adsorption in photocatalyzed reactions of organic molecules in aqueous titania suspensions. *Langmuir* **1992,** *8* (2), 481-486.

15. Vulliet, E.; Chovelon, J.-M.; Guillard, C.; Herrmann, J.-M., Factors influencing the photocatalytic degradation of sulfonylurea herbicides by TiO2 aqueous suspension. *Journal of Photochemistry and Photobiology A: Chemistry* **2003,** *159* (1), 71-79.

16. Ksibi, M.; Zemzemi, A.; Boukchina, R., Photocatalytic degradability of substituted phenols over UV irradiated TiO2. *Journal of Photochemistry and Photobiology A: Chemistry* **2003,** *159* (1), 61-70.

17. Einaga, H.; Futamura, S.; Ibusuki, T., Heterogeneous photocatalytic oxidation of benzene, toluene, cyclohexene and cyclohexane in humidified air: comparison of decomposition behavior on photoirradiated TiO2 catalyst. *Applied Catalysis B: Environmental* **2002,** *38* (3), 215-225.

18. Nørskov, J. K.; Studt, F.; Abild-Pedersen, F.; Bligaard, T., Surface Electrocatalysis. In *Fundamental Concepts in Heterogeneous Catalysis*, John Wiley & Sons, Inc: **2014**; pp 155-174.

19. Herrmann, J.-M., Photocatalysis fundamentals revisited to avoid several misconceptions. *Applied Catalysis B: Environmental* **2010,** *99* (3–4), 461-468.

20. Herrmann, J.-M., Photocatalysis. In *Kirk-Othmer Encyclopedia of Chemical Technology*, John Wiley & Sons, Inc.: **2000**.

21. Janssen, F. J. J. G.; van Santen, R. A., *Environmental Catalysis*. **1999**.

22. Kondarides, D. I., PHOTOCATALYSIS In *Catalysis in Encyclopedia of Life Support Systems (EOLSS), Developed under the Auspices of the UNESCO.*, Centi, G., Ed. EOLSS Publishers: Oxford, UK, **2010**.

23. Schneider, J.; Matsuoka, M.; Takeuchi, M.; Zhang, J. L.; Horiuchi, Y.; Anpo, M.; Bahnemann, D. W., Understanding TiO2 Photocatalysis: Mechanisms and Materials. *Chemical Reviews* **2014,** *114* (19), 9919-9986.

24. (a) Maeda, K.; Domen, K., Photocatalytic Water Splitting: Recent Progress and Future Challenges. *Journal of Physical Chemistry Letters* **2010,** *1* (18), 2655-2661; (b) Abe, R., Recent progress on photocatalytic and photoelectrochemical water splitting under visible light irradiation. *Journal of Photochemistry and Photobiology C-Photochemistry Reviews* **2010,** *11* (4), 179-209.

25. Banerjee, A. N., The design, fabrication, and photocatalytic utility of nanostructured semiconductors: focus on TiO(2)-based nanostructures. *Nanotechnology, Science and Applications* **2011,** *4*, 35-65.

26. Kisch, H., Semiconductor Photocatalysis: Principles and Applications. Kisch, H., Ed. WILEY-VCH Verlag GmbH & Co. KGaA: Weinheim, Germany, **2014**; pp. 85-210. http://onlinelibrary.wiley.com.ezproxy.lib.ou.edu/book/10.1002/9783527673315.

27. Zhang, J.; Zhou, P.; Liu, J.; Yu, J., New understanding of the difference of photocatalytic activity among anatase, rutile and brookite TiO2. *Physical Chemistry Chemical Physics* **2014,** *16* (38), 20382-20386.

28. Hanaor, D. A. H.; Sorrell, C. C., Review of the anatase to rutile phase transformation. *Journal of Materials Science* **2011,** *46* (4), 855-874.

29. Augustynski, J., The role of the surface intermediates in the photoelectrochemical behaviour of anatase and rutile TiO2. *Electrochimica Acta* **1993,** *38* (1), 43-46.

30. Sclafani, A.; Herrmann, J. M., Comparison of the Photoelectronic and Photocatalytic Activities of Various Anatase and Rutile Forms of Titania in Pure Liquid Organic Phases and in Aqueous Solutions. *The Journal of Physical Chemistry* **1996,** *100* (32), 13655-13661.

31. Deák, P.; Aradi, B.; Frauenheim, T., Band Lineup and Charge Carrier Separation in Mixed Rutile-Anatase Systems. *The Journal of Physical Chemistry C* **2011,** *115* (8), 3443-3446.

32. Kavan, L.; Grätzel, M.; Gilbert, S. E.; Klemenz, C.; Scheel, H. J., Electrochemical and Photoelectrochemical Investigation of Single-Crystal Anatase. *Journal of the American Chemical Society* **1996,** *118* (28), 6716-6723.

33. Scanlon, D. O.; Dunnill, C. W.; Buckeridge, J.; Shevlin, S. A.; Logsdail, A. J.; Woodley, S. M.; Catlow, C. R. A.; Powell, M. J.; Palgrave, R. G.; Parkin, I. P.; Watson, G. W.; Keal, T. W.; Sherwood, P.; Walsh, A.; Sokol, A. A., Band alignment of rutile and anatase TiO2. *Nat Mater* **2013,** *12* (9), 798-801.

34. Henderson, M. A., A surface science perspective on TiO2 photocatalysis. *Surface Science Reports* **2011,** *66*, 185–297.

35. (a) Hirakawa, T.; Kominami, H.; Ohtani, B.; Nosaka, Y., Mechanism of photocatalytic production of active oxygens on highly crystalline TiO2 particles by means of chemiluminescent probing and ESR spectroscopy. *Journal of Physical Chemistry B* **2001,** *105* (29), 6993-6999; (b) Salvador, P., On the nature of photogenerated radical species active in the oxidative degradation of dissolved pollutants with TiO2 aqueous suspensions: A revision in the light of the electronic structure of adsorbed water. *Journal of Physical Chemistry C* **2007,** *111* (45), 17038-17043.

36. Idriss, H.; Legare, P.; Maire, G., Dark and photoreactions of acetates on TiO2(110) single crystal surface. *Surface Science* **2002,** *515* (2-3), 413-420.

37. Stevanovic, A.; Buttner, M.; Zhang, Z.; Yates, J. T., Photoluminescence of TiO2: Effect of UV Light and Adsorbed Molecules on Surface Band Structure. *Journal of the American Chemical Society* **2012,** *134* (1), 324-332.

38. Mu, W.; Herrmann, J.-M.; Pichat, P., Room temperature photocatalytic oxidation of liquid cyclohexane into cyclohexanone over neat and modified TiO2. *Catal Lett* **1989,** *3* (1), 73-84.

39. Letcher, T., Scott, J., and Patterson, D., Chemical Processes for a Sustainable Future. The Royal Society of Chemistry 2015: Cambridge, UK, **2014**.

40. Faust, B., Ultraviolet/visible spectroscopy. In *Modern Chemical Techniques*, CHEMISTRY, T. R. S. O., Ed. 1997; p 105.

41. X. Fu, W. A. Z. a. M. A., Applications in PhotoCatalytic Purification of Air, Semiconductor Nanoclusters. *Physical, Chemical, and Catalytic Aspects,* **1996,** *103,* 445.

42. Muggli, D. S.; Falconer, J. L., UV-enhanced exchange of O-2 with H2O adsorbed on TiO2. *Journal of Catalysis* **1999,** *181* (1), 155-159.

43. Lukaski, A. C.; Muggli, D. S., Photocatalytic oxidation of methyl formate on TiO2: a transient DRIFTS study. *Journal of Catalysis* **2004,** *223* (2), 250-261.

44. (a) Nagaveni, K.; Hegde, M. S.; Ravishankar, N.; Subbanna, G. N.; Madras, G., Synthesis and structure of nanocrystalline TiO2 with lower band gap showing high photocatalytic activity. *Langmuir* **2004,** *20* (7), 2900-2907; (b) M El-Maazawi, A. F., AB Nair, VH Grassian, Adsorption and Photocatalytic Oxidation of Acetone on TiO< sub> 2</sub>: An< i> in Situ</i> Transmission FT-IR Study. *Journal of catalysis* **2000,** *191*, 138-146; (c) Shang, J.; Du, Y. G.; Xu, Z. L., Photocatalytic oxidation of heptane in the gas-phase over TiO2. *Chemosphere* **2002,** *46* (1), 93-99.

45. Dutta, P. K.; Ray, A. K.; Sharma, V. K.; Millero, F. J., Adsorption of arsenate and arsenite on titanium dioxide suspensions. *Journal of Colloid and Interface Science* **2004,** *278* (2), 270-275.

46. Romão, J. Photocatalytic Water Treatment: Substrate-Specific Activity of Titanium Dioxide University of Twente, Enschede, The Netherlands **2015**.

47. Hoffmann, M. R.; Martin, S. T.; Choi, W. Y.; Bahnemann, D. W., ENVIRONMENTAL APPLICATIONS OF SEMICONDUCTOR PHOTOCATALYSIS. *Chemical Reviews* **1995,** *95* (1), 69-96.

48. Leytner, S.; Hupp, J. T., Evaluation of the energetics of electron trap states at the nanocrystalline titanium dioxide/aqueous solution interface via time-resolved photoacoustic spectroscopy. *Chemical Physics Letters* **2000,** *330* (3-4), 231-236.

49. (a) Yoshihara, T.; Katoh, R.; Furube, A.; Tamaki, Y.; Murai, M.; Hara, K.; Murata, S.; Arakawa, H.; Tachiya, M., Identification of reactive species in photoexcited nanocrystalline TiO2 films by wide-wavelength-range (400-2500 nm) transient absorption spectroscopy. *Journal of Physical Chemistry B* **2004,** *108* (12), 3817-3823; (b) Yamakata, A.; Ishibashi, T.; Onishi, H., Time-resolved infrared absorption spectroscopy of photogenerated electrons in platinized TiO2 particles. *Chemical Physics Letters* **2001,** *333* (3-4), 271-277; (c) Peiro, A. M.; Colombo, C.; Doyle, G.; Nelson, J.; Mills, A.; Durrant, J. R., Photochemical reduction of oxygen adsorbed to nanocrystalline TiO2 films: A transient absorption and oxygen scavenging study of different TiO2 preparations. *Journal of Physical Chemistry B* **2006,** *110* (46), 23255-23263; (d) Haque, S. A.; Tachibana, Y.; Willis, R. L.; Moser, J. E.; Gratzel, M.; Klug, D. R.; Durrant, J. R., Parameters influencing charge recombination kinetics in dye-sensitized nanocrystalline titanium dioxide films. *Journal of Physical Chemistry B* **2000,** *104* (3), 538-547;

(e) Katoh, R.; Furube, A., Tunneling-Type Charge Recombination in Nanocrystalline TiO2 Films at Low Temperature. *Journal of Physical Chemistry Letters* **2011,** *2* (15), 1888-1891.

50. Klein, D. R., *Organic chemistry*. John Wiley: Hoboken, N.J., **2012**.

51. Du, P.; Moulijn, J. A.; Mul, G., Selective photo(catalytic)-oxidation of cyclohexane: Effect of wavelength and TiO2 structure on product yields. *Journal of Catalysis* **2006,** *238* (2), 342-352.

52. Almeida, A. R.; Moulijn, J. A.; Mul, G., In Situ ATR-FTIR Study on the Selective Photo-oxidation of Cyclohexane over Anatase TiO2. *The Journal of Physical Chemistry C* **2008,** *112* (5), 1552-1561.

53. Carneiro, J. T.; Yang, C.-C.; Moma, J. A.; Moulijn, J. A.; Mul, G., How Gold Deposition Affects Anatase Performance in the Photo-catalytic Oxidation of Cyclohexane. *Catal Lett* **2009,** *129* (1), 12-19.

54. Carneiro, J. T.; Moulijn, J. A.; Mul, G., Photocatalytic oxidation of cyclohexane by titanium dioxide: Catalyst deactivation and regeneration. *Journal of Catalysis* **2010,** *273* (2), 199-210.

55. Carneiro, J. T.; Almeida, A. R.; Moulijn, J. A.; Mul, G., Cyclohexane selective photocatalytic oxidation by anatase TiO2: influence of particle size and crystallinity. *Physical Chemistry Chemical Physics* **2010,** *12* (11), 2744-2750.

56. Boarini, P.; Carassiti, V.; Maldotti, A.; Amadelli, R., Photocatalytic Oxygenation of Cyclohexane on Titanium Dioxide Suspensions: Effect of the Solvent and of Oxygen. *Langmuir* **1998,** *14* (8), 2080-2085.

57. Almquist, C. B.; Biswas, P., The photo-oxidation of cyclohexane on titanium dioxide: an investigation of competitive adsorption and its effects on product formation and selectivity. *Applied Catalysis A: General* **2001,** *214* (2), 259-271.

58. Brusa, M. A.; Di Iorio, Y.; Churio, M. S.; Grela, M. A., Photocatalytic air oxidation of cyclohexane in CH2Cl2–C6H12 mixtures over TiO2 particles: An attempt to rationalize the positive effect of dichloromethane on the yields of valuable oxygenates. *Journal of Molecular Catalysis A: Chemical* **2007,** *268* (1–2), 29-35.

59. Brusa, M. A.; Grela, M. A., Photon flux and wavelength effects on the selectivity and product yields of the photocatalytic air oxidation of neat cyclohexane on TiO2 particles. *Journal of Physical Chemistry B* **2005,** *109* (5), 1914-1918.

60. Li, X. Y.; Chen, G. H.; Po-Lock, Y.; Kutal, C., Photocatalytic oxidation of cyclohexane over TiO2 nanoparticles by molecular oxygen under mild conditions. *Journal of Chemical Technology and Biotechnology* **2003,** *78* (12), 1246-1251.

61. Yoon, S. B.; Kim, J.-Y.; Kim, J. H.; Park, Y. J.; Yoon, K. R.; Park, S.-K.; Yu, J.-S., Synthesis of monodisperse spherical silica particles with solid core and mesoporous shell: mesopore channels perpendicular to the surface. *Journal of Materials Chemistry* **2007,** *17* (18), 1758-1761.

62. Deng, Y.; Qi, D.; Deng, C.; Zhang, X.; Zhao, D., Superparamagnetic High-Magnetization Microspheres with an Fe3O4@SiO2 Core and Perpendicularly Aligned Mesoporous SiO2 Shell for Removal of Microcystins. *Journal of the American Chemical Society* **2008,** *130* (1), 28-29.

63. Prazeres, T. J. V.; Beija, M.; Fernandes, F. V.; Marcelino, P. G. A.; Farinha, J. P. S.; Martinho, J. M. G., Determination of the critical micelle concentration of surfactants and amphiphilic block copolymers using coumarin 153. *Inorganica Chimica Acta* **2012,** *381*, 181-187.

64. Zapata, P. A.; Faria, J.; Ruiz, M. P.; Jentoft, R. E.; Resasco, D. E., Hydrophobic Zeolites for Biofuel Upgrading Reactions at the Liquid–Liquid Interface in Water/Oil Emulsions. *Journal of the American Chemical Society* **2012,** *134* (20), 8570-8578.

65. Weston, J. S.; Jentoft, R. E.; Grady, B. P.; Resasco, D. E.; Harwell, J. H., Silica Nanoparticle Wettability: Characterization and Effects on the Emulsion Properties. *Industrial & Engineering Chemistry Research* **2015,** *54* (16), 4274-4284.

66. Tripp, C. P.; Hair, M. L., An infrared study of the reaction of octadecyltrichlorosilane with silica. *Langmuir* **1992,** *8* (4), 1120-1126.

67. Cendrowski, K.; Chen, X.; Zielinska, B.; Kalenczuk, R. J.; Rümmeli, M. H.; Büchner, B.; Klingeler, R.; Borowiak-Palen, E., Synthesis, characterization, and photocatalytic properties of core/shell mesoporous silica nanospheres supporting nanocrystalline titania. *Journal of Nanoparticle Research* **2011,** *13* (11), 5899-5908.

68. Shang, J.; Flury, M.; Harsh, J. B.; Zollars, R. L., Comparison of different methods to measure contact angles of soil colloids. *Journal of Colloid and Interface Science* **2008,** *328* (2), 299-307.

69. Arkles, B. Hydrophobicity, Hydrophilicity and Silanes. http://www.gelest.com/goods/pdf/Library/advances/HydrophobicityHydrophilicityandSilanes.pdf (accessed 07/21).

70. Miller, D., Kempe, M. , Kennedy, C., and Kurtz, S. *Analysis of Transmitted Optical Spectrum Enabling Accelerated Testing of CPV Designs*; National Renewable Energy Laboratory (NREL): Golden, CO, USA, **2009**.

71. Ikeda, S.; Kowata, Y.; Ikeue, K.; Matsumura, M.; Ohtani, B., Asymmetrically modified titanium(IV) oxide particles having both hydrophobic and hydrophilic parts of their surfaces for liquid–liquid dual-phase photocatalytic reactions. *Applied Catalysis A: General* **2004,** *265* (1), 69-74.

72. Ahmadi, F.; Zarrin, L.; Sharifnia, S.; Hosseini, S. N., ANALYZED AND PROPOSED MECHANISM OF PHOTOCATALYTIC DEGRADATION OF FURFURAL AT TIO2 NANO-PARTICLES BY HPLC-UV AND LC-MASS METHODS. *Journal of Liquid Chromatography & Related Technologies* **2014,** *37* (12), 1750-1762.

73. Hoffmann, N., Photocatalytic Transformations of Furfural and its Derivatives In *9th Green Chemistry Conference*, Alcalá de Henares, Spain, **2011**.

74. Abdollahi, Y.; Abdullah, A. H.; Zainal, Z.; Yusof, N. A., Photodegradation of m-cresol by Zinc Oxide under Visible-light Irradiation. *2011* **2011,** *3* (3).

75. Abdollahi, Y.; Zakaria, A.; Sairi, N. A., Degradation of High Level m-Cresol by Zinc Oxide as Photocatalyst. *CLEAN – Soil, Air, Water* **2014,** *42* (9), 1292-1297.

76. Hatipoğlu, A.; San, N.; Çınar, Z., An experimental and theoretical investigation of the photocatalytic degradation of meta-cresol in TiO2 suspensions: a model for the product distribution. *Journal of Photochemistry and Photobiology A: Chemistry* **2004,** *165* (1–3), 119-129.

77. Choquette-Labbé, M.; Shewa, W.; Lalman, J.; Shanmugam, S., Photocatalytic Degradation of Phenol and Phenol Derivatives Using a Nano-TiO2 Catalyst: Integrating Quantitative and Qualitative Factors Using Response Surface Methodology. *Water* **2014,** *6* (6), 1785.

APPENDIX: TiO_2@mSiO_2 core-shell + OTS

This section is dedicated to the study of TiO_2@mSiO_2 core-shell + OTS, which is illustrated in Figure 63. This catalyst consists of TiO_2 particle coated with a mesoporous SiO_2 shell and functionalized with octadecyltrichlorosilane (OTS). Table 8 summarizes the chemical hazards and the safety precautions for the different compounds employed during the catalyst synthesis.

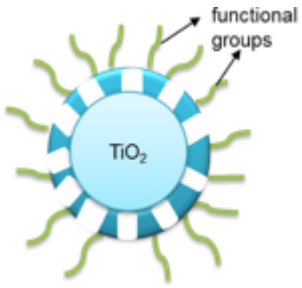

Figure 63. Illustration of TiO_2@mSiO_2 core-shell + OTS.

The catalyst was characterized by transmission electron microscopy (TEM), Brunauer, Emmett and Teller (BET) surface analysis, Fourier transform infrared spectroscopy (FTIR), diffuse Reflectance UV-vis Spectroscopy (DR UV-Vis), and contact angle measurement. These characterization techniques provided fairly detailed information about the structure and functionality of the catalysts.

Table 8. Chemical hazards of the different compounds used and safety precautions.

Compounds	Chemical Hazard	Hazard Code	Safety precautions
Octadecyl trichlorosilane (OTS)	Combustible liquid. Causes severe skin burns and eye damage. Causes serious eye damage.		Keep away from heat/sparks/open flames/hot surfaces. Wash skin thoroughly after handling. Store in a well-ventilated place. Keep cool.
Ammonium Hydroxide solution (NH_4OH)	Harmful if swallowed. Causes severe skin burns and eye damage. Causes serious eye damage. Very toxic to aquatic life.		Wash skin thoroughly after handling. Avoid release to the environment. Store locked up.
Tetraethyl orthosilicate (TEOS)	Flammable liquid and vapor. Causes serious eye irritation. Harmful if inhaled. May cause respiratory irritation.		Keep away from heat/sparks/open flames/hot surfaces. Keep container tightly closed. Avoid breathing dust/ fume/ gas/ mist/ vapors/ spray. Wash skin thoroughly after handling. Use only in a well-ventilated area.
Titanium (IV) isopropoxide	Flammable liquid and vapor. Causes serious eye irritation. May cause drowsiness or dizziness.		Keep away from heat/sparks/open flames/hot surfaces. Keep container tightly closed. Avoid breathing dust/ fume/ gas/ mist/ vapors/ spray. Wash skin thoroughly after handling. Use and store only in a well-ventilated area. Keep cool.

Catalyst characterization techniques

Transmission electron microscopy (TEM)

Figure 64 displays the TEM images of the TiO_2@mSiO_2 core-shell catalyst. It is hard to differentiate the SiO_2 spheres from the TiO_2 However, the thickness of the shell was measured to be around 4 ± 1 nm. Electron diffraction, dark field, and bright field images were taken in order to attempt to differentiate the silica from the crystalline TiO_2.

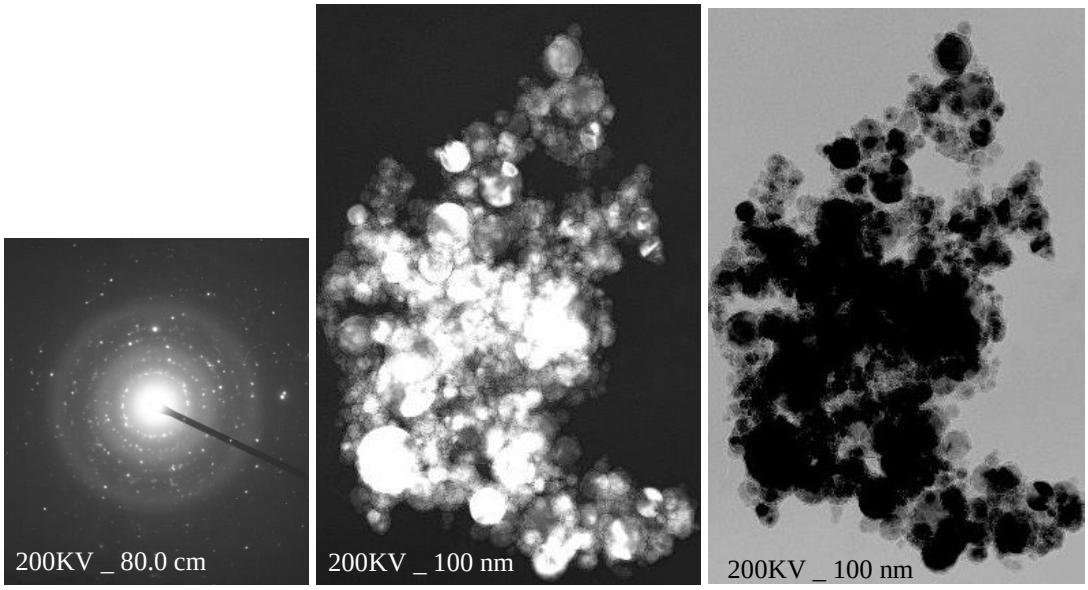

Figure 64. a) Electron diffraction, b) and c) Bright and dark field images.

Brunauer–Emmett–Teller (BET) surface area

Specific surface areas were determined by the classical BET procedure. Table 9 summarizes the BET surfaces areas and pore volumes of the TiO_2@mSiO_2 core-shell and TiO_2@mSiO_2 core-shell + OTS catalysts compared to the BET surfaces areas and pore volumes of commercial hydrophobic TiO_2 and TiO_2, anatase, 99.9%. Concerning the TiO_2@mSiO_2 core-shell catalyst, the incorporation of the SiO_2 shell causes a

noticeable increase in surface area compared to the TiO_2, anatase, 99.9%. In regard to the $TiO_2/mSiO_2$, the surface area of the mesoporous SiO_2 decreases after the impregnation of TiO_2. On the other hand, the surface area and pore volume markedly drop off for both catalysts after the OTS functionalization because the mesoporous SiO_2 may become partially blocked by the silane.

Table 9. BET surface area and pore volumes of the catalysts.

Catalyst	BET Surface area ± 5 (m^2/g)	Pore volume (cm^3/g)
Commercial hydrophobic TiO_2	48.12	0.31
TiO_2, anatase, 99.9%	51.04	0.27
TiO_2@$mSiO_2$ core-shell	118.29	0.32
TiO_2@$mSiO_2$ core-shell + OTS	67.46	0.28
mSiO2	936.86	0.24
$TiO_2/mSiO_2$	696.6	0.24
$TiO_2/mSiO_2$ + OTS	490.78	0.15

Contact angle measurement

High contact angle means that the surface is hydrophobic and has poor wetting property. A well-known technique, the sessile drop method was used for the contact angle measurement. Results for the functionalized nanoparticles are summarized in Table 10. Both surfaces, $TiO_2/mSiO_2$ nanoparticles and TiO_2@$mSiO_2$ core-shell nanoparticles treated with OTS, presented contact angles higher than 90° and close to the contact angle obtained for the commercial hydrophobic TiO_2.[69]

Table 10. Static contact angles for hydrophobic nanoparticles.

Sample	DSA contact angle, degrees
Commercial hydrophobic TiO_2	164
TiO_2@$mSiO_2$ core-shell + OTS	161
TiO_2/$mSiO_2$ + OTS	156

FTIR

Figure 65 depicts the FTIR spectra of TiO_2@$mSiO_2$ core-shell + OTS. The presence of water causes the broad band at 3250-3600 cm^{-1} and the band at 1620 cm^{-1}. Addition of OTS to the TiO_2@$mSiO_2$ core-shell causes the antisymmetric and symmetric CH stretching band positions occurring at 2916 and 2851 cm^{-1}, respectively.[66] The characteristic bands of OH groups are located at 3740, 3729, and 3756 cm^{-1}.[55] It can also be observed that the surface hydroxyl groups' vibrational frequency decreased after impregnation of TiO_2 on the $mSiO_2$ and decreased even more with addition of OTS (green line). The complete removal of the CTAB micelles can be corroborated by the absence of the CH_2 vibration frequency in the spectra for TiO_2@$mSiO_2$ (red line).

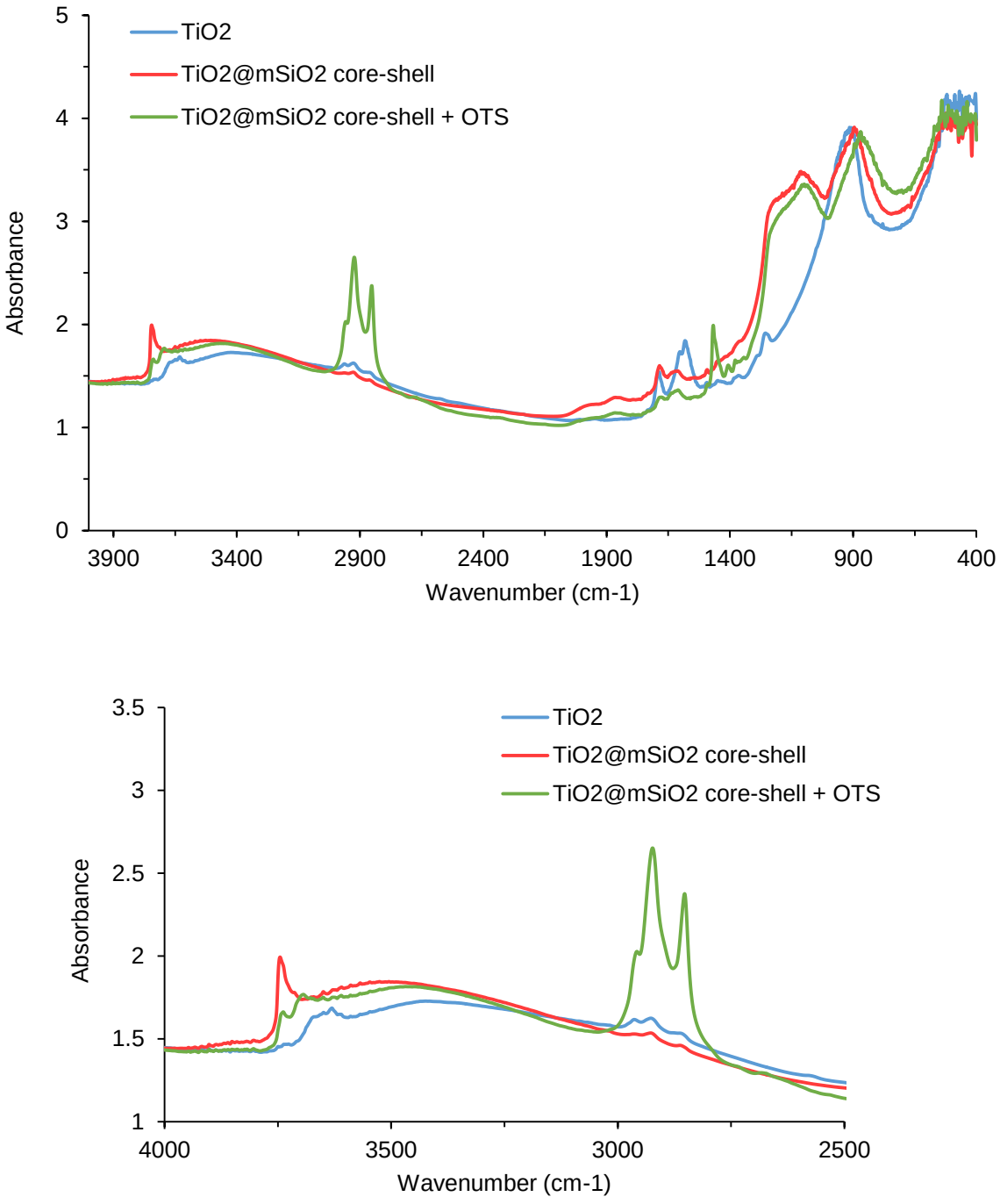

Figure 65. FTIR spectrum on TiO_2, TiO_2@$mSiO_2$ core-shell + OTS, and TiO2@$mSiO_2$ core-shell + OTS. Top: Full range, wavenumber range 500 to 4000 cm-1. Bottom: Wavenumber range 2500 to 4000 cm^{-1}.

DR-UV/Vis

The resulting UV-vis diffuse reflectance spectrum of the studied samples is presented in Figure 66. This figure clearly shows that the absorption edge of the modified catalysts shifted towards shorter wavelength in comparison to the TiO_2, anatase, 99.9%. Figure 67 shows that the bandgap energy increased a little after addition of OTS, being approximately 3.05 eV for TiO_2, anatase, 99.9%, 3.1 for eV for commercial hydrophobic TiO_2 and TiO_2@$mSiO_2$ core-shell + OTS, and 3.14 eV for TiO_2/$mSiO_2$ + OTS.

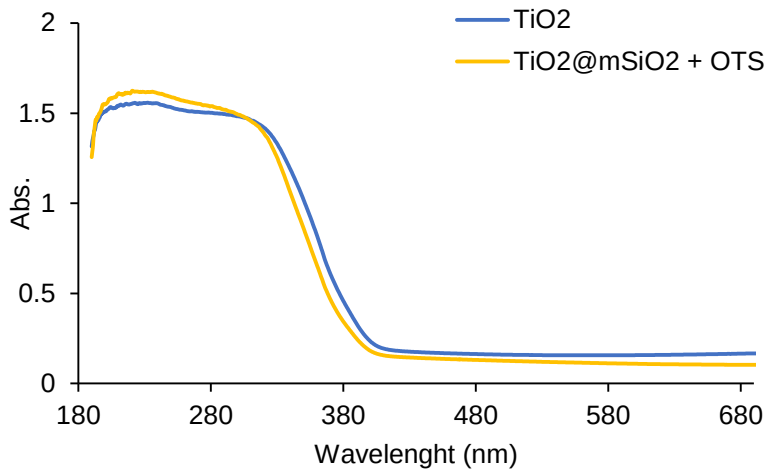

Figure 66. UV-vis diffuse reflectance spectrum for TiO_2 *and* TiO_2@$mSiO_2$ core-shell + OTS.

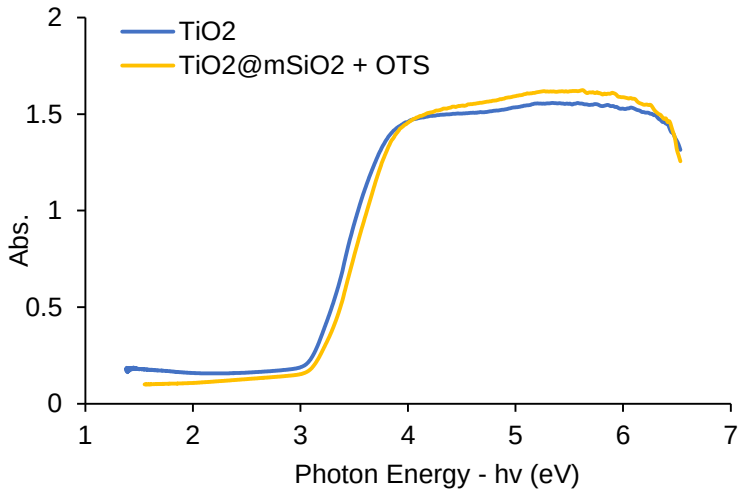

Figure 67. Tauc Plot for TiO_2 and TiO_2 and TiO_2@$mSiO_2$ core-shell + OTS.